

PREPARATION OF PALLADIUM, PALLADIUM SULFIDE, CADMIUM SELENIDE
NANOPARTICLES AND MAGNESIUM OXYCHLORIDE, MAGNESIUM HYDROXIDE
NANORODS

by

ZHIQIANG YANG

B.S., East China University of Science & Technology, 1994
M.S., East China University of Science & Technology, 1997

AN ABSTRACT OF A DISSERTATION

submitted in partial fulfillment of the requirements for the degree

DOCTOR OF PHILOSOPHY

Department of Chemistry
College of Art and Science

KANSAS STATE UNIVERSITY
Manhattan, Kansas

2008

Abstract

First, a new tiara Pd(II) thiolate complex-[Pd(SC₁₂H₂₅)₂]₆ has been synthesized and fully characterized. Then the complex was further used as a single-source precursor to prepare nearly monodisperse palladium sulfide (PdS) nanoparticles through the high-temperature-induced decomposition in diphenyl ether.

Secondly, the influence of dodecanethiol on the product distribution upon heating a Pd(II)-octylamine system was investigated. The molar ratio of octylamine to Pd(II) was fixed at 20:1, and the concentration of dodecanethiol was changed systematically. Without thiol ligand, only aggregated Pd(0) particles were obtained due to the reduction of Pd(II) by octylamine. When the molar ratio of dodecanethiol to Pd(II) was increased to 0.5, highly monodisperse sulfurized palladium nanoparticles with diameter 7.55 ± 0.73 nm were generated. When the molar ratio reached to 2, only a thiolate complex-[Pd(SC₁₂H₂₅)₂]₆ was found as the final product.

Thirdly, we report a facile method to prepare nearly monodisperse Pd nanoparticles by heating Pd(II) ions in 4-*tert*-butyltoluene solvent, in the presence of oleylamine and trioctylphosphine (TOP) ligands. It has been found the concentration of TOP ligand was highly pivotal for the formation of Pd nanoparticles. Without TOP, only aggregated Pd particles were obtained due to the reduction of Pd(II) by oleylamine. When the molar ratio of TOP to Pd(II) was less than two, well-protected Pd nanoparticles were obtained. However, when the molar ratio reached to two, only Pd(II)-TOP coordination complexes were obtained as the final product.

Fourthly, we present a novel way to synthesize cadmium selenide (CdSe) nanoparticles from a heterogeneous system only containing cadmium oxide, trioctylphosphine, and trioctylphosphine selenide.

Last, the formation of magnesium oxychloride (Mg_x(OH)_yCl_z·nH₂O) nanorods from the system MgO-MgCl₂-H₂O was investigated. By changing the amounts of the starting materials, short nanorods (< 1 micron) or long nanorods (up to 20 micron) could be obtained readily with the aspect ratio in the range of 10-70. The resulting magnesium oxychloride nanorods could be further transformed to magnesium hydroxide (Mg(OH)₂) nanorods by treating with NaOH.

PREPARATION OF PALLADIUM, PALLADIUM SULFIDE, CADMIUM SELENIDE
NANOPARTICLES AND MAGNESIUM OXYCHLORIDE, MAGNESIUM HYDROXIDE
NANORODS

by

ZHIQIANG YANG

B.S., East China University of Science & Technology, 1994
M.S., East China University of Science & Technology, 1997

A DISSERTATION

submitted in partial fulfillment of the requirements for the degree

DOCTOR OF PHILOSOPHY

Department of Chemistry
College of Art and Science

KANSAS STATE UNIVERSITY
Manhattan, Kansas

2008

Approved by:

Major Professor
Kenneth J. Klabunde

Abstract

First, a new tiara Pd(II) thiolate complex-[Pd(SC₁₂H₂₅)₂]₆ has been synthesized and fully characterized. Then the complex was further used as a single-source precursor to prepare nearly monodisperse palladium sulfide (PdS) nanoparticles through the high-temperature-induced decomposition in diphenyl ether.

Secondly, the influence of dodecanethiol on the product distribution upon heating a Pd(II)-octylamine system was investigated. The molar ratio of octylamine to Pd(II) was fixed at 20:1, and the concentration of dodecanethiol was changed systematically. Without thiol ligand, only aggregated Pd(0) particles were obtained due to the reduction of Pd(II) by octylamine. When the molar ratio of dodecanethiol to Pd(II) was increased to 0.5, highly monodisperse sulfurized palladium nanoparticles with diameter 7.55 ± 0.73 nm were generated. When the molar ratio reached to 2, only a thiolate complex-[Pd(SC₁₂H₂₅)₂]₆ was found as the final product.

Thirdly, we report a facile method to prepare nearly monodisperse Pd nanoparticles by heating Pd(II) ions in 4-*tert*-butyltoluene solvent, in the presence of oleylamine and trioctylphosphine (TOP) ligands. It has been found the concentration of TOP ligand was highly pivotal for the formation of Pd nanoparticles. Without TOP, only aggregated Pd particles were obtained due to the reduction of Pd(II) by oleylamine. When the molar ratio of TOP to Pd(II) was less than two, well-protected Pd nanoparticles were obtained. However, when the molar ratio reached to two, only Pd(II)-TOP coordination complexes were obtained as the final product.

Fourthly, we present a novel way to synthesize cadmium selenide (CdSe) nanoparticles from a heterogeneous system only containing cadmium oxide, trioctylphosphine, and trioctylphosphine selenide.

Last, the formation of magnesium oxychloride (Mg_x(OH)_yCl_z·nH₂O) nanorods from the system MgO-MgCl₂-H₂O was investigated. By changing the amounts of the starting materials, short nanorods (< 1 micron) or long nanorods (up to 20 micron) could be obtained readily with the aspect ratio in the range of 10-70. The resulting magnesium oxychloride nanorods could be further transformed to magnesium hydroxide (Mg(OH)₂) nanorods by treating with NaOH.

Table of Contents

List of figures	viii
List of tables	xi
Acknowledgements	xii
Dedication	xiii
Preface	xiv
CHAPTER 1 - Introduction.....	1
CHAPTER 2 - Synthesis and characterization of a new tiara Pd(II) thiolate complex- [Pd(SC ₁₂ H ₂₅) ₂] ₆ and its solution-phase thermolysis to prepare nearly monodisperse palladium sulfide nanoparticles.....	3
2.1 Introduction.....	3
2.2 Experimental Section.....	6
2.2.1 Materials.....	6
2.2.2 Preparation of Pd(II) thiolate complex [Pd(SC ₁₂ H ₂₅) ₂] ₆	6
2.2.3 Solution-phase thermolysis.....	7
2.2.4 Equipment and analysis.....	7
2.3 Results and discussion.....	8
2.3.1 Preparation of [Pd(SC ₁₂ H ₂₅) ₂] ₆	8
2.3.2 Structure and properties of [Pd(SC ₁₂ H ₂₅) ₂] ₆	9
2.3.3 Thermolysis of [Pd(SC ₁₂ H ₂₅) ₂] ₆ in diphenyl ether.....	14
2.4 Conclusions.....	18
2.5 References.....	19
2.6 Supporting information.....	22
CHAPTER 3 - From monodisperse sulfurized palladium nanoparticles to tiara Pd(II) thiolate clusters: the influence of thiol ligand on the thermal treatment of a Pd(II)-amine system.....	32
3.1 Introduction.....	32
3.2 Experimental Section.....	34
3.2.1 Materials.....	34
3.2.2 Thermolysis without dodecanethiol.....	34

3.2.3 Thermolysis with different amounts of dodecanethiol.....	35
3.2.4 Equipment and analysis.....	35
3.3 Results.....	36
3.3.1 Heating of Pd(II)-octylamine mixture without thiol	36
3.3.2 Heating of Pd(II)-octylamine-dodecanethiol systems.....	39
3.4 Discussion.....	46
3.5 Conclusions.....	52
3.6 References.....	52
3.7 Supporting information.....	55
CHAPTER 4 - Synthesis of nearly monodisperse palladium (Pd) nanoparticles by using oleylamine and trioctylphosphine mixed ligands.....	60
4.1 Introduction.....	60
4.2 Experimental Section.....	61
4.2.1 Materials.....	61
4.2.2 Thermolysis without TOP.....	62
4.2.3 Thermolysis with different amounts of TOP.....	62
4.2.4 Equipment and analysis.....	63
4.3 Results and discussion.....	63
4.3.1 Reduction of Pd(II) ions by oleylamine.....	63
4.3.2 Reduction of Pd(II) ions in the presence of oleylamine and TOP.....	67
4.3.3 The function of TOP.....	71
4.3.4 The cooperative protecting effects of oleylamine.....	76
4.4 Conclusions.....	79
4.5 References.....	79
4.6 Supporting information.....	82
CHAPTER 5 - An unusual fluorescence evolution of cadmium selenide (CdSe) nanoparticles generated from a cadmium oxide / trioctylphosphine selenide / trioctylphosphine heterogeneous system.....	87
5.1 Introduction.....	87
5.2 Experimental Section.....	89
5.2.1 Materials.....	89

5.2.2 Preparation of CdSe nanoparticles from CdO/TOPSe/TOP system.....	89
5.2.3 Equipment and analysis.....	90
5.3 Results and discussion.....	91
5.3.1 The fluorescence evolution at 320 °C.....	91
5.3.2 The fluorescence evolution at 270 °C.....	98
5.3.3 Discussion.....	100
5.4 Conclusions.....	100
5.5 References.....	101
CHAPTER 6 - Synthesis of magnesium oxychloride nanorods with controllable morphology and their transformation to magnesium hydroxide nanorods via treatment with sodium hydroxide.	103
6.1 Introduction.....	103
6.2 Experimental Section.....	105
6.2.1 Materials.....	105
6.2.2 Preparation of magnesium oxychlorides.....	105
6.2.3 Transformation of MgCl ₂ ·6H ₂ O nanorods to Mg(OH) ₂ nanorods.....	105
6.2.4 Equipment and analysis.....	106
6.3 Results and discussion.....	108
6.3.1 Synthesis of magnesium oxychloride nanorods.....	108
6.3.2 Conversion of magnesium oxychlorides to Mg(OH) ₂	114
6.4 Conclusions.....	116
6.5 References.....	116

List of Figures

Figure 2.1 Perspective view of the complex $[\text{Pd}(\text{SC}_{12}\text{H}_{25})_2]_6$. Yellow balls represent S atoms, while green balls represent Pd atoms umber.....	10
Figure 2.2 ^1H NMR (room temperature in deutero-benzene) spectrum of $[\text{Pd}(\text{SC}_{12}\text{H}_{25})_2]_6$. (3.04 ppm, 12H (t); 2.81 ppm, 12H (t); 2.16 ppm, 12H (q); 2.02 ppm, 12H (q); 1.70-1.34 ppm, 216H(m); 0.94 ppm, 36H (m).).....	11
Figure 2.3 UV/Vis spectrum of $[\text{Pd}(\text{SC}_{12}\text{H}_{25})_2]_6$. (0.2×10^{-4} M in <i>n</i> -heptane)	12
Figure 2.4 MALDI spectrum of $[\text{Pd}(\text{SC}_{12}\text{H}_{25})_2]_6$	13
Figure 2.5 UV-Vis spectra of the colloidal solution at different reaction times. The arrows indicate the decrease of the peaks	14
Figure 2.6 TEM of the obtained nanoparticles after refluxing $[\text{Pd}(\text{SC}_{12}\text{H}_{25})_2]_6$ for 6 hours in diphenyl ether. (scale bar = 100 nm).....	16
Figure 2.7 Histogram of the nanoparticles showing the size distribution. (diameter = 2.87 ± 0.51 nm, obtained by measuring 100 particles).....	16
Figure 2.8 Powder XRD pattern of the PdS product obtained by refluxing $[\text{Pd}(\text{SC}_{12}\text{H}_{25})_2]_6$ for 6 hr. (The standard PdS pattern is from JCPDS file 25-1234)	17
Figure 3.1 Powder XRD pattern of Sample (0 X) indicating the formation of Pd(0) crystals. The standard pattern is based on JCPDS file 46-1043	37
Figure 3.2 TEM image of Sample (0 X) shows aggregated particles	38
Figure 3.3 Solutions with different amounts of dodecanethiol before (upper) and after (lower) heating. The molar ratios of thiol to Pd(II) are 0, 0.125, 0.25, 0.5, 1, 1.5, 2 from left to right	39
Figure 3.4 TEM image of Sample (0.5 X)	41
Figure 3.5 Powder XRD of Sample (0.5 X). The standard patterns are from JCPDS file 30-884 (Pd_{16}S_7 , marked with \circ) and 73-1387 (Pd_4S , marked with Δ).....	42
Figure 3.6 TEM images for Sample (1 X); (upper row) Sample (1.5 X) and Sample (2 X). (lower row, from left to right).....	44
Figure 3.7 UV/vis pattern of Sample (2 X) in <i>n</i> -heptane	45

Figure 3.8 UV/vis patterns of the solutions after heating. (50 μ l of solution in 3 ml of <i>n</i> -heptane)	49
Figure 3.9 TEM images indicating the growth of the particles in Sample (0.5 X) along with heating time. (from left to right: 30 min, 45 min, 2 h)	51
Figure 4.1 Powder XRD pattern of Sample (0 \times) indicating the formation of Pd(0) crystallites. The standard pattern (the vertical lines) is based on JCPDS file 46-1043. (Notice: a small amount of water was added during wash in order to remove NaCl that was generated in the reaction.)	64
Figure 4.2 TEM image of Sample (0 \times) shows aggregated particles.....	66
Figure 4.3 Powder XRD patterns of Sample (0.4 \times) (a), Sample (0.6 \times) (b) and Sample (1.0 \times) (c).....	68
Figure 4.4 TEM images of (a) Sample (0.4 \times), (b) Sample (0.6 \times), (c) Sample (1.0 \times), (d) Sample (1.4 \times). Scale bar = 100 nm	70
Figure 4.5 UV/vis absorbance for Sample (1.0 \times) before and after adding TOP at room temperature to show the generation of Pd(II)-TOP complexes. For each measurement, 30 μ l of the solution was taken and then mixed with 3 ml of hexane, which was also used as the reference.....	72
Figure 4.6 UV/vis patterns of the sample solutions after heating. For each measurement, an aliquot of 30 μ l was taken and then mixed with 3 ml of hexane. Reference: hexane	74
Figure 4.7 TEM images of the particles prepared according to Sample (0.6 \times) except changing the molar ratio of oleylamine to Pd(II). (a) Decreasing the ratio to 3, (b) increasing the ratio to 60. Scale bar = 100 nm. Also see the TEM image of Sample (0.6 \times) in Figure 4.4 (b) for comparison.....	77
Figure 4.8 TEM images of the sample prepared according to Sample (0.6 \times) except increasing the molar ratio of oleylamine to Pd(II) to 60 and heating for 17 h. (A) Small magnification to show the hexagonal close-packing pattern in short range. (B) Large magnification to show the faceted quasi-spherical shape. Scale bar = 100 nm	78
Figure 5.1 Powder XRD pattern of the sample collected after heating at 320 $^{\circ}$ C for 4 h to show the generation of CdSe nanocrystallites with wurtzite structure. The standard pattern (vertical lines) is drawn according to JCPDS file No. 02-0330.....	92

Figure 5.2 TEM images to show the temporal evolution of CdSe nanoparticles. A: 0.5 h; B: 1 h; C: 1.5 h; D: 2 h; E: 3 h; F: 4 h. scale bar = 100 nm. Heating temperature: 320 °C	94
Figure 5.3 Photoluminescence (PL) evolution of CdSe nanoparticles. Heating temperature: 320 °C	95
Figure 5.4 Changes of the PL peak position and the full width of half-maximum (FWHM) as the function of heating time. Heating temperature: 320 °C.....	96
Figure 5.5 UV/vis absorbance patterns of the obtained samples.....	97
Figure 5.6 Temporal fluorescence evolution of CdSe nanoparticles. Heating temperature: 270 °C	98
Figure 5.7 Changes of the peak position and the full width of half-maximum (FWHM) as the function of heating time. Heating temperature: 270 °C.....	99
Figure 6.1 Powder XRD patterns of samples A-F. The peaks are appointed according to JCPDS file 73-2119 (phase 3), file 07-0420 (phase 5), and 75-1527 (Mg(OH) ₂)	109
Figure 6.2 TEM images of samples A-F. The scale bar in each image is equal to 2 μm.....	110
Figure 6.3 TEM images of samples G-M. The scale bar in each image is equal to 2 μm	114
Figure 6.4 Powder XRD pattern and TEM image of sample D after NaOH treatment. The peaks in the XRD pattern are appointed according to JCPDS file 75-1527.....	115

List of Tables

Table 6.1 Experimental conditions for the synthesis of magnesium oxychlorides	107
---	-----

Acknowledgements

I would like to acknowledge many people for helping me during my Ph.D. studies. First of all, I would like to thank my advisor Dr. Kenneth J. Klabunde for supporting and guiding me in his wonderful research group. As a successful scientist and chemist himself, he is always encouraging me to think and work in an analytical and scientific way. From him, I have learned a lot of things about the qualities to be a good scientist. His kindness in nature let all of us work in a pleasant atmosphere; and his profound knowledge assure our success in research. Also, I would like to thank him for helping me in paper-writing and job-hunting.

I would like to express my deep appreciation to my committee members: Dr. Sameer Madanshetty, Dr. Christopher Sorensen, Dr. Daniel Higgins, Dr. Duy Hua, and my major advisor Dr. Kenneth Klabunde.

I would like to thank my colleagues in our research group, Dr. Jeevanandam Pethaiyan, Dr. Uma Sitharaman, Dr. Ranjit Koodali, Dr. Shalini Rodriguez, Dr. Igor Martyanov, Dr. Gavin Medine, Dr. David Heroux, Dr. Aldo Ponce, Dr. Johanna Haggstrom, Dr. Dmytro Demydov, Dr. Kennedy Kalebaila, Sreeram Cingarapu, Dambar Hamal, Erin Beavers, Yanting Kuo, XiangXin Yang, Khadga Shrestha, for everything they did for me. Specially, I would like to thank Dr. Alexander Smetana, for helping me a lot in SMAD.

I am very grateful for the helps that Yanli and I got from Earline Dikeman, a lady with all kindness and generosity.

Thanks also give to Dr.Dan Boyle for the help with TEM.

Last, to my beloved wife, Yanli Chen. Without her, I could not achieve anything.

Dedication

To my wife and my parents.

Preface

For the small, we pursue.

CHAPTER 1 - Introduction

In recent years, considerable efforts have been made to study nanoscale materials. Generally speaking, nanomaterials are materials with size smaller than one micron in at least one dimension. If saying in more specific way, most people think that the size range for nanomaterials is in 1 to 100 nm.

Materials in nanoscale may possess different physical/chemical properties compared with their bulk counterparts. For example, gold nanoparticles can serve as catalyst even though bulk gold is very inert and stable; cadmium selenide nanoparticles have fluorescence emission changing from blue to red due to the size-related quantum effects. The potential applications of nanomaterials in optical, electronic, magnetic, and biological fields are quite attractive and promising.

To prepare nanomaterials, a variety of methods and strategies have been established. Although it can be achieved by pure physical methods, the most common strategy to prepare nanomaterials is to generate the required materials by chemical reactions. And the reactions are usually carried out in liquid phases, which are much easier to be handled and controlled compared to gas-phases and solid-phase reactions. The newly generated nanomaterials from the so-called wet chemistry have quite large surface areas and very reactive. To stabilize them, protecting agents are generally applied. For the reactions carried out in organic phase, organic ligands with long C-

chains such as alkylthiols, alkylamines and phosphines are widely used, as demonstrated in the following chapters.

The main research goal of this dissertation is to develop novel and facile methods to prepare nanomaterials including metals, metal chalcogenides, and metal oxides on large scale. For this purpose, wet chemical processes were implemented for all the productions, and organic ligands were applied in some cases to obtain high monodisperse nanoparticles.

CHAPTER 2 - Synthesis and characterization of a new tiara Pd(II) thiolate complex-[Pd(SC₁₂H₂₅)₂]₆ and its solution-phase thermolysis to prepare nearly monodisperse palladium sulfide nanoparticles*

* It has been published in *Inorganic Chemistry* 2007, 46, 2427-2431.

2.1 Introduction

A variety of metal alkanethiolates have been synthesized and characterized because of their interesting structural features for coordination chemistry and wide applications for monolayer-protected clusters and surface chemistry.

According to their solubility, metal alkanethiolates can be roughly separated into two groups. Ag(I),^{1, 2, 3} Cu(I),⁴ Pb(II)^{5, 6} ions react with primary alkanethiols and form insoluble precipitates in most organic solvents. Through powder XRD analysis, these alkanethiolates show equally separated peaks and can be inferred to have layered structures. On the other hand, Ni(II) and Pd(II) ions produce soluble cyclic (tiara) compounds with primary alkanethiols or other functionalized thiols. In such structures, every metal ion is coordinated to four sulfur atoms in an approximate square plane and each -SR ligand is connected to two metal ions. Depending on the properties of the

ligands and the reaction conditions, tiara Ni(II) thiolates with 4, 5, 6, 8, 9 or 11-membered Ni(II) ring have been prepared.^{7, 8} Compared to Ni(II) thiolates, fewer tiara Pd(II) thiolates with short C-chain ligands have been prepared and characterized, including $[\text{Pd}(\text{SCH}_2\text{CH}_2\text{OH})_2]_6$,⁹ $[\text{Pd}(\text{SCH}_2\text{CH}_2\text{CH}_3)_2]_6$ ¹⁰ and $[\text{Pd}(\text{SCH}_2\text{CH}_2\text{CH}_3)_2]_8$.¹¹ Some theoretical articles described the important role that metal–S π bonds play to stabilize such tiara-like structures.^{12, 13, 14}

An important application of metal thiolates is to produce metals or metal sulfides through the heat-induced decomposition, which can be carried out in solvents with high boiling point or under solventless conditions. Carotenuto et al. reported a general method to synthesize metal or metal sulfide clusters embedded in polymer matrices.¹⁵ Nakamoto et al. presented the thermolysis of a series of gold thiolate precursors $[\text{RN}(\text{CH}_3)_3][\text{Au}(\text{SC}_{12}\text{H}_{25})_2]$ ($\text{R} = \text{C}_8\text{H}_{17}$, $\text{C}_{12}\text{H}_{25}$, and $\text{C}_{14}\text{H}_{29}$) to produce spherical Au nanoparticles.^{16, 17} Korgel et al. reported the solventless synthesis of nickel sulfide and copper sulfide through the decomposition of the corresponding thiolate precursors in the presence of octanoate.^{18, 19} Through changing the reaction conditions, nanorods or triangular nanoprisms for NiS, and nanorods or spherical nanoparticles for Cu_2S were obtained. Wu et al. reported the synthesis of Cu_2S nanowires²⁰ and Ag nanodisks²¹ through the thermolysis of the respective metal thiolates. Titanium sulfide (TiS_2) and niobium sulfide (NbS_2) thin films have been prepared through the chemical vapor deposition by using the corresponding metal tert-butylthiolates.^{22, 23} Recently, copper-indium sulfide nanocrystal heterostructures with interesting shapes were

obtained from the thermolysis of a mixture composed of Cu-oleate, In-oleate and an alkanethiol.²⁴

PdS is a semiconductor with an energy gap about 2eV and has a variety of applications in materials science and catalysis.²⁵ PdS films have been prepared by laser or thermal vapor deposition from a single-source precursor Pd(S₂COCHMe₂)₂.²⁶ Yamamoto et al. reported the preparation of PdS organosols through the reaction of Pd acetate with hydrogen sulfide.²⁷ Also, the first trioctylphosphine oxide (TOPO)-capped PdS nanoparticles have been synthesized through the thermolysis of Pd(S₂CNMe(Hex))₂ in the presence of TOPO.²⁸ The tetragonal crystal structure of PdS has been precisely determined by single crystal analysis.²⁹

Here we report the synthesis and full characterization of a new tiara Pd(II) thiolate complex-[Pd(SC₁₂H₂₅)₂]₆, which was further used as a single-source precursor to prepare nearly monodisperse palladium sulfide (PdS) nanoparticles. This will not only enlarge our understanding about metal thiolate complexes with tiara structures, but also offer a novel and facile method to prepare palladium sulfide nanoparticles.

2.2 Experimental section

2.2.1 Materials

Sodium tetrachloropalladate(II) (99%) and 1-dodecanethiol (98%) were obtained from Aldrich Chem. Co. Diphenyl ether and 4-tert-butyltoluene (96%) were bought from ACROS Organics. Other chemicals were purchased and used as received.

2.2.2 Preparation of Pd(II) thiolate complex $[\text{Pd}(\text{SC}_{12}\text{H}_{25})_2]_6$

In a glass tube equipped with a rubber septum which was connected to a vacuum line and an argon gas-tank through needles, 0.588 g of Na_2PdCl_4 (2×10^{-3} mol), 10 ml of 4-tert-butyltoluene, and 0.98 ml of dodecanethiol (4×10^{-3} mol) were added sequentially. The mixture was degassed and then flushed with argon several times. Then, it was refluxed (about 192°C) in a preheated sand-bath for 1 hour under an atmosphere of argon. After that, the tube was removed from the sand-bath and left to cool. The obtained orange-red solution was then dropped into 100 ml of 95% ethanol which was stirred violently. Orange precipitates and a few red oil droplets formed immediately. Stirring overnight caused the droplets to also form orange precipitates. The final product was separated by centrifugation and washed with 95% ethanol (30 ml \times 4) and then pure ethanol (30 ml \times 4). After drying at 45°C under vacuum overnight, 0.93 g of orange powder was obtained. Yield: 91.2%. Elemental analysis: found Pd: 20.56, S: 12.56, C: 56.26, H: 9.42; calcd. Pd: 20.92, S: 12.60, C: 56.65, H: 9.83. For the UV/Vis analysis, certain amounts of dry powder were dissolved in n-heptane.

2.2.3 Solution-phase thermolysis

In a glass tube, 0.102 g of the obtained orange powder was added into 4 ml of diphenyl ether. The mixture was degassed and flushed with argon several times. After that, the mixture was refluxed (about 259 °C) in a preheated sand-bath for 6 hours under the protection of argon. During this process, the original clear orange-red solution became black, which indicated the formation of palladium sulfide nanoparticles. For the UV-Vis tracking, the reaction was stopped at different times and cooled to room temperature. Then 16 µl of solution was taken out and mixed with 3 ml of toluene. The UV-Vis absorbance was measured using pure toluene as reference. For TEM analysis, some colloidal solution was taken out and washed with acetone (30 ml × 4) by centrifugation and then redissolved into 4-tert-butyltoluene. For elemental analysis, the washed sample was further dried at 45°C under vacuum overnight.

2.2.4 Equipment and analysis

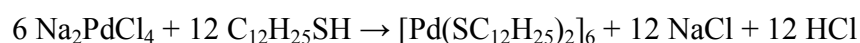
UV/Vis absorption analysis was carried out on a Cary 500 UV-VIS-NIR spectrophotometer. Transmission electron microscopy (TEM) was performed on a Philips CM100 microscope operated at 100 kV. To prepare a TEM sample, a drop of colloidal solution was dropped onto a carbon-coated Formvar copper grid and then allowed to dry in air. IR spectra were obtained using a NEXUS 670 FT-IR system produced by Nicolet Instrument Corporation. ¹H NMR spectra were obtained on a Varian Unity 400 Plus 400-MHz NMR system. A [Pd(SC₁₂H₂₅)₂]₆ single crystal was analyzed through a Bruker SMART 1000 CCD instrument with Mo X-ray irradiation.

To obtain the single crystal, product was dissolved in a THF/4-tert-butyltoluene mixture (volume ratio: 1/1) and then left uncovered on the bench for several days at room temperature. MALDI mass analysis was performed on an Applied Biosystem DE-Pro MALDI-Tof system. The sample was dissolved in THF and then mixed with 2, 5-dihydrobenzoic acid (a matrix) and a cationizing agent (CF₃COONa). Positive scan was carried out. Powder X-ray diffraction (XRD) patterns were recorded by a Bruker D8 X-ray diffractometer with Cu K α radiation.

2.3 Results and discussion

2.3.1 Preparation of [Pd(SC₁₂H₂₅)₂]₆

To prepare the Pd(II) thiolate complex, Na₂PdCl₄ was used as the Pd(II) source and dodecanethiol as ligand, while 4-tert-butyltoluene was applied as a solvent. The reaction is assumed to happen according to the following equation:



When the thiol ligand was added into the suspension of Na₂PdCl₄ in 4-tert-butyltoluene at room temperature, a white fog formed, which was assumed to be the release of the HCl. In the meantime, the color of the solution changed from colorless to orange-red and part of the brown-colored Na₂PdCl₄ faded into colorless crystals, which indicated the formation of NaCl.

Although this reaction could initiate at room temperature, as described above, it was found not to go to completion unless heated. A control experiment was carried out to show this. When other conditions remained the same, the mixture of the starting materials was stirred at room temperature for one hour under argon, instead of refluxing. A similar orange powder could be obtained, but more reddish compared with the refluxed sample. Through thin-layer-chromatography analysis, three products were found for the room temperature sample, while only one sample-point existed for the refluxed sample. (See supporting information, Figure 2.S1) These results clearly indicate that without heating, only a mixture can be obtained, which probably contains $[\text{Pd}(\text{SC}_{12}\text{H}_{25})_2]_6$ and other Pd(II) complexes.

2.3.2 Structure and properties of $[\text{Pd}(\text{SC}_{12}\text{H}_{25})_2]_6$

Through single crystal X-ray analysis, the obtained product was revealed to be a new Pd(II) thiolate complex with a tiara structure. (Figure 2.1) The crystal was found to be in P-1 space group with $a = 13.2189(14) \text{ \AA}$, $b = 18.2919(18) \text{ \AA}$, $c = 19.1575(19) \text{ \AA}$; $\alpha = 66.529(5)^\circ$, $\beta = 70.892(8)^\circ$, $\gamma = 77.054(7)^\circ$. In each cluster, the six palladium atoms form a nearly planar hexagonal ring with the average Pd-Pd distance about 3.11 \AA . Each palladium atom is coordinated to four sulfur atoms with an approximately square planar geometry and the average Pd-S bond length is 2.32 \AA . The total twelve sulfur atoms form two S_6 hexagons parallel to the center Pd_6 ring from both sides. The average S-S distance in each S_6 ring is 3.50 \AA . Such a triple-layered tiara structure is about 3.04 \AA in height with a D_{6h} symmetry. (See supporting information Table 2.S1, Table 2.S2, Table 2.S3 for detailed structural data)

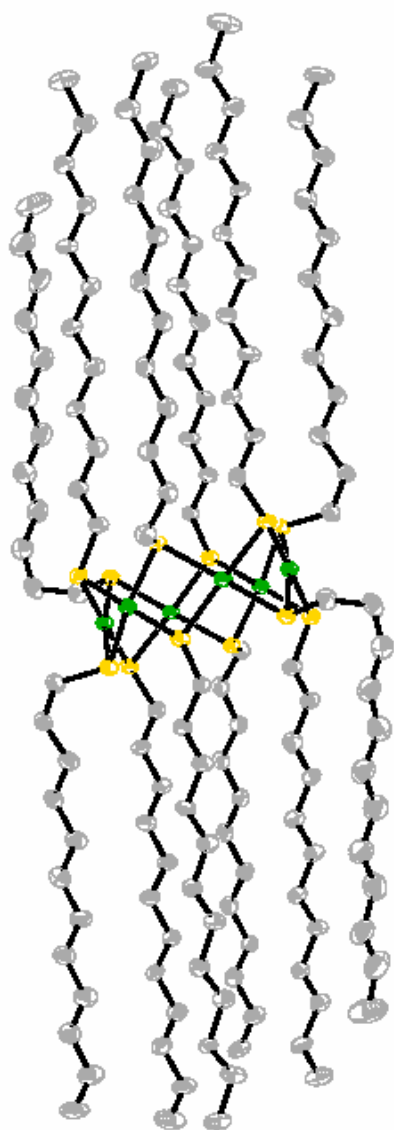


Figure 2.1. Perspective view of the complex $[\text{Pd}(\text{SC}_{12}\text{H}_{25})_2]_6$. Yellow balls represent S atoms, while green balls represent Pd atoms.

As shown in Figure 2.1, the S-C bonds are alternately directed either parallel or perpendicular to the S_6 rings. Such an arrangement is attributed to the steric repulsion and has been found in other $[Pd(SR)_2]_6$ or $[Ni(SR)_2]_6$ complexes with much shorter substituents.⁷⁻¹¹ The 1H NMR spectrum clearly shows this structural feature. (Figure 2.2)

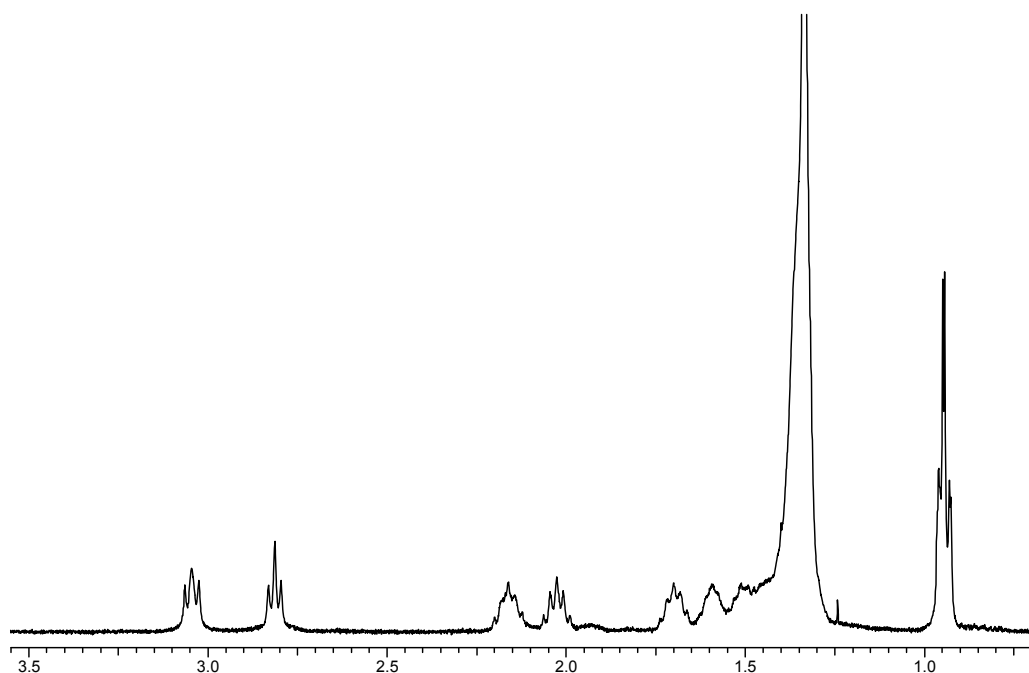


Figure 2.2. 1H NMR (room temperature in deuterio-benzene) spectrum of $[Pd(SC_{12}H_{25})_2]_6$. (3.04 ppm, 12H (t); 2.81 ppm, 12H (t); 2.16 ppm, 12H (q); 2.02 ppm, 12H (q); 1.70-1.34 ppm, 216H(m); 0.94 ppm, 36H (m).)

The two triplets at 3.04 ppm and 2.81 ppm represent the H atoms in SCH_2 groups. Because of the different orientation, the chemical shift differs by 0.23 ppm. Similar situations occur for H atoms in $(SCH_2)CH_2$ groups, and such differences

decrease when the CH₂ groups are further away from the tiara ring. Also, a high-temperature ¹H NMR (80°C) spectrum shows no significant changes in shift, which indicates the relatively stable steric arrangement. (See supporting information, Figure 2.S2)

As also indicated in Figure 2.1, all the long chains of the C backbone are packed roughly parallel to each other regardless of the orientation the S-C bonds. So the overall geometry of this cluster is C_i.

In the UV/Vis spectrum, three main peaks (412 nm, 320 nm, 272 nm) and one shoulder peak (248 nm) are observed. (Figure 2.3) They are tentatively assigned to ligand-to-metal charge-transfer transition (412 nm), metal-centered transition (320 nm) and ligand-centered transition (272 nm and 248 nm).³⁰

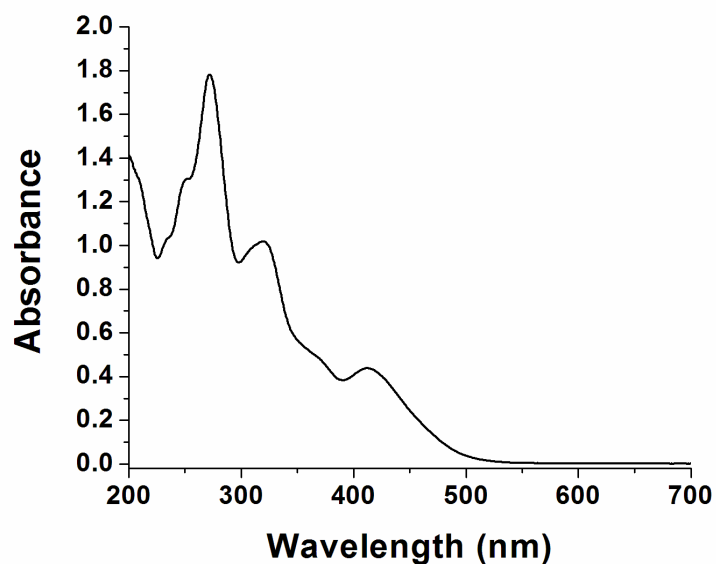


Figure 2.3. UV/Vis spectrum of [Pd(SC₁₂H₂₅)₂]₆. (0.2×10^{-4} M in n-heptane)

In the IR spectrum of the complex, main peaks are found at 2918 cm^{-1} , 2849 cm^{-1} , 1468 cm^{-1} , and 720 cm^{-1} , which indicate CH stretching (the first two peaks) modes and CH bending modes. (See supporting information Figure 2.S3) In the Raman spectrum, one slightly-split peak is found at 345 cm^{-1} , indicating the Pd-S vibration. (See supporting information Figure 2.S4) The powder XRD pattern of the complex reveals it has a more complicated crystalline structure than other layered-structured metal thiolates. (See supporting information Figure 2.S5) In the MALDI mass spectrum, the highest peak at 3076.0 is assumed to be the molecular ion peak of $[\text{Pd}(\text{SC}_{12}\text{H}_{25})_2]_6$ (3053.0) plus Na^+ ion resulted from the cationizing agent CF_3COONa . The second strongest peak at 2568.0 is assumed to be $\{[\text{Pd}(\text{SC}_{12}\text{H}_{25})_2]_5\text{Na}\}^+$ (2567.0), a big fragment induced by the ionization. (Figure 2.4)

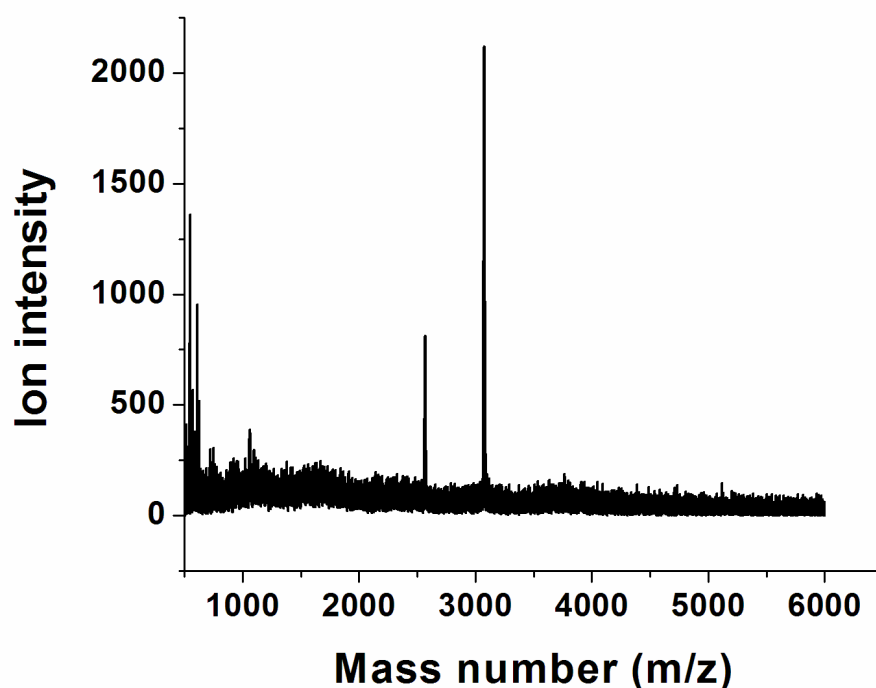


Figure 2.4. MALDI spectrum of $[\text{Pd}(\text{SC}_{12}\text{H}_{25})_2]_6$

2.3.3 Thermolysis of $[\text{Pd}(\text{SC}_{12}\text{H}_{25})_2]_6$ in diphenyl ether

The thermolysis of the obtained complex was carried out in diphenyl ether (boiling point 259 °C) under the protection of argon. At room temperature, the complex was partially dissolved in diphenyl ether under the experimental conditions. When heated, it was totally dissolved and became a clear orange-red solution. At the beginning of reflux, the color of the solution changed to black in 10 min because of the formation of nanoparticles. Then it became darker and darker with longer reaction time. Through tracking the change of the UV spectra, the reaction was found to be complete after 6 hours. (Figure 2.5)

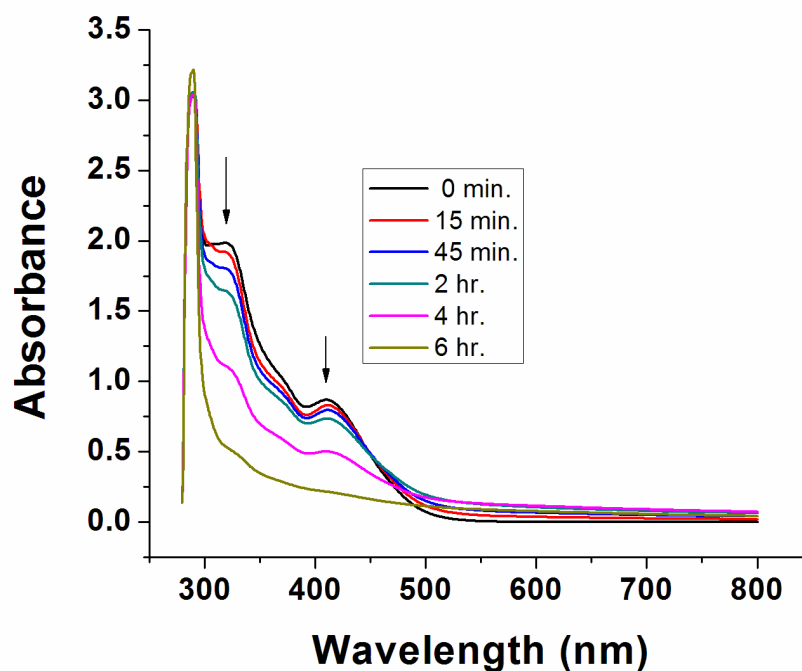


Figure 2.5. UV-Vis spectra of the colloidal solution at different reaction times.

The arrows indicate the decrease of the peaks.

As mentioned before, the complex $[\text{Pd}(\text{SC}_{12}\text{H}_{25})_2]_6$ has three absorbance peaks (272 nm, 320 nm, 412 nm) in the UV-Vis spectrum. Because of the interference of the solvent, the peak at 272 nm is not suitable for the tracking. The other two peaks decrease with reaction time as the complex is gradually transformed to nanoparticles. After 6 hours, almost no peaks can be found at these two places and only the scattering effect of the nanoparticles can be observed.

Through TEM analysis, the obtained nanoparticles were found to be spherical, with an average diameter of 2.87 nm and a standard deviation of 0.51 nm. (Figure 2.6 and Figure 2.7) It is also noticeable that the nanoparticles are well separated with an average distance about 2.0 nm, which resembles other monolayer-protected nanoparticles.³¹

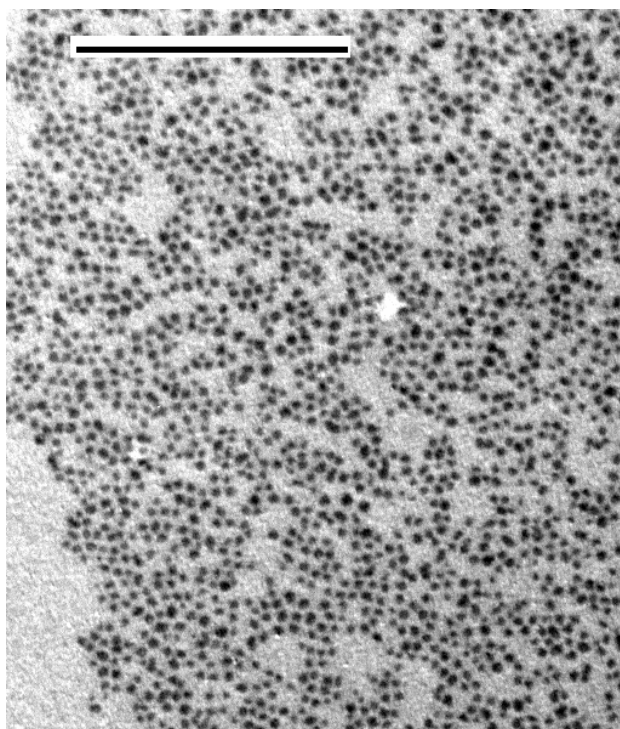


Figure 2.6. TEM of the obtained nanoparticles after refluxing $[\text{Pd}(\text{SC}_{12}\text{H}_{25})_2]_6$ for 6 hours in diphenyl ether. (scale bar = 100 nm)

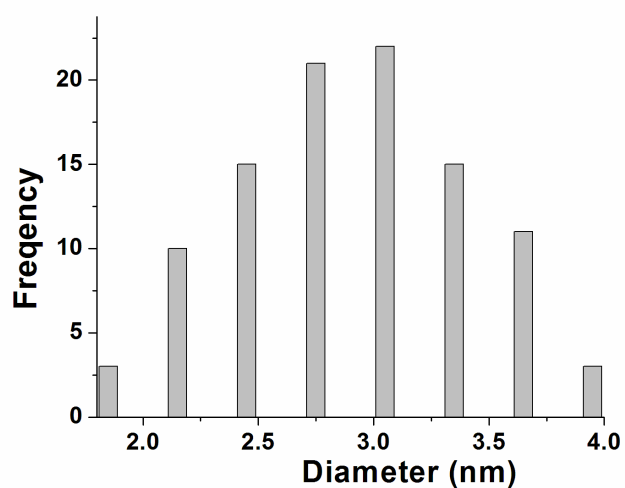


Figure 2.7. Histogram of the nanoparticles showing the size distribution. (diameter = 2.87 ± 0.51 nm, obtained by measuring 100 particles)

The colloidal solution obtained after refluxing was very stable. In a capped vial, it could be kept for months without any color change or sedimentation. It could be washed and separated by polar solvents like ethanol or acetone, and the obtained black precipitates were readily redissolved into nonpolar solvents, such as hexane, toluene, or 4-tert-bulyltoluene. Elemental analysis of the dry product shows it contains a rather high content of organic species (Pd: 42.6, S: 15.9, C: 29.01, H: 4.79 in wt%), and the molar ratio of Pd to S is about 0.8. Due to the high content of the organic species and the small size of the nanoparticles, the powder XRD analysis shows a rather broad peak with fine features, which indicate the presence of very small PdS crystals. (Figure 2.8)

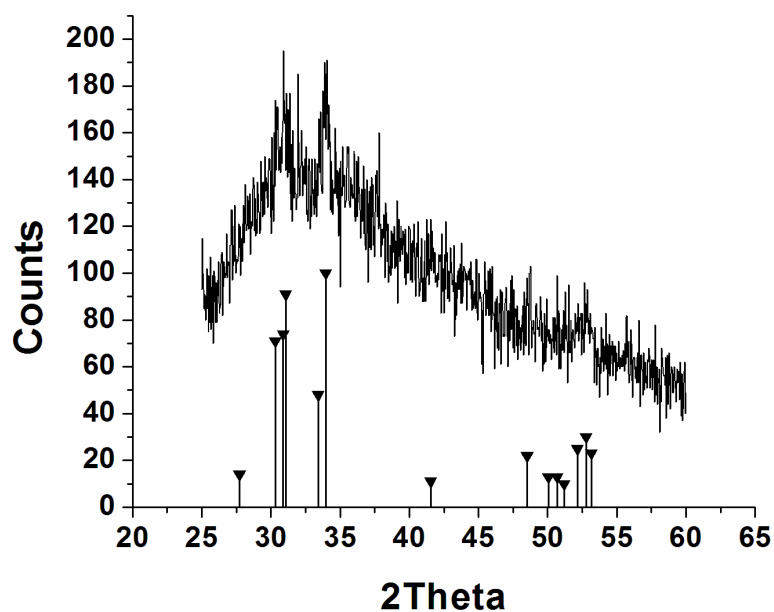


Figure 2.8. Powder XRD pattern of the PdS product obtained by refluxing $[\text{Pd}(\text{SC}_{12}\text{H}_{25})_2]_6$ for 6 hr. (The standard PdS pattern is from JCPDS file 25-1234)

When the system was refluxed for longer times than 6 hours, the nanoparticles gradually aggregated together and precipitated from the solution. A TEM image and a XRD pattern for the sample refluxed for 8 hr. indicate some aggregated particles and clearer PdS XRD pattern because of the growth of the crystals. (See supporting information Figure 2.S6 and Figure 2.S7) It has been found that the aggregation can be prevented by adding additional ligands. For example, when 98 μl of dodecanthiol was injected after 6 hours, the system could be refluxed for another 6 hours without any appreciable precipitates.

According to all the above-mentioned experimental results, we infer that the obtained product is PdS nanoparticles passivated by a layer of dodecanethiolate species ($-\text{SC}_{12}\text{H}_{25}$), which may be produced when thermolyzing the complex $[\text{Pd}(\text{SC}_{12}\text{H}_{25})_2]_6$. Also, the molar ratio of C to H is 2.0 according to the elemental analysis, which is close to 2.1 in $-\text{SC}_{12}\text{H}_{25}$ species.

2.4 Conclusions

A new tiara Pd(II) thiolate complex $[\text{Pd}(\text{SC}_{12}\text{H}_{25})_2]_6$ was first synthesized with high yield (91.2 %) through a simple one-pot reaction and its structure and properties were further studied by a variety of methods. These results help clarify the reaction system that involves Pd(II) ion and long chain alkanethiol ligands, which is an usual situation when preparing protected Pd nanoparticles. Also, it gives clues to synthesize other Pd(II) thiolates with long alkyl chain.

Furthermore, nearly monodisperse palladium sulfide nanoparticles (2.87 ± 0.51 nm) have been synthesized through the thermolysis of the obtained $[\text{Pd}(\text{SC}_{12}\text{H}_{25})_2]_6$ clusters. The particles were spontaneously passivated by in-situ-formed thiolate species. It will be interesting to study the thermolysis of other Pd(II) alkanethiolates and test the possible influence of chain length of the ligands on the size of the protected nanoparticles.

We believe this sample strategy, i.e., the thermolysis of metal thiolates, can be easily expanded to other metal ions and now we are investigating the similar methods to prepare metal or metal sulfide nanoparticles of high quality.

2.5 References

- (1) Bensebaa, F.; Ellis, T. H.; Hruus, E.; Voicu, R.; Zhou, Y. *Langmuir* **1998**, *14*, 6579-6587.
- (2) Baena, M. J.; Espinet, P.; Lequerica, M. C.; Levelut, A. M. *J. Am. Chem. Soc.* **1992**, *114*, 4182-4185.
- (3) Dance, I. G.; Fisher, K. J.; Herath Banda, R. M.; Scudder, M. L. *Inorg. Chem.* **1991**, *30*, 183-187.
- (4) Sandhyarani, N.; Predeep, T. *J. Mater. Chem.* **2001**, *11*, 1294-1299.
- (5) Shaw, R. A.; Woods, M. *J. Chem. Soc. A.* **1971**, *10*, 1569-1571.
- (6) Tiers, G. V. D.; Brostrom, M. L. *J. Appl. Cryst.* **2000**, *33*, 915-920.

- (7) Woodward, P.; Dahl, L. F.; Abel, E. W.; Crosse, B. C. *J. Am. Chem. Soc.* **1965**, *87*, 5251-5253.
- (8) Ivanov, S. A.; Kozee, M. A.; Merrill, W. A.; Agarwal, S.; Dahl, L. F. *J. Chem. Soc., Dalton Trans.* **2002**, 4105-4115.
- (9) Gould, R. O.; Harding, M. M. *J. Chem. Soc. A* **1970**, 875-881.
- (10) Kunchur, N. R. *Acta cryst.* **1968**, *B24*, 1623-1633.
- (11) Higgins, J. D. III; Suggs, J. W. *Inorg. Chim. Acta* **1988**, *145*, 247-252.
- (12) Nobusada, K.; Yamaki, T. *J. Phys. Chem A* **2004**, *108*, 1813-1817.
- (13) Alemany, P.; Hoffmann, R. *J. Am. Chem. Soc.* **1993**, *115*, 8290-8297.
- (14) Datta, A.; John, N. S.; Kulkarni, G. U.; Pati, S. K. *J. Phys. Chem A* **2005**, *109*, 11647-11649.
- (15) Carotenuto, G.; Martorana, B.; Perlo, P.; Nicolais, L. *J. Mater. Chem.* **2003**, *13*, 2927-2930.
- (16) Nakamoto, M.; Yamamoto, M.; Fukusumi, M. *J. Chem. Soc., Chem. Commun.* **2002**, 1622-1623.
- (17) Nakamoto, M.; Kashiwagi, Y.; Yamamoto, M. *Inorg. Chim. Acta*, **2005**, *358*, 4229-4236.
- (18) Ghezelbash, A.; Sigman, M. B. Jr.; Korgel, B. A. *Nano Lett.* **2004**, *4*, 537-542.
- (19) Larsen, T. H.; Sigman, M. B.; Ghezelbash, A.; Doty, R. C.; Korgel, B. A. *J. Am. Chem. Soc.* **2003**, *125*, 5638-5639.
- (20) Chen, L.; Chen, Y. B.; Wu, L. M. *J. Am. Chem. Soc.* **2004**, *126*, 16334-16335.
- (21) Chen, Y. B.; Chen, L.; Wu, L. M. *Inorg. Chem.* **2005**, *44*, 9817-9822.

- (22) Carmalt, C. J.; O'Neill, S. A.; Parkin, I. P.; Peters, E. S. *J. Mater. Chem.* **2004**, *14*, 830-834.
- (23) Carmalt, C. J.; Manning, T. D.; Parkin, I. P.; Peters, E. S.; Hector, A. L. *J. Mater. Chem.* **2004**, *14*, 290-291.
- (24) Choi, S. H.; Kim, E. G.; Hyeon, T. *J. Am. Chem. Soc.* **2006**, *128*, 2520-2521.
- (25) Dey, S.; Jain, V. K. *Platinum Metals Review* **2004**, *48*, 16-29.
- (26) Cheon, J.; Talaga, D. S.; Zink, J. I. *Chem. Mater.* **1997**, *9*, 1208-1212.
- (27) Yamamoto, T.; Taniguchi, A.; Dev, S.; Osakada, K.; Kubota, K. *Colloid Polym. Sci.* **1991**, *269*, 969-971.
- (28) Malik, M. A.; O'Brien, P.; Revaprasadu, N. *J. Mater. Chem.* **2002**, *12*, 92-97.
- (29) Brese, N. E.; Squattrito, P. S.; Ibers, J. A. *Acta Cryst.* **1985**, *C41*, 1829-1830.
- (30) Tzeng, B. C.; Yeh, H. T.; Huang, Y. C.; Chao, H. Y.; Lee, G. H.; Peng, S. M. *Inorg. Chem.* **2003**, *42*, 6008-6014.
- (31) Ponce, A. A.; Smetana, A.; Stoeva, S.; Klabunde, K. J.; Sorensen, C. M. *Nanostructured and Advanced Materials.* **2005**, 309-316.

2.6 Supporting information

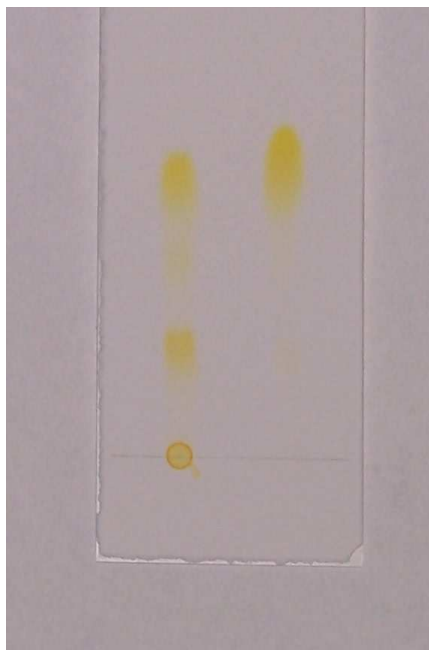


Figure 2.S1. Thin-Layer-Chromatography (TLC) analysis (developed in heptane) Left: the sample obtained at room temperature, Right: the refluxed sample. It was noticeable that, 1) for the sample obtained at room temperature, some product (the lowest yellow point) was left on the starting line, which did not occur for the heated sample. It implies that in the room temperature sample, there are some species so strongly adsorbed on the TLC substrate that can not be developed. 2) the highest point of the room temperature sample was roughly at the same level as the point of the refluxed sample, indicating that the Pd₆ tiara product was formed in both cases.

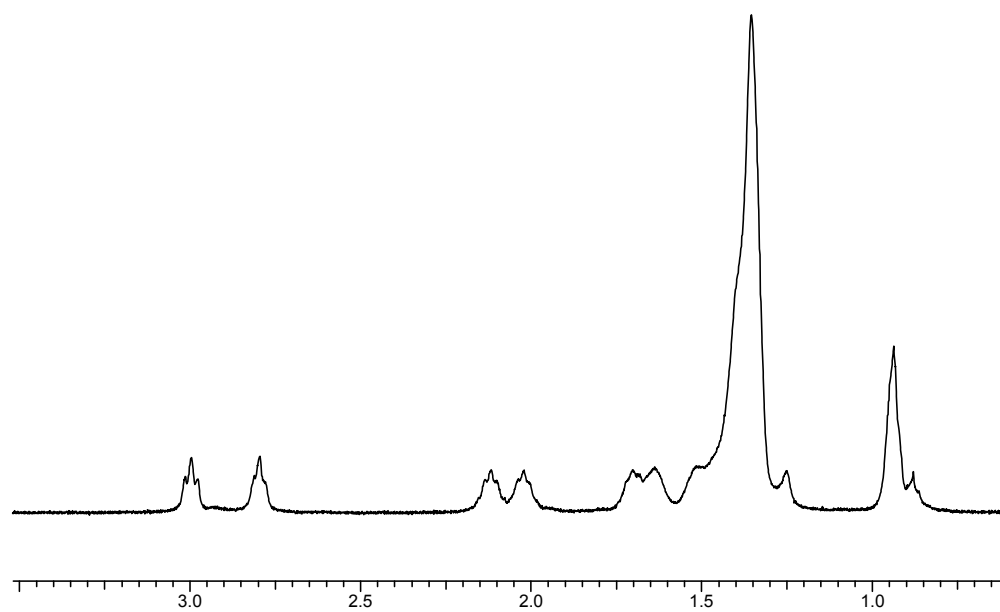


Figure 2.S2. ^1H NMR (80 °C in deuterio-benzene, sealed MNR tube) spectrum of $[\text{Pd}(\text{SC}_{12}\text{H}_{25})_2]_6$. (3.00 ppm, 12H (t); 2.80 ppm, 12H (t); 2.12 ppm, 12H (q); 2.02 ppm, 12H (q); 1.70-1.36 ppm, 216H(m); 0.94 ppm, 36H (m).)

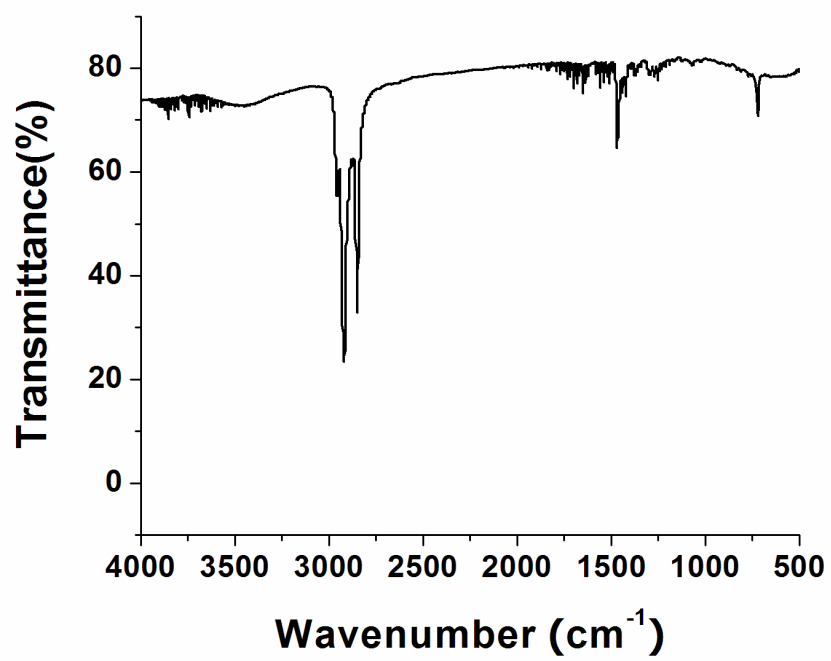


Figure 2.S3. IR spectrum of $[\text{Pd}(\text{SC}_{12}\text{H}_{25})_2]_6$. (in KBr pellet)

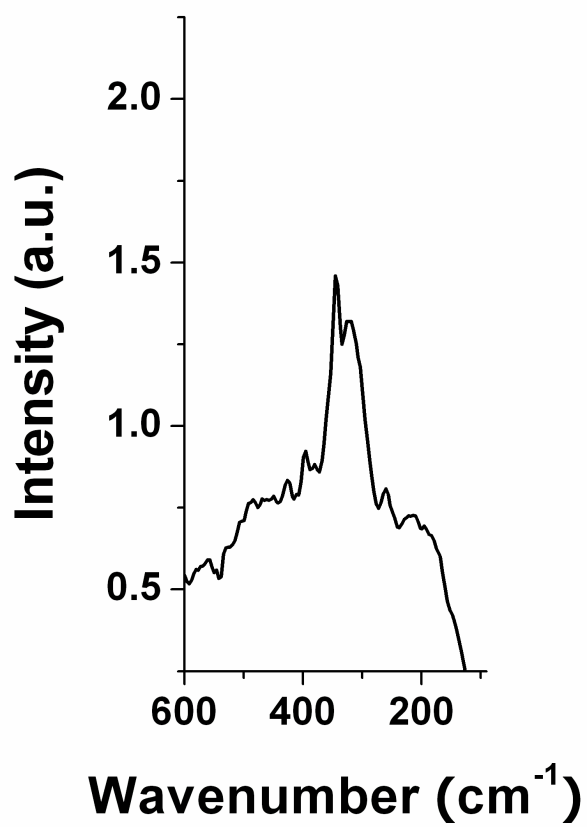


Figure 2.S4. Raman spectrum of $[\text{Pd}(\text{SC}_{12}\text{H}_{25})_2]_6$.

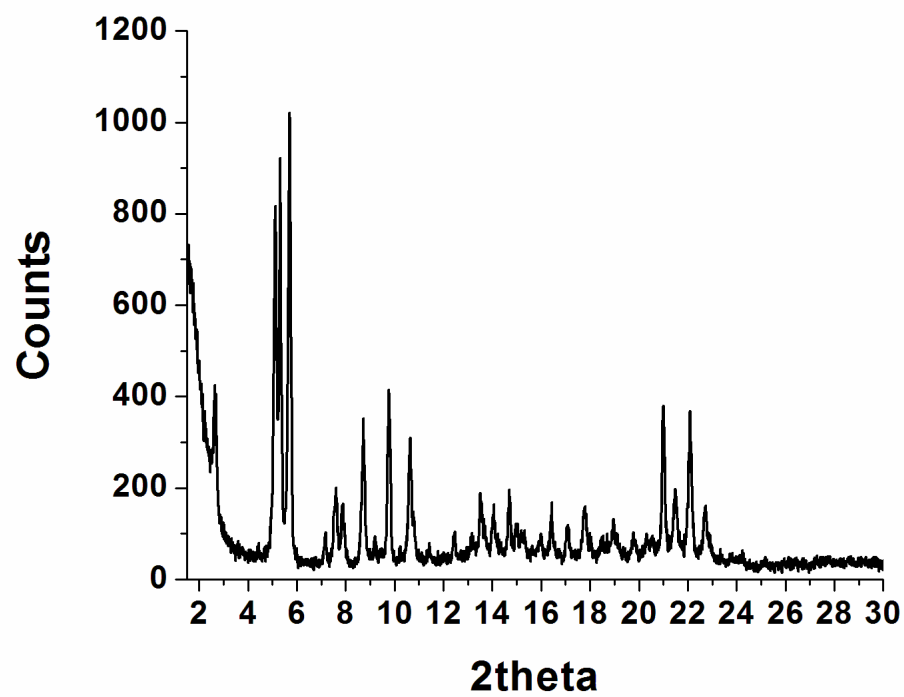


Figure 2.S5. Powder XRD pattern of $[\text{Pd}(\text{SC}_{12}\text{H}_{25})_2]_6$.

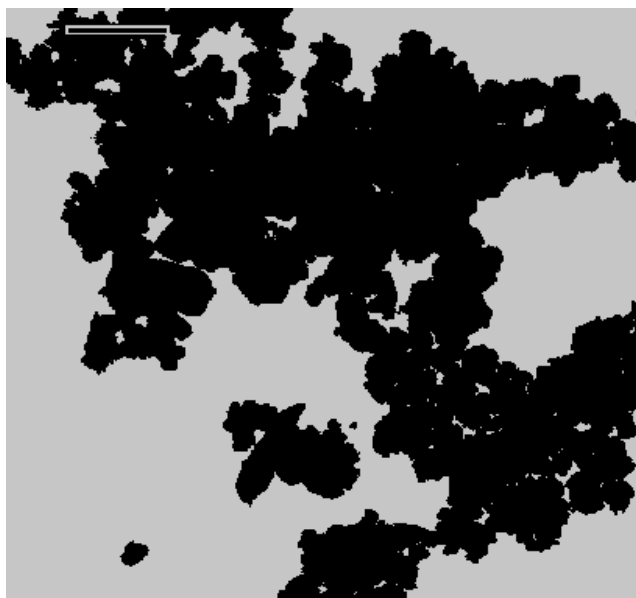


Figure 2.S6. Some aggregated particles obtained after refluxing [Pd(SC₁₂H₂₅)₂]₆ for 8 hr. (scale bar = 2 μm)

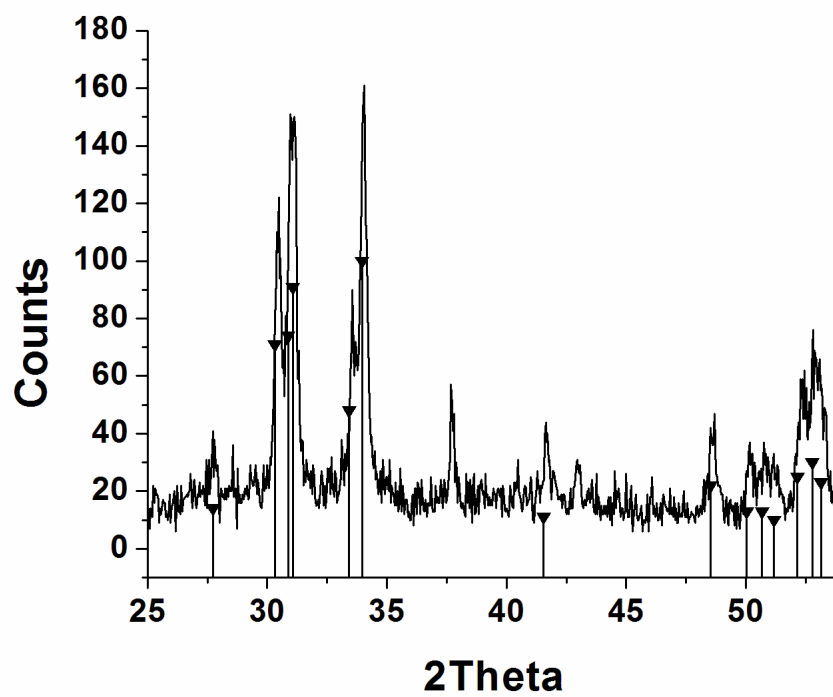


Figure 2.S7. Powder XRD pattern of the products obtained by refluxing $[\text{Pd}(\text{SC}_{12}\text{H}_{25})_2]_6$ for 8 hr. (The standard PdS pattern is from JCPDS file 25-1234)

Table 2.S1. Crystal data and structure refinement of [Pd(SC₁₂H₂₅)₂]₆.

Empirical formula	C ₂₄ H ₅₀ Pd S ₂	
Formula weight	509.16	
Temperature	173(2) K	
Wavelength	0.71073 Å	
Crystal system	Triclinic	
Space group	P-1	
Unit cell dimensions	a = 13.2189(14) Å	α = 66.529(5)°.
	b = 18.2919(18) Å	β = 70.892(8)°.
	c = 19.1575(19) Å	γ = 77.054(7)°.
Volume	3991.4(7) Å ³	
Z	6	
Density (calculated)	1.271 g/cm ³	
Absorption coefficient	0.862 mm ⁻¹	
F(000)	1632	
Crystal size	0.40 x 0.20 x 0.10 mm ³	
Theta range for data collection	1.64 to 27.51°.	
Index ranges	-16 ≤ h ≤ 17, -23 ≤ k ≤ 21, -24 ≤ l ≤ 24	
Reflections collected	28432	
Independent reflections	17309 [R(int) = 0.1073]	
Completeness to theta = 27.51°	94.4 %	
Absorption correction	None	
Refinement method	Full-matrix least-squares on F ²	
Data / restraints / parameters	17309 / 0 / 736	
Goodness-of-fit on F ²	0.859	

Final R indices [$I > 2\sigma(I)$]	R1 = 0.0618, wR2 = 0.1342
R indices (all data)	R1 = 0.1456, wR2 = 0.1616
Largest diff. peak and hole	1.336 and -1.150 e.Å ⁻³

Table 2.S2. Main bond lengths [Å] of [Pd(SC₁₂H₂₅)₂]₆.

Pd(1)-S(1)	2.3119(19)	Pd(3)-S(6)	2.3117(17)
Pd(1)-S(6)#1	2.3141(19)	Pd(3)-S(4)	2.3151(19)
Pd(1)-S(2)	2.3195(19)	Pd(3)-S(5)	2.3257(19)
Pd(1)-S(5)#1	2.3220(19)	Pd(3)-S(3)	2.3279(17)
Pd(1)-Pd(2)	3.0430(8)	Pd(3)-Pd(1)#1	3.1355(8)
Pd(1)-Pd(3)#1	3.1356(8)	S(1)-C(01)	1.816(7)
Pd(2)-S(3)	2.3113(19)	S(2)-C(13)	1.816(6)
Pd(2)-S(2)	2.3127(19)	S(3)-C(25)	1.815(7)
Pd(2)-S(1)	2.3170(17)	S(4)-C(37)	1.828(7)
Pd(2)-S(4)	2.3211(17)	S(5)-C(49)	1.818(7)
Pd(2)-Pd(3)	3.1643(8)	S(6)-C(61)	1.810(7)

Table 2.S3. Main bond angles [°] for [Pd(SC₁₂H₂₅)₂]₆.

S(1)-Pd(1)-S(6)#1	98.67(7)	S(4)-Pd(3)-S(5)	177.10(7)
S(1)-Pd(1)-S(2)	81.00(7)	S(6)-Pd(3)-S(3)	168.32(7)
S(6)#1-Pd(1)-S(2)	170.16(6)	S(4)-Pd(3)-S(3)	82.90(6)
S(1)-Pd(1)-S(5)#1	178.33(7)	S(5)-Pd(3)-S(3)	97.11(7)
S(6)#1-Pd(1)-S(5)#1	82.95(7)	S(6)-Pd(3)-Pd(1)#1	47.36(5)
S(2)-Pd(1)-S(5)#1	97.33(7)	S(4)-Pd(3)-Pd(1)#1	130.31(5)
S(1)-Pd(1)-Pd(2)	48.97(4)	S(5)-Pd(3)-Pd(1)#1	47.52(5)
S(6)#1-Pd(1)-Pd(2)	124.11(5)	S(3)-Pd(3)-Pd(1)#1	125.32(5)
S(2)-Pd(1)-Pd(2)	48.84(5)	S(6)-Pd(3)-Pd(2)	125.62(5)
S(5)#1-Pd(1)-Pd(2)	129.71(5)	S(4)-Pd(3)-Pd(2)	47.04(4)

S(1)-Pd(1)-Pd(3)#1	133.46(5)	S(5)-Pd(3)-Pd(2)	131.30(5)
S(6)#1-Pd(1)-Pd(3)#1	47.29(4)	S(3)-Pd(3)-Pd(2)	46.77(5)
S(2)-Pd(1)-Pd(3)#1	126.78(5)	Pd(1)#1-Pd(3)-Pd(2)	120.57(2)
S(5)#1-Pd(1)-Pd(3)#1	47.62(5)	C(01)-S(1)-Pd(1)	113.4(2)
Pd(2)-Pd(1)-Pd(3)#1	117.73(2)	C(01)-S(1)-Pd(2)	113.0(2)
S(3)-Pd(2)-S(2)	172.73(7)	Pd(1)-S(1)-Pd(2)	82.20(6)
S(3)-Pd(2)-S(1)	98.69(6)	C(13)-S(2)-Pd(2)	106.6(3)
S(2)-Pd(2)-S(1)	81.04(6)	C(13)-S(2)-Pd(1)	108.7(3)
S(3)-Pd(2)-S(4)	83.13(6)	Pd(2)-S(2)-Pd(1)	82.13(6)
S(2)-Pd(2)-S(4)	97.33(7)	C(25)-S(3)-Pd(2)	103.9(3)
S(1)-Pd(2)-S(4)	177.73(7)	C(25)-S(3)-Pd(3)	111.0(2)
S(3)-Pd(2)-Pd(1)	125.79(5)	Pd(2)-S(3)-Pd(3)	86.01(6)
S(2)-Pd(2)-Pd(1)	49.03(5)	C(37)-S(4)-Pd(3)	108.5(2)
S(1)-Pd(2)-Pd(1)	48.83(5)	C(37)-S(4)-Pd(2)	107.7(2)
S(4)-Pd(2)-Pd(1)	130.98(5)	Pd(3)-S(4)-Pd(2)	86.08(7)
S(3)-Pd(2)-Pd(3)	47.21(4)	C(49)-S(5)-Pd(1)#1	107.4(2)
S(2)-Pd(2)-Pd(3)	128.84(5)	C(49)-S(5)-Pd(3)	107.6(2)
S(1)-Pd(2)-Pd(3)	135.39(5)	Pd(1)#1-S(5)-Pd(3)	84.85(6)
S(4)-Pd(2)-Pd(3)	46.88(5)	C(61)-S(6)-Pd(3)	109.9(2)
Pd(1)-Pd(2)-Pd(3)	121.69(2)	C(61)-S(6)-Pd(1)#1	106.9(3)
S(6)-Pd(3)-S(4)	96.47(7)	Pd(3)-S(6)-Pd(1)#1	85.35(6)
S(6)-Pd(3)-S(5)	82.93(6)		

Symmetry transformations used to generate equivalent atoms: #1 -x+1,-y+1,-z+1

CHAPTER 3 - From monodisperse sulfurized palladium nanoparticles to tiara Pd(II) thiolate clusters: the influence of thiol ligand on the thermal treatment of a Pd(II)-amine system*

* It has been published in *Journal of Physical Chemistry C* **2007**, 111, 18143-18147.

3.1 Introduction

Organic ligands with long C-chains such as alkyl carboxyl acids, alkylthiols, alkylamines and phosphines are widely applied as protecting agents to synthesize monolayer-protected clusters (MPC) of metal, metal oxide, metal chalcogenide, etc. According to the literature, the functions of these ligands may be more complicated than the obvious chemical adsorption on the particle surface. The digestive ripening method established in our lab indicates that pre-prepared polydisperse metal particles can react with certain organic ligands and then transform to highly monodisperse nanoparticles.²⁻⁴ For systems where the ligands are added before the formation of nanoparticles, it is possible that metal ion-ligand complexes (coordination compounds) form initially, followed by chemical reactions that lead to nanoparticles. In some cases, the ligands may undergo decomposition and release certain components to form the nanoparticles. For example, metal sulfides such as NiS, Cu₂S with controllable shapes (nanorod,

nanosphere, or nanoprism) have been synthesized through the thermolysis of the corresponding metal thiolates;^{5, 6} a variety of metal oxide nanoparticles have been produced by the decomposition of metal oleate complexes;^{7, 8} nanorods of metal phosphide including MnP, Co₂P, FeP, Ni₂P have been prepared via the thermal decomposition of metal-phosphine complexes.⁹ In these cases, the ligands serve as both the protecting agents and the source materials for S, O, P, respectively. Furthermore, to achieve the best control over particle size, shape, and size distribution, mixed ligands are generally employed, which makes the situation more complicated. In most cases, the functions of each ligand in a ligand-mixed system are not completely specified.

As highly active catalysts with enlarged surface area, Pd nanoparticles have been attracting attention and some preparation methods have been established. Reducing agents such as lithium triethylborohydride (Superhydride),¹⁰ lithium borohydride,¹¹ sodium borohydride,¹² hydrazine,¹³ sodium hypophosphite¹⁴ are generally applied to convert Pd(II) ions to Pd metal. The reduction can also be achieved by refluxing Pd(II) in ethanol/water solution.¹⁵⁻¹⁷ To control the particle size and size distribution, a variety of protecting agents have been applied, including hydrophilic ones such as sodium dodecyl sulphate,¹⁴ polyvinylpyrrolidone (PVP);^{15, 16} or hydrophobic ones such as alkanethiols,^{10, 12, 17} phosphines.^{18, 19}

As mild reducing agents, alkylamines have been used to prepare gold and silver nanoparticles.²⁰ To the best of our knowledge, the amine-induced reduction of Pd(II) has not been reported. In this paper, the reduction of Pd(II) by octylamine and the

influence of dodecanethiol on this process were investigated. The results provide a facile method to synthesize highly monodisperse sulfurized Pd nanoparticles, which are good catalysts for some reactions.^{21, 22} More importantly, it is a good example about how different ligands may play special roles in a ligand-mixed system and either pure coordination compounds or monodisperse nanoparticles can be prepared based on this very simple approach.

3.2 Experimental Section

3.2.1 Materials

Sodium tetrachloropalladate(II) (99%), octylamine (99%) and 1-dodecanethiol (98%) were obtained from Aldrich Chem. Co. 4-*tert*-butyltoluene (96%) was bought from ACROS Organics. Other chemicals were purchased and used as received.

3.2.2 Thermolysis without dodecanethiol

In a glass tube, 0.029 g of Na₂PdCl₄ (1.0×10^{-4} mol), 10 ml of 4-*tert*-butyltoluene, and 0.33 ml of octylamine (2.0×10^{-3} mol) were added sequentially. The mixture was sonicated for 30 min to form a colorless solution. Then, the tube was connected to a vacuum line and an argon gas-tank through a rubber septum equipped with needles. The mixture was degassed and then flushed with argon several times. After that, it was heated (about 192 °C) in a preheated sand-bath for 1 h under the protection of argon. During that time, black precipitates were produced. After 1 h, the tube was removed from the sand-bath and left to cool. Finally, the black precipitates

were collected by centrifugation and washed with 95% ethanol (30 ml × 4) and then pure ethanol (30 ml × 4).

3.2.3 Thermolysis with different amounts of dodecanethiol

In a glass tube, 0.029 g of Na₂PdCl₄ (1.0×10^{-4} mol), 10 ml of 4-*tert*-butyltoluene, 0.33 ml of octylamine (2.0×10^{-3} mol), and certain amounts of dodecanethiol were added sequentially. The molar ratios of thiol to Pd(II) were altered systematically from 0.125, 0.25, 0.5, 1, 1.5, to 2. After sonication for 30 min, the Pd(II) salt was dissolved and the solution's color changed to yellow or orange-red, depending on the concentration of thiol. Then the thermal reaction and the product collection were carried out in the same way as described above. For convenience, the obtained products are labeled as Sample (n X) in this paper. (n = the molar ratio of thiol to Pd(II) ion).

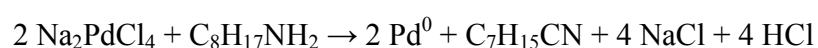
3.2.4 Equipment and analysis

Transmission electron microscopy (TEM) was performed on a Philips CM100 microscope operated at 100 kV. To prepare a TEM sample, products were dispersed with toluene and then a drop of solution was dropped onto a carbon-coated Formvar copper grid, which was allowed to dry in air. UV/vis absorption analysis was carried out on a Cary 500 UV-VIS-NIR spectrophotometer. IR spectra were obtained using a NEXUS 670 FT-IR system produced by Nicolet Instrument Corporation. Powder X-ray diffraction (XRD) patterns were recorded by a Bruker D8 X-ray diffractometer with Cu K α radiation. ¹H NMR spectra were obtained on a Varian Unity 400 Plus 400-MHz NMR system.

3.3 Results

3.3.1 Heating of Pd(II)-octylamine mixtures without thiol

First, brown-colored Na_2PdCl_4 powder and excess amounts of octylamine were added into 4-*tert*-butyltoluene, which served as a high boiling point solvent. After sonication, the brown color of the Pd(II) salt faded and a colorless solution formed. A likely explanation for this phenomenon is the formation of certain Pd(II)-amine complexes, which are colorless and soluble in the solvent. When heated at the boiling temperature of the solvent (192 °C), the system turned to black in minutes. After one hour, black-colored precipitates were obtained as Sample (0 X). The powder XRD pattern of this sample indicates that pure fcc palladium crystals had been generated. (Figure 3.1) The formation of Pd(0) is attributed to the reduction of Pd(II) by amine at high temperature, in which the amine ligands are oxidized to nitriles.²³ The reaction is assumed to happen according to the following equation:



In support of this idea, a peak at 2239 cm^{-1} (the normal position for the CN stretching vibration) was found in the IR spectrum of the solution after heating.

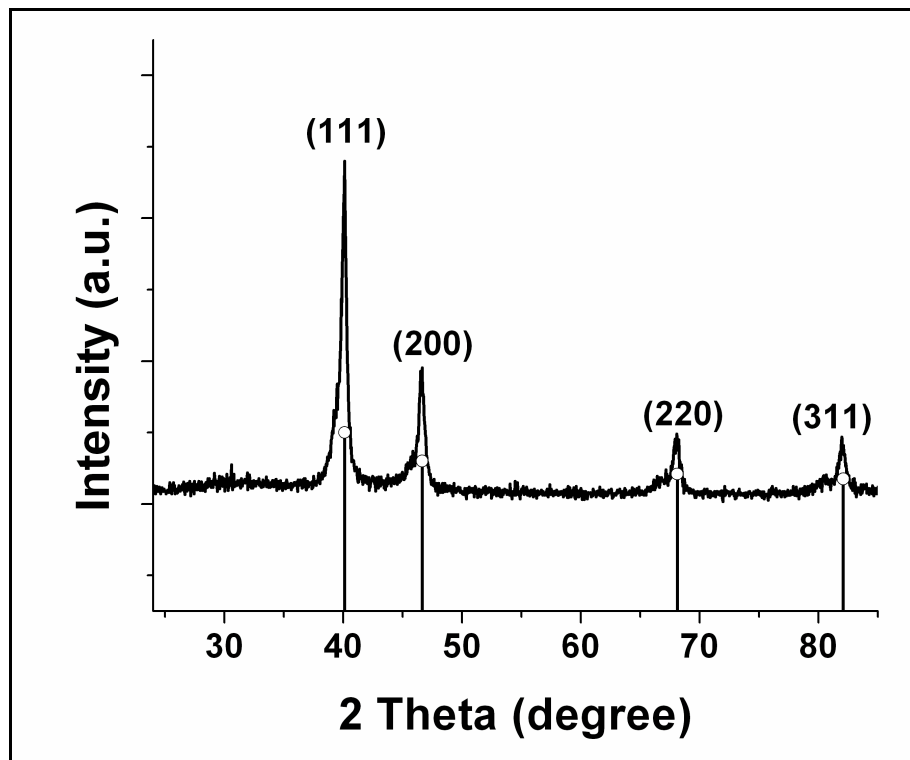


Figure 3.1. Powder XRD pattern of Sample (0 X) indicating the formation of Pd(0) crystals. The standard pattern is based on JCPDS file 46-1043.

A typical TEM image shows that the resulting crystallites aggregate into big roughly spherical particles about 300-700 nm. (Figure 3.2) This result is consistent with the observation of the reaction mixture after heating, i.e., the generated Pd(0) particles are not stable in the solution and ready to settle down as black precipitates.

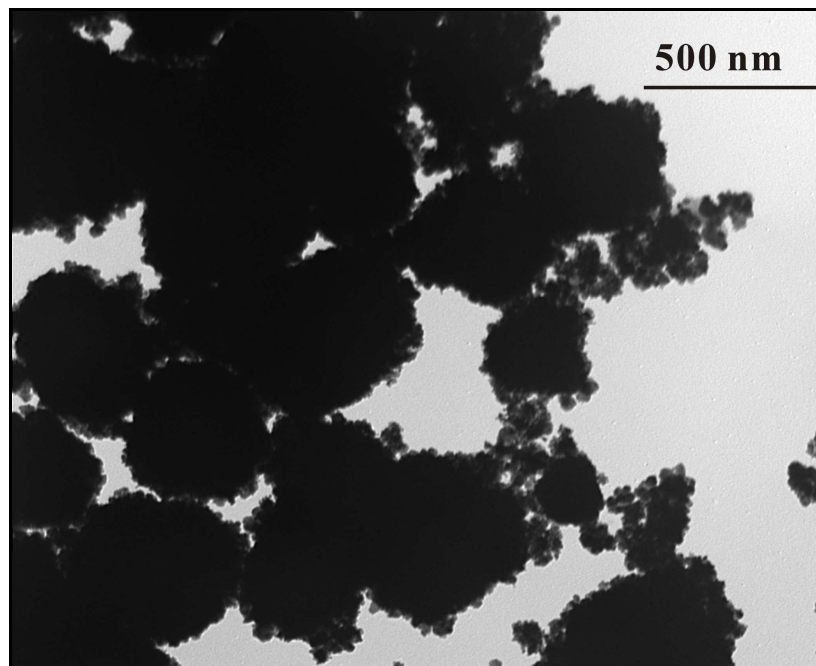


Figure 3.2. TEM image of Sample (0 X) shows aggregated particles.

3.3.2 Heating of Pd(II)-octylamine-dodecanethiol systems

In order to investigate the influence of thiol ligands, different amounts of dodecanethiol were added (molar ratio of thiol to Pd(II): 0.125, 0.25, 0.5, 1, 1.5, 2) before heating, while the molar ratio of octylamine to Pd(II) was fixed as 20. After sonication to dissolve the Pd(II) salt precursor, a series of solutions with the color changing from yellow to orange-red were obtained. (Figure 3.3, upper row) Compared with the colorless solution of Pd(II)-amine complex, it was obvious that certain colored Pd(II)-thiol complexes were generated.

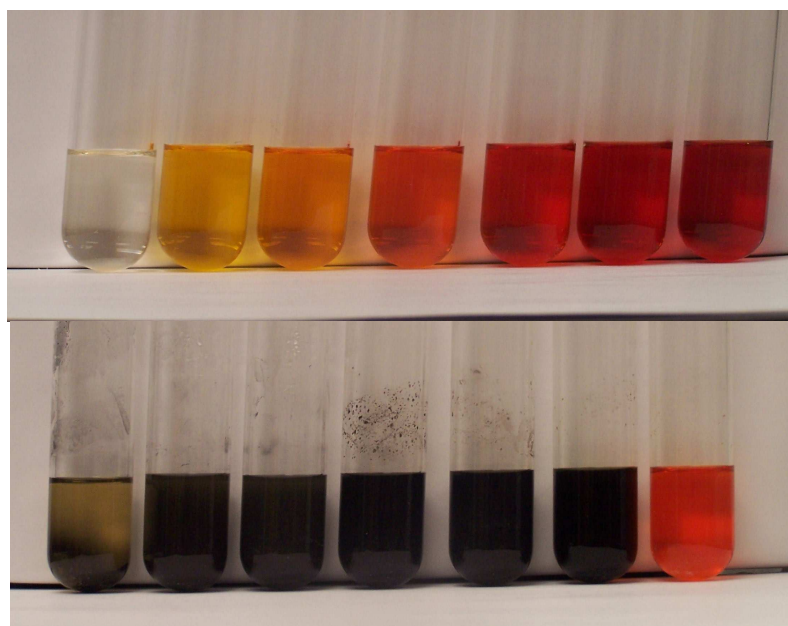


Figure 3.3. Solutions with different amounts of dodecanethiol before (upper) and after (lower) heating. The molar ratios of thiol to Pd(II) are 0, 0.125, 0.25, 0.5, 1, 1.5, 2 from left to right.

After heating for 1 h, the solutions turned black for the systems with the molar ratio of thiol to Pd(II) ≤ 1.5 , while the sample with molar ratio equal to 2 remained as an orange-red solution. (Figure 3.3, lower row) As seen in Figure 3.3, Sample (0.125 X) and Sample (0.25 X) were more stable than Sample (0 X), but they still precipitated out of the solutions after days. TEM microphotos indicate the formation of smaller aggregated particles compared to Sample (0 X). (see Supporting Information , Figure 3.S1)

When the molar ratio of thiol to Pd(II) was increased to 0.5, a stable black colloidal solution was obtained after heating, which could be stored in a capped vial for months without observable precipitates. TEM observation (Figure 3.4) demonstrates highly monodisperse nanoparticles, which self-assemble into hexagonal close-packing pattern on the TEM grid like other monolayer-protected clusters. The average diameter of the particles is 7.55 ± 0.73 nm, with the standard deviation of 9.7 %. (see Supporting Information , Figure 3.S2 for the histogram pattern)

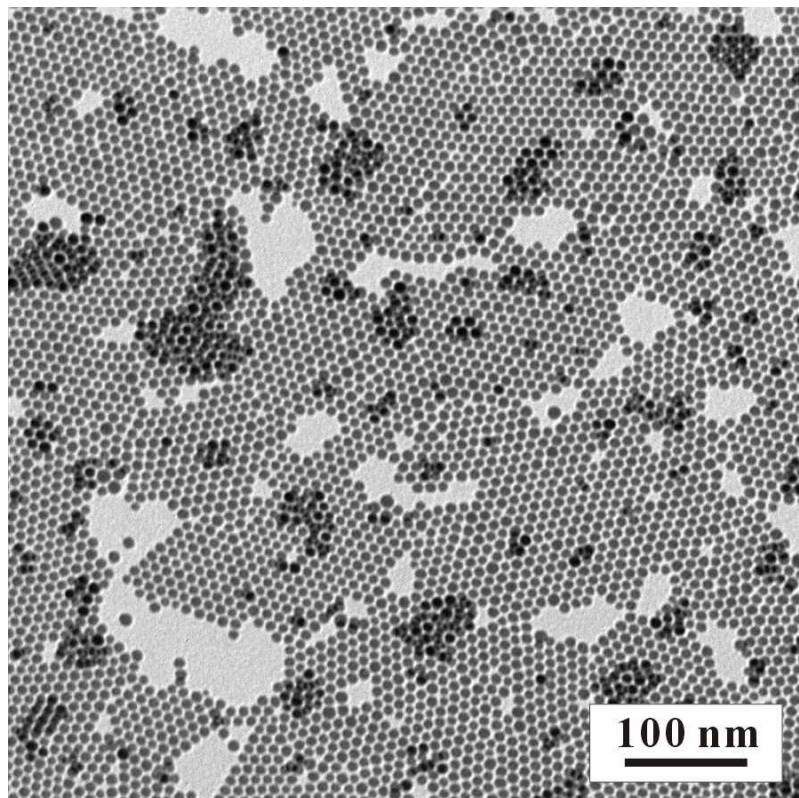


Figure 3.4. TEM image of Sample (0.5 X).

The powder XRD pattern (Figure 3.5) shows that the obtained nanoparticles are sulfurized palladium instead of pure Pd(0). Peaks standing for Pd₁₆S₇ and Pd₄S are found and the former is dominating according to the peak intensity. An elemental analysis (C: 18.28, H: 3.29, S: 11.65, Pd: 52.73, N:<0.5 in %wt) points out the high S contents in the sample. If assuming the nanoparticles are covered with SC₁₂H₂₅ species, a calculation based on the elemental analysis result indicates the molar ratio of Pd to S in the particle cores is about 2.1. This value is close to that in Pd₁₆S₇ (2.3) and consistent with the XRD results. Further calculation based on the particle size and density (estimated to be 7 g/cm³) reveals that the composition of each nanoparticle is close to (Pd₁₆S₇)₁₄(SC₁₂H₂₅)₅₇. Since there are no other S sources in the reaction system, the S in the particle cores is attributed to the decomposition of the thiol ligand. More details will be discussed later.

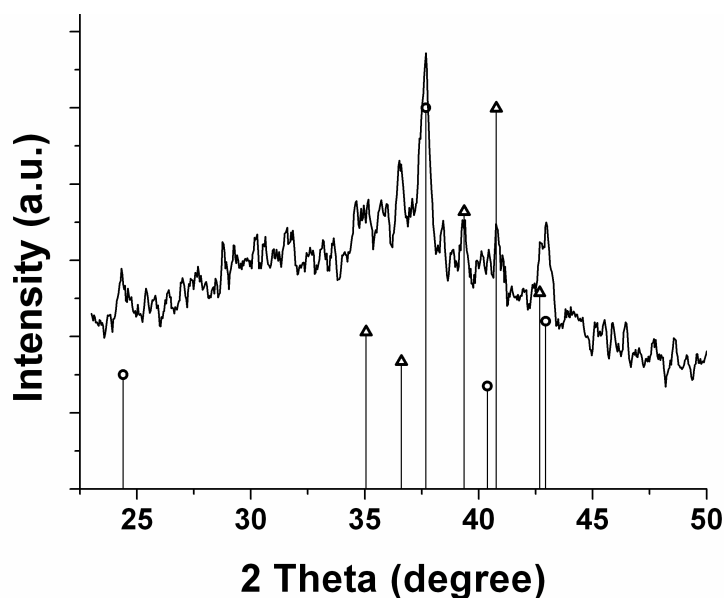


Figure 3.5. Powder XRD of Sample (0.5 X). The standard patterns are from JCPDS file 30-884 (Pd₁₆S₇, marked with ○) and 73-1387 (Pd₄S, marked with Δ).

The solution color of Sample (1 X) and Sample (1.5 X) was not as dark as in Sample (0.5 X). The optical density decreased with the increase of thiol ligand. Also, even though the basic color was black, an increase in yellow-orange tint from Sample (0.5 X) to Sample (1.5 X) was noticeable. At the end, the solution of Sample (2 X) was not dark at all and only exhibited an orange-red color. This trend can be seen more clearly when the samples were precipitated out of the solution with 95 % ethanol. Compared with the black-colored precipitates in Sample (0.5 X), precipitates with brown color, yellowish-brown-color, and bright orange color were obtained for Sample (1 X), Sample (1.5 X) and Sample (2 X), respectively. (see Supporting Information , Figure 3.S3) All of these observations strongly suggest that, with the increase of dodecanethiol, the formation of nanoparticles will be hindered and some orange-colored species will become dominant in the final products.

The results from TEM confirm the viewpoint mentioned above. (Figure 3.6) The typical TEM image of Sample (1 X) shows both nanoparticles with average diameter about 6.5 nm and big snowflake-like patterns with the size in the dimension of tens of microns. For Sample (1.5 X), smaller but much darker snowflake patterns and extremely small nanoparticles were observed. For Sample (2 X), the TEM image indicates only rod-like patterns and no nanoparticles can be found.

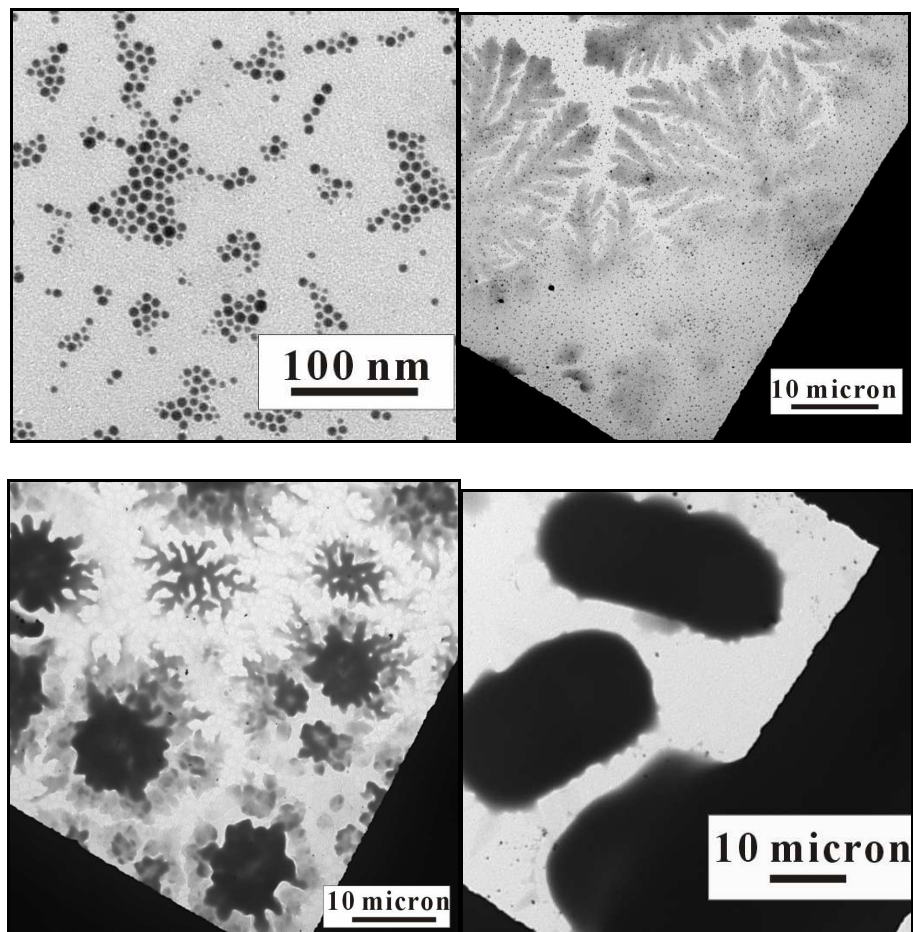


Figure 3.6. TEM images for Sample (1 X); (upper row) Sample (1.5 X) and Sample (2 X). (lower row, from left to right)

To understand the chemistry, Sample (2 X) was collected as dry product and then characterized. The orange-colored powder was not soluble in polar solvents such as ethanol or acetone, but readily dissolved in nonpolar solvents like hexanes or toluene. In the UV/vis spectrum of Sample (2 X) (Figure 3.7), three main peaks are found at 272, 318, 413 nm, which are consistent with the UV/vis features of a tiara Pd(II) thiolate complex-[Pd(SC₁₂H₂₅)₂]₆ that has been fully characterized in our early studies.¹ This was further confirmed by comparing the ¹H NMR and powder XRD patterns of Sample (2 X) (see Supporting Information , Figure 3.S4, 3.S5) with those data previously obtained from [Pd(SC₁₂H₂₅)₂]₆. All the results have very good matches.

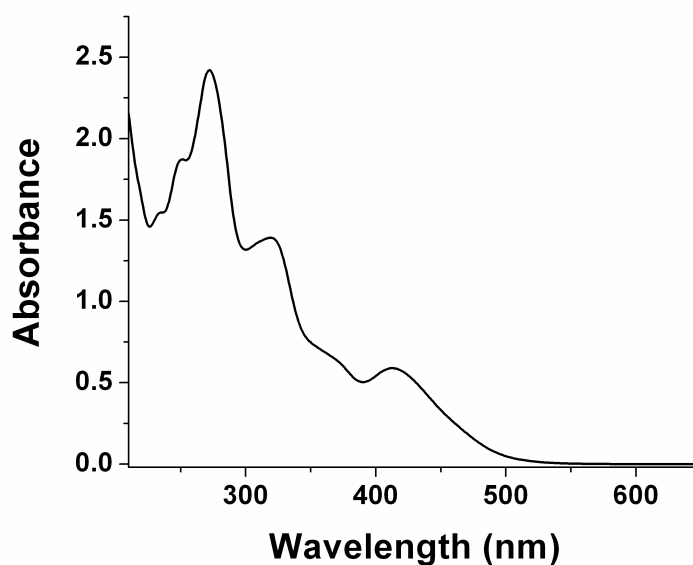


Figure 3.7. UV/vis pattern of Sample (2 X) in *n*-heptane.

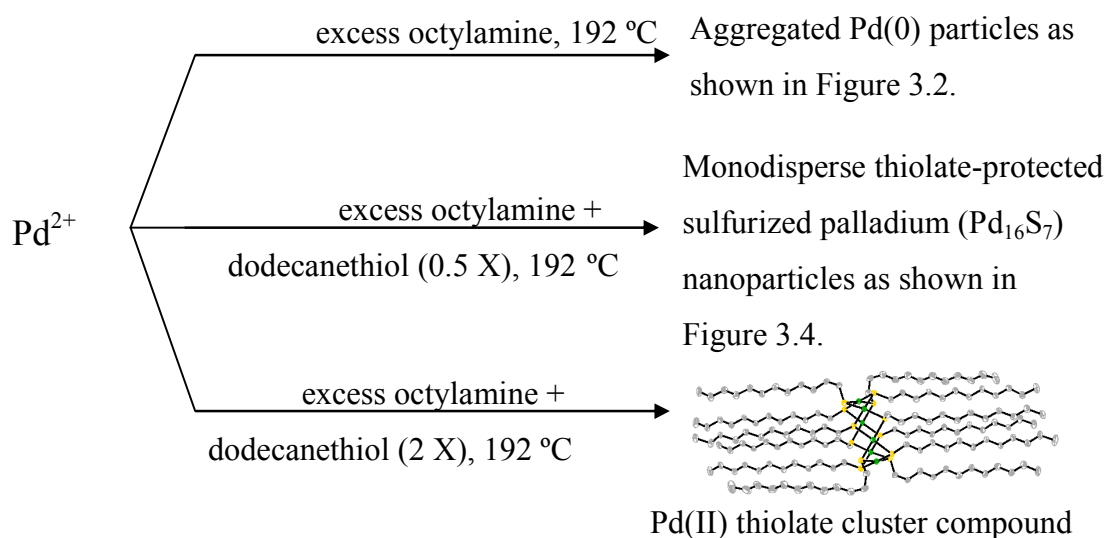
3.4 Discussion

Before heating, as good ligands, both octylamine and dodecanethiol could coordinate with Pd(II) ions to form soluble coordination complexes in the solvent. Without adding thiol, the solution of Pd(II)-amine complex was colorless. When coordinated with dodecanethiol, it had yellow to orange-red color depending on the thiol concentration. Since octylamine was in a large excess (20 X) and dodecanethiol was not enough in most cases (≤ 2 X), the color change of the solutions also indicated that dodecanethiol was a much stronger ligand than octylamine. So, in any solution, Pd(II) ions strongly coordinate with dodecanethiol, but remaining coordination sites would be filled by octylamine.

During heating, three main reactions could happen according to the experimental results. One was the amine-induced reduction of Pd(II) to Pd(0); the other was the formation of a tiara Pd(II) thiolate complex-[Pd(SC₁₂H₂₅)₂]₆; and the third was the chemical adsorption and decomposition of Pd(II) thiolate species on the as-synthesized nanoparticles. In the case of Sample (0 X), only the first reaction happened and aggregated Pd(0) particles were generated, which indicated octylamine was not a good protecting ligand for the particles in this system. For Sample (2 X), according to the experimental results, all of the Pd(II) ions were consumed to form [Pd(SC₁₂H₂₅)₂]₆ and no reduction took place. This cluster compound has a stable sandwich-like ring structure and only undergoes decomposition at much higher temperature.¹ For Sample (0.125 X) to Sample (1.5 X), since the amounts of dodecanethiol were limited, some

Pd(II) ions were consumed to form $[\text{Pd}(\text{SC}_{12}\text{H}_{25})_2]_6$, while others were still reduced by octylamine. Along with the formation of Pd(0) particles, thiolate species were chemically adsorbed onto the particle surface. After adsorption, the thiolate species were not stable anymore and the decomposition process occurred, which resulted in the sulfurization of Pd(0) nanoparticles. The control of the chemical paths by thiol concentration is indicated in Scheme 3.1. The breaking of S-C bond in thiol ligands on as-synthesized palladium nanoparticles or films has also been reported by others.²⁴⁻²⁶

According to the sequence mentioned above, the composition change in the final products is reasonable. Besides visual observations and TEM, the increase of $[\text{Pd}(\text{SC}_{12}\text{H}_{25})_2]_6$ in the final products with increasing dodecanethiol was further indicated by measuring the UV/vis absorbance of the solutions after heating, in which the featured peak at 413 nm of $[\text{Pd}(\text{SC}_{12}\text{H}_{25})_2]_6$ was employed. (Figure 3.8)



Scheme 3.1. Different products controlled by thiol concentration. The molecular structure of the cluster compound is from our early studies.¹

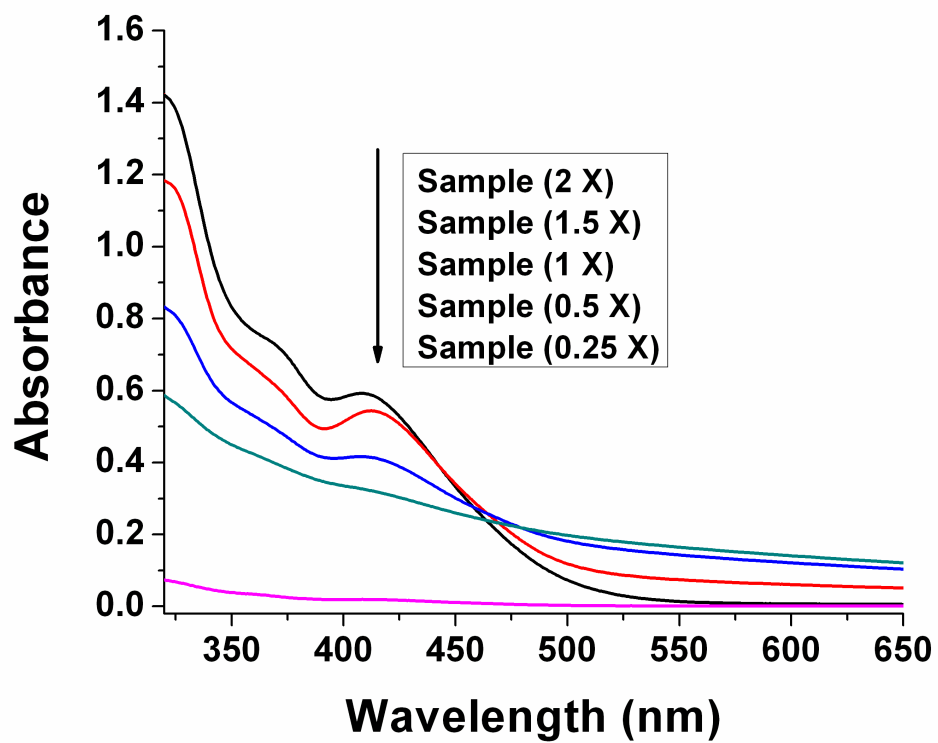


Figure 3.8. UV/vis patterns of the solutions after heating. (50 μ l of solution in 3 ml of *n*-heptane)

It is obvious that Sample (2 X) has the highest concentration of $[\text{Pd}(\text{SC}_{12}\text{H}_{25})_2]_6$, followed by Sample (1.5 X) and Sample (1 X) due to the partial adsorption and decomposition. In Sample (0.5 X), this peak disappears and the pattern only reflects the scattering effects of the nanoparticles. This means almost all of $[\text{Pd}(\text{SC}_{12}\text{H}_{25})_2]_6$ has been consumed. The overall results are the formation of thiolate-protected sulfurized palladium nanoparticles as shown in Fig. 3.4. If this sample is heated for another 1 h, aggregation of the nanoparticles will happen due to the further decomposition of the adsorbed thiolates. The evolution of the particles along with heating time in Sample (0.5 X) is shown in Figure 3.9. (also see Figure 3.4 for the TEM of the sample at 1 h) For Sample (0.25 X), the UV/vis pattern indicates no $[\text{Pd}(\text{SC}_{12}\text{H}_{25})_2]_6$ existing and the scattering effects are also low due to the large size of the obtained particles.

A similar influence of thiol ligands on the synthesis of Pd(0) nanoparticles using NaBH_4 as reducing agent was reported previously.¹² With increasing thiol concentration, the final products changed from thiolate-protected nanoparticles to certain Pd(II) thiolate complexes. For other metal ions, Lin et al. reported the influence of oleic acid on the growth of Co(0) nanocrystals.²⁷ Increasing the concentration of oleic acid also resulted in the transform action from Co(0) nanoparticles to Co(II) cluster compounds. The results described herein add to our understanding of these sensitive chemical processes that are ligand controlled.

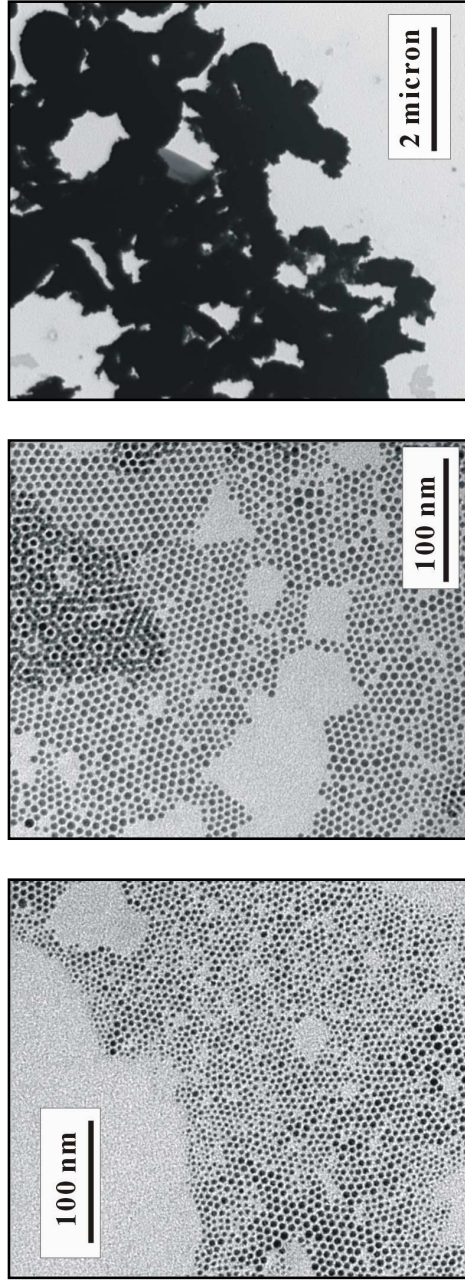


Figure 3.9. TEM images indicating the growth of the particles in Sample (0.5 X) along with heating time. (from left to right: 30 min, 45 min, 2 h)

3.5 Conclusions

We report the influence of thiol ligand on the formation of Pd nanoparticles through amine-induced reduction. When increasing the concentration of thiol, the final products changed from monodisperse sulfurized palladium nanoparticles (7.55 ± 0.73 nm), to a mixture of nanoparticles and Pd(II) thiolate complex-[Pd(SC₁₂H₂₅)₂]₆, and then to the pure complex at last.

3.6 References

1. Yang, Z.; Smetana, A. B.; Sorensen, C. M.; Klabunde, K. J. *Inorganic Chemistry* **2007**, 46, (7), 2427-2431.
2. Prasad, B. L. V.; Stoeva, S. I.; Sorensen, C. M.; Klabunde, K. J. *Chemistry of Materials* **2003**, 15, (4), 935-942.
3. Smetana, A. B.; Klabunde, K. J.; Sorensen, C. M. *Journal of Colloid and Interface Science* **2005**, 284, (2), 521-526.
4. Stoeva, S.; Klabunde, K. J.; Sorensen, C. M.; Dragieva, I. *Journal of the American Chemical Society* **2002**, 124, (10), 2305-2311.
5. Ghezelbash, A.; Sigman, M. B., Jr.; Korgel, B. A. *Nano Letters* **2004**, 4, (4), 537-542.
6. Larsen, T. H.; Sigman, M.; Ghezelbash, A.; Doty, R. C.; Korgel, B. A. *Journal of the American Chemical Society* **2003**, 125, (19), 5638-5639.
7. Jana, N. R.; Chen, Y.; Peng, X. *Chemistry of Materials* **2004**, 16, (20), 3931-3935.

8. Jun, Y.-w.; Choi, J.-s.; Cheon, J. *Angewandte Chemie, International Edition* **2006**, 45, (21), 3414-3439.
9. Park, J.; Koo, B.; Yoon, K. Y.; Hwang, Y.; Kang, M.; Park, J.-G.; Hyeon, T. *Journal of the American Chemical Society* **2005**, 127, (23), 8433-8440.
10. Yee, C. K.; Jordan, R.; Ulman, A.; White, H.; King, A.; Rafailovich, M.; Sokolov, J. *Langmuir* **1999**, 15, (10), 3486-3491.
11. Martin, J. E.; Wilcoxon, J. P.; Odinek, J.; Provencio, P. *Journal of Physical Chemistry B* **2002**, 106, (5), 971-978.
12. Zamborini, F. P.; Gross, S. M.; Murray, R. W. *Langmuir* **2001**, 17, (2), 481-488.
13. Veisz, B.; Kiraly, Z. *Langmuir* **2003**, 19, (11), 4817-4824.
14. Chen, M.; Falkner, J.; Guo, W.-H.; Zhang, J.-Y.; Sayes, C.; Colvin, V. L. *Journal of Colloid and Interface Science* **2005**, 287, (1), 146-151.
15. Narayanan, R.; El-Sayed, M. A. *Journal of the American Chemical Society* **2003**, 125, (27), 8340-8347.
16. Teranishi, T.; Miyake, M. *Chemistry of Materials* **1998**, 10, (2), 594-600.
17. Thomas, P. J.; Kulkarni, G. U.; Rao, C. N. R. *Journal of Physical Chemistry B* **2000**, 104, (34), 8138-8144.
18. Son, S. U.; Jang, Y.; Yoon, K. Y.; Kang, E.; Hyeon, T. *Nano Letters* **2004**, 4, (6), 1147-1151.
19. Kim, S.-W.; Park, J.; Jang, Y.; Chung, Y.; Hwang, S.; Hyeon, T.; Kim, Y. W. *Nano Letters* **2003**, 3, (9), 1289-1291.
20. Hiramatsu, H.; Osterloh, F. E. *Chemistry of Materials* **2004**, 16, (13), 2509-2511.
21. Dey, S.; Jain, V. K. *Platinum Metals Review* **2004**, 48, (1), 16-29.

22. Koizumi, N.; Miyazawa, A.; Furukawa, T.; Yamada, M. *Chemistry Letters* **2001**, 30, 1282-1283.
23. Capdevielle, P.; Lavigne, A.; Sparfel, D.; Baranne-Lafont, J.; Nguyen Kim, C.; Maumy, M. *Tetrahedron Letters* **1990**, 31, (23), 3305-3308.
24. Murayama, H.; Ichikuni, N.; Negishi, Y.; Nagata, T.; Tsukuda, T. *Chemical Physics Letters* **2003**, 376, (1,2), 26-32.
25. Teranishi, T.; Inoue, Y.; Nakaya, M.; Oumi, Y.; Sano, T. *Journal of the American Chemical Society* **2004**, 126, (32), 9914-9915.
26. Love, J. C.; Wolfe, D. B.; Haasch, R.; Chabinye, M. L.; Paul, K. E.; Whitesides, G. M.; Nuzzo, R. G. *Journal of the American Chemical Society* **2003**, 125, (9), 2597-2609.
27. Samia, A. C. S.; Hyzer, K.; Schlueter, J. A.; Qin, C.-J.; Jiang, J. S.; Bader, S. D.; Lin, X.-M. *Journal of the American Chemical Society* **2005**, 127, (12), 4126-4127.

3.7 Supporting information

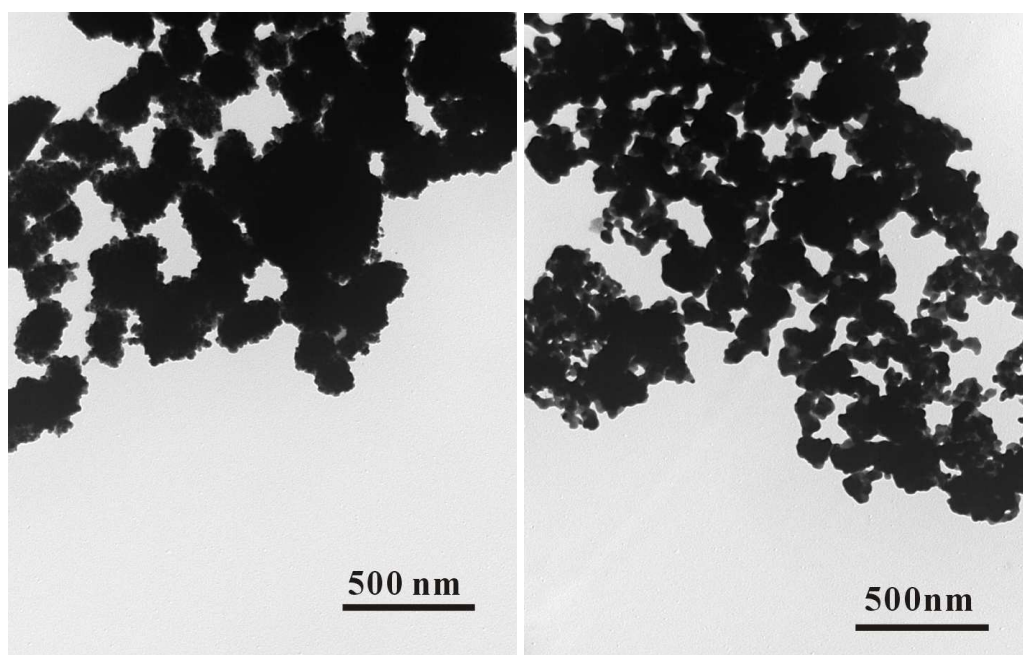


Figure 3.S1. TEM images of Sample (0.125 X) (left) and Sample (0.25 X) (right).

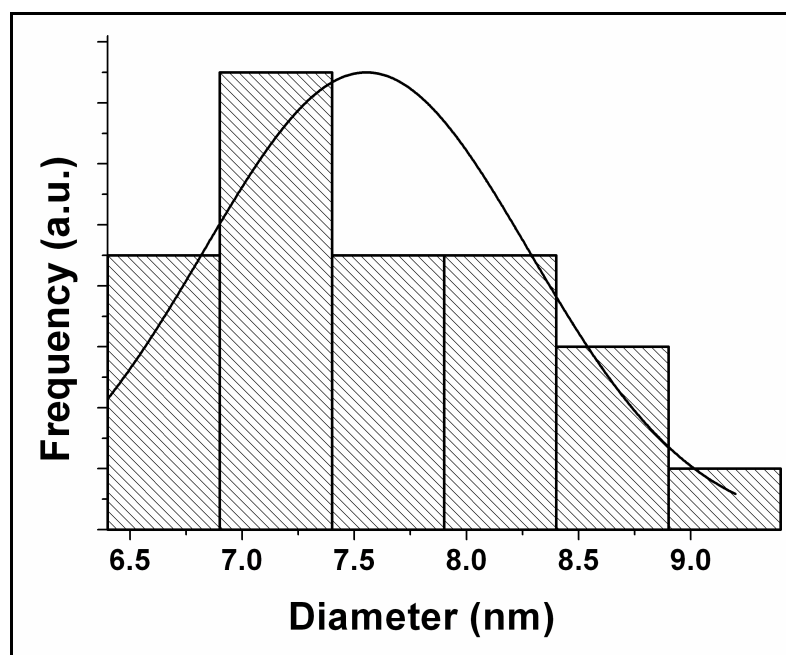


Figure 3.S2. Histogram of Sample (0.5 X) showing the size distribution. (diameter = 7.55 ± 0.73 nm, obtained by measuring 100 particles)



Figure 3.S3. Photo indicating different color when precipitated with 95 % ethanol for Sample (0.5 X), (1 X), (1.5 X) and (2 X). (from left to right)

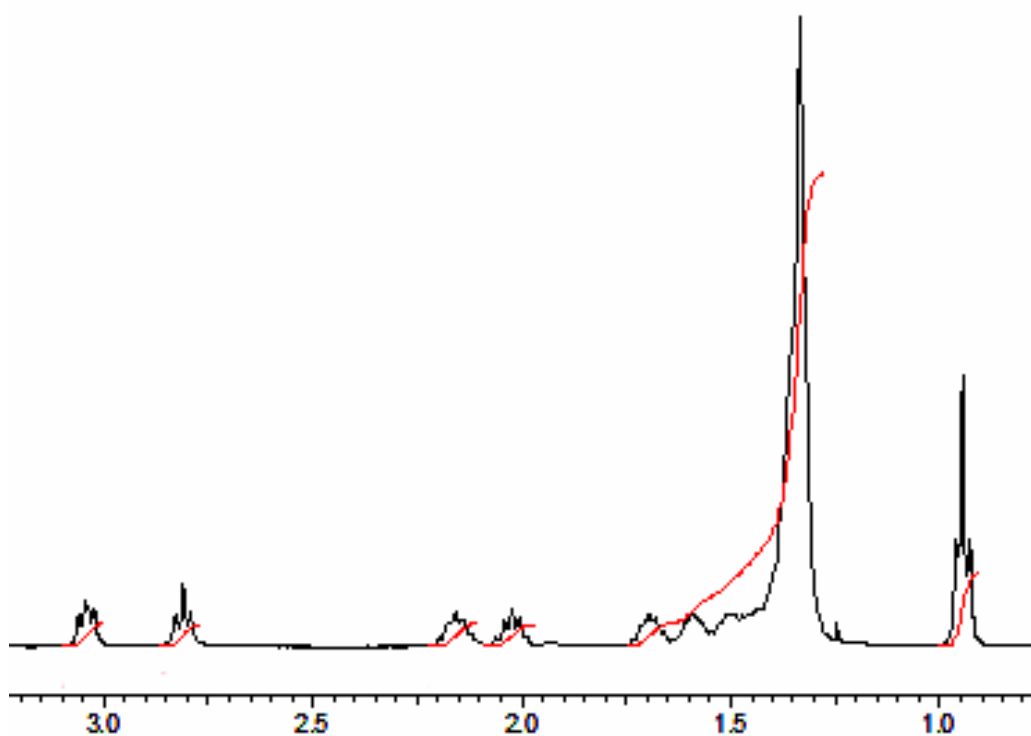


Figure 3.S4. ^1H NMR spectrum (in deuterobenzene) of Sample (2 X). (3.04 ppm (t), 2.81 ppm (t), 2.16 ppm (q), 2.02 ppm (q), 1.70-1.34 ppm (m), 0.94 ppm (m). Area ratio: 1:1:1:1:18:3 from left to right)

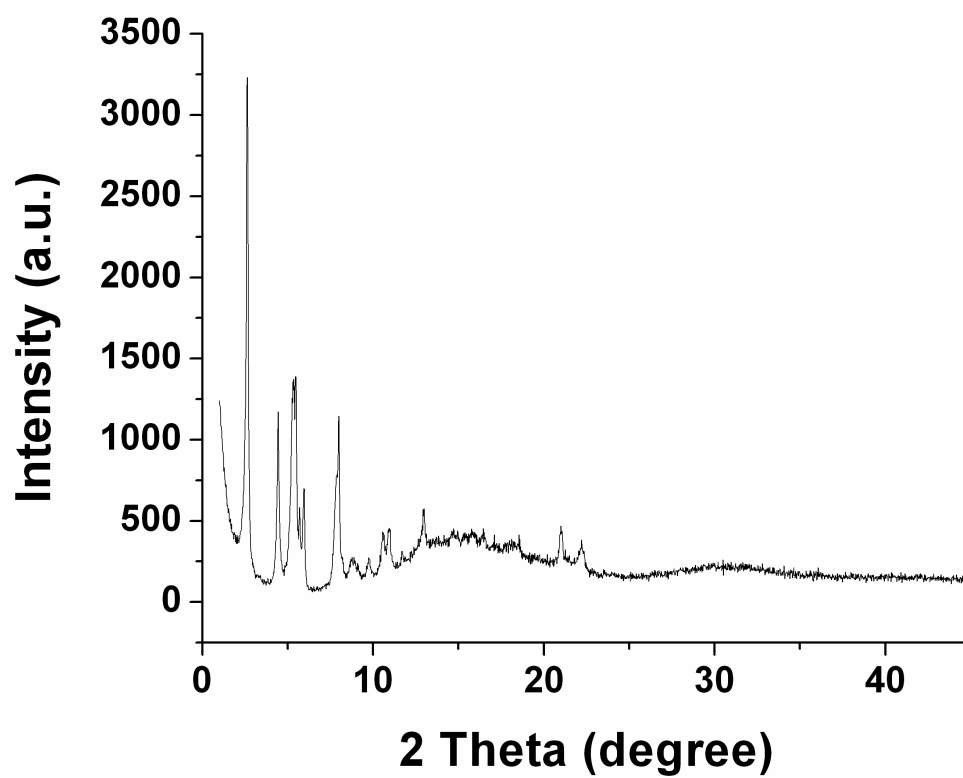


Figure 3.S5. Powder XRD of Sample (2 X).

CHAPTER 4 - Synthesis of nearly monodisperse palladium (Pd) nanoparticles by using oleylamine and trioctylphosphine mixed ligands

4.1 Introduction

In recent years, considerable efforts have been made to synthesize metal nanoparticles. When the particle size is in the nano-range, different physical/chemical properties compared with the bulk counterparts may occur, which is extremely attractive for both academic studies and practical applications.¹ To prepare high quality metal nanoparticles that are soluble in organic solvents, organic ligands with long C-chains such as alkyl carboxyl acids, alkylthiols, alkylamines and phosphines are widely applied. The ligands can chemically adsorb on the particle surface and then protect them from aggregation. Furthermore, to achieve the best control over particle size, shape, and size distribution, mixed ligands are generally employed. In these cases, it is very important to understand the function of each ligand, but unfortunately, this is not usually possible.

Pd nanoparticles have proven to be highly active catalysts. For example, polyvinylpyrrolidone (PVP)-protected Pd nanoparticles were applied to catalyze the Suzuki reaction between phenylboronic acid and iodobenzene;² non-supported Pd

nanoparticles were used for the selective hydrogenation of 1-hexyne.³ Some preparation methods have been established to prepare Pd nanoparticles. The reactions may be carried out in aqueous solutions,⁴⁻⁷ inverse micelle systems,^{8, 9} or high-boiling-point organic solvents.^{10, 11} Reducing agents such as lithium triethylborohydride (Superhydride),¹² lithium borohydride,⁸ sodium borohydride,^{5,13} hydrazine,⁴ sodium hypophosphite⁹ are generally applied to convert Pd(II) ions to Pd metal. The reduction can also be achieved by heating Pd(II) species in ethylene glycol^{14, 15} or ethanol/water solutions.^{16, 17} To control the particle size and size distribution, a variety of protecting agents have been applied, including surfactants,^{4, 7, 9} polymers,^{15, 16, 18} dendrimers,^{5, 6, 19} alkanethiols,^{12, 13, 17} phosphines,^{10, 11} thioethers,²⁰ and alkanecyanides.²¹

Alkylamines have been employed as mild reducing agents to prepare gold and silver nanoparticles.^{22, 23} In our early studies, octylamine and dodecanethiol were used to synthesize highly monodisperse sulfurized Pd nanoparticles.²⁴ To the best of our knowledge, no other amine-induced reduction of Pd(II) has been reported. In this chapter, the reduction of Pd(II) by oleylamine and the influence of trioctylphosphine on this reaction, is presented. This approach provides a facile method to synthesize nearly monodisperse Pd nanoparticles with controllable size. In addition, it is a good example to show how different ligands may play special roles in a ligand-mixed system. If you need to create additional chapters, use Heading 1 style for the main heading of the chapter.

4.2 Experimental Section

4.2.1 Materials

Sodium tetrachloropalladate(II) (Na_2PdCl_4 , 99%), trioctylphosphine ($[\text{CH}_3(\text{CH}_2)_7]_3\text{P}$, 90%) were purchased from Aldrich Chem. Co. Oleylamine ($\text{CH}_3(\text{CH}_2)_7\text{CH}=\text{CH}(\text{CH}_2)_7\text{CH}_2\text{NH}_2$, 97%) and 4-*tert*-butyltoluene ($(\text{CH}_3)_3\text{CC}_6\text{H}_4\text{CH}_3$, 96%) were bought from ACROS Organics. Other chemicals were purchased and used as received.

4.2.2 Thermolysis without TOP

In a glass tube, 0.029 g of Na_2PdCl_4 (1.0×10^{-4} mol), 10 ml of 4-*tert*-butyltoluene, and 0.50 ml of oleylamine (1.5×10^{-3} mol) were added sequentially. The mixture was sonicated for 20 min. Then, the tube was connected to a vacuum line and an argon gas-tank through a rubber septum equipped with needles. The mixture was degassed and then flushed with argon several times. After that, it was heated (about 192 °C) in a preheated sand-bath for 1 h under the protection of argon. During that time, black precipitates were produced. After 1 h, the tube was removed from the sand-bath and left to cool. Finally, the black precipitates were collected by centrifugation and washed with acetone several times.

4.2.3 Thermolysis with different amounts of TOP

In a glass tube, 0.029 g of Na_2PdCl_4 , 10 ml of 4-*tert*-butyltoluene, 0.50 ml of oleylamine, and certain amounts of TOP were added sequentially. The molar ratios of TOP to Pd(II) were altered systematically from 0.4, 0.6, 1.0, 1.4, to 2.0. After sonication for 20 min, the thermal reaction and the product collection were carried out in the same

way as described above. For convenience, the obtained products are labeled as Sample (n ×) in this paper (n = the molar ratio of TOP to Pd(II) ions).

4.2.4 Equipment and analysis

Transmission electron microscopy (TEM) was performed on a Philips CM100 microscope operated at 100 kV. To prepare a TEM sample, the washed products were redispersed into toluene and then a drop of solution was dropped onto a carbon/Formvar co-coated copper grid, which was then allowed to dry in air. UV/vis absorption analysis was carried out on a Cary 500 UV-VIS-NIR spectrophotometer. Powder X-ray diffraction (XRD) patterns were recorded by a Bruker D8 X-ray diffractometer with Cu K α radiation.

4.3 Results and discussion

4.3.1 Reduction of Pd(II) ions by oleylamine

In the reaction system, oleylamine was applied in an excess amount (the molar ratio of amine to Pd(II) was 15) to facilitate the completion of the reduction. 4-*tert*-butyltoluene was used as a high-boiling-point (192 °C), non-coordinating solvent. After sonication for 20 minutes at room temperature, the reddish-brown-colored Na₂PdCl₄ powder was mostly dissolved and a colorless solution was formed, which was attributed to the generation of certain Pd(II)-oleylamine complexes. When boiled at ca.192 °C under the protection of argon, the system turned to black in ten minutes, indicating the formation of small particles. After one hour, black-colored precipitates were collected as Sample (0 ×). The powder XRD pattern of this sample shows the features of pure face-centred cubic palladium crystallites (Figure 4.1).

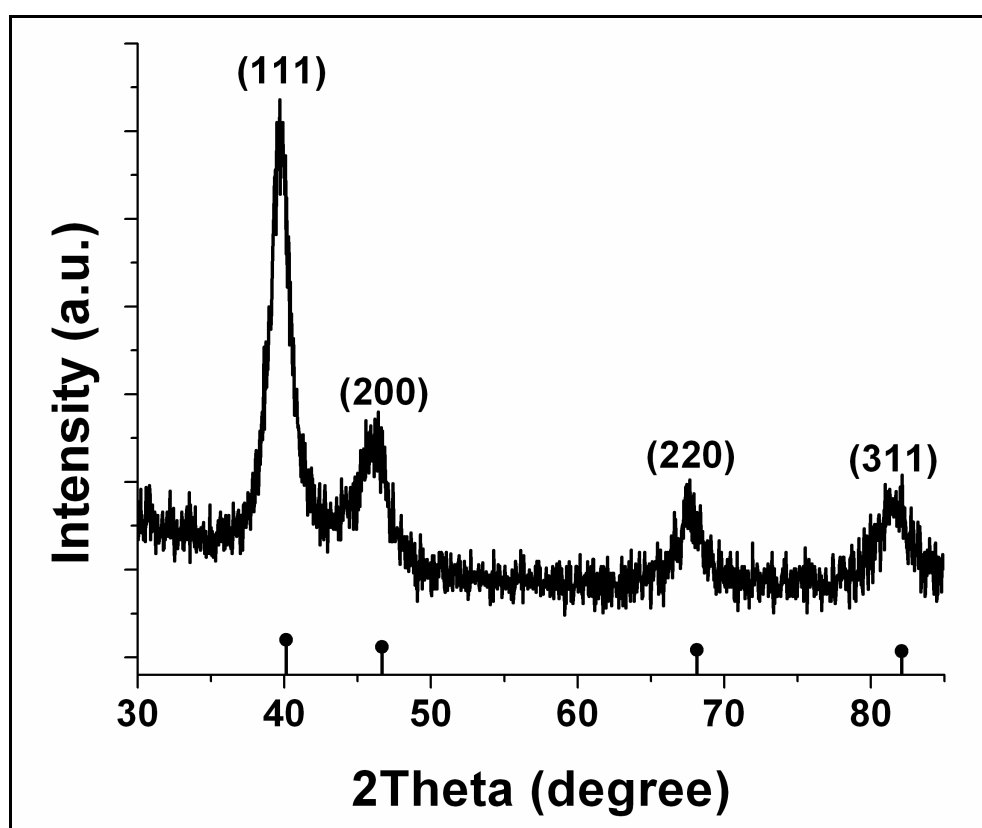
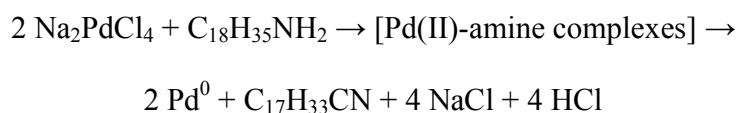


Figure 4.1. Powder XRD pattern of Sample (0 ×) indicating the formation of Pd(0) crystallites. The standard pattern (the vertical lines) is based on JCPDS file 46-1043. (Notice: a small amount of water was added during wash in order to remove NaCl that was generated in the reaction.)

The formation of Pd(0) is attributed to the reduction of Pd(II) ions by oleylamine at high temperature, in which the amine ligands are oxidized to nitriles.²⁵ The formation of soluble Pd(II)-oleylamine coordination complexes occurs before the heat treatment, and the amine-induced reduction occurs during the heating step. The overall reaction is assumed to happen according to the following equation via Pd(II)-amine intermediates:



A typical TEM image (Figure 4.2) of Sample (0 ×) shows large, irregular aggregates in the dimension of tens of micrometers. They are composed of numerous stacked small Pd(0) nanoparticles, which can be observed at the edge of the aggregates. Although oleylamine has been applied successfully as the protecting ligand for the synthesis of a variety of metal nanoparticles, our results indicate it may not be the best capping ligand for Pd nanoparticles. To further confirm that, another experiment was carried out under the same conditions except that the molar ratio of oleylamine to Pd(II) was increased to 150. The obtained particles were still not stable in the solution and ready to settle down as black precipitates as seen in Sample (0 ×).

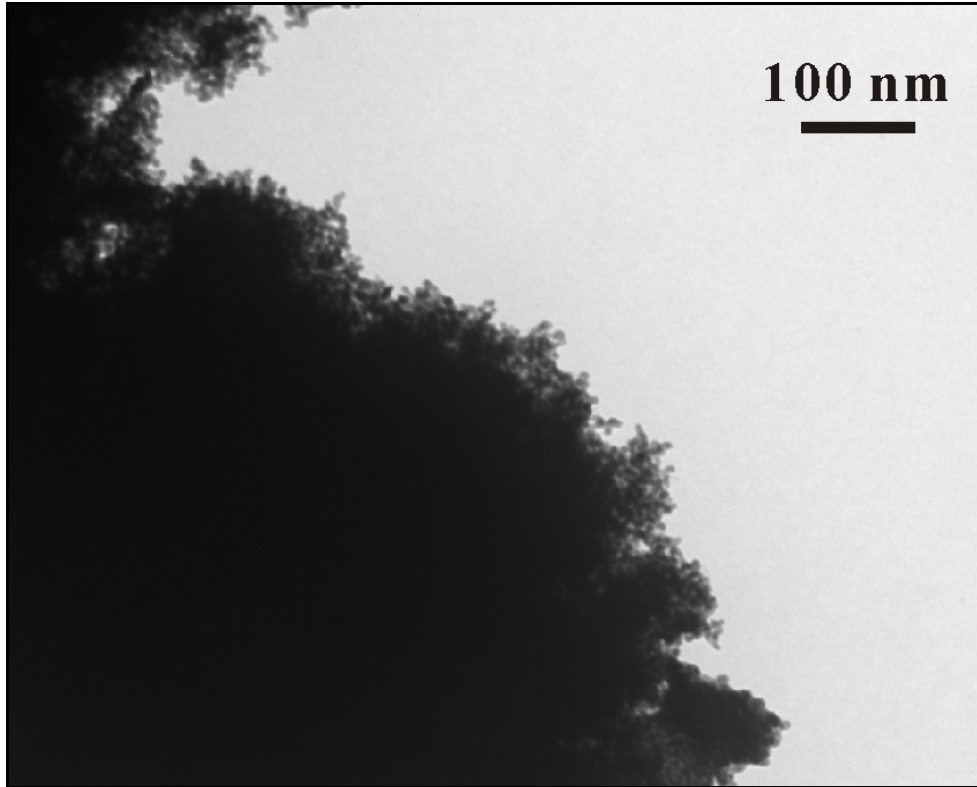


Figure 4.2. TEM image of Sample (0 ×) shows aggregated particles.

4.3.2 Reduction of Pd(II) ions in the presence of oleylamine and TOP

When other experimental conditions were fixed, different amounts of TOP were added before heating. The molar ratio of TOP to Pd(II) were set as 0.4, 0.6, 1.0, 1.4, and 2.0. After heating, stable black colloidal solutions were obtained for Sample (0.4 ×) to Sample (1.4 ×), while Sample (2.0 ×) remained as a clear lightly yellow solution. While the optical densities for Sample (0.4 ×), Sample (0.6 ×), and Sample (1.0 ×) were indistinguishable to the naked eye, the decrease of the darkness for Sample (1.4 ×) was obvious (see Supporting Information Figure 4.S1 for the different appearance of the as-synthesized samples).

The powder XRD patterns of the obtained samples still show the features of pure face-centred-cubic Pd(0) nanocrystallites (Figure 4.3). The broadening of the (111) peak and the disappearance of other peaks indicate that, when increasing the molar ratio of TOP to Pd(II), the generated nanocrystallites decrease in size.

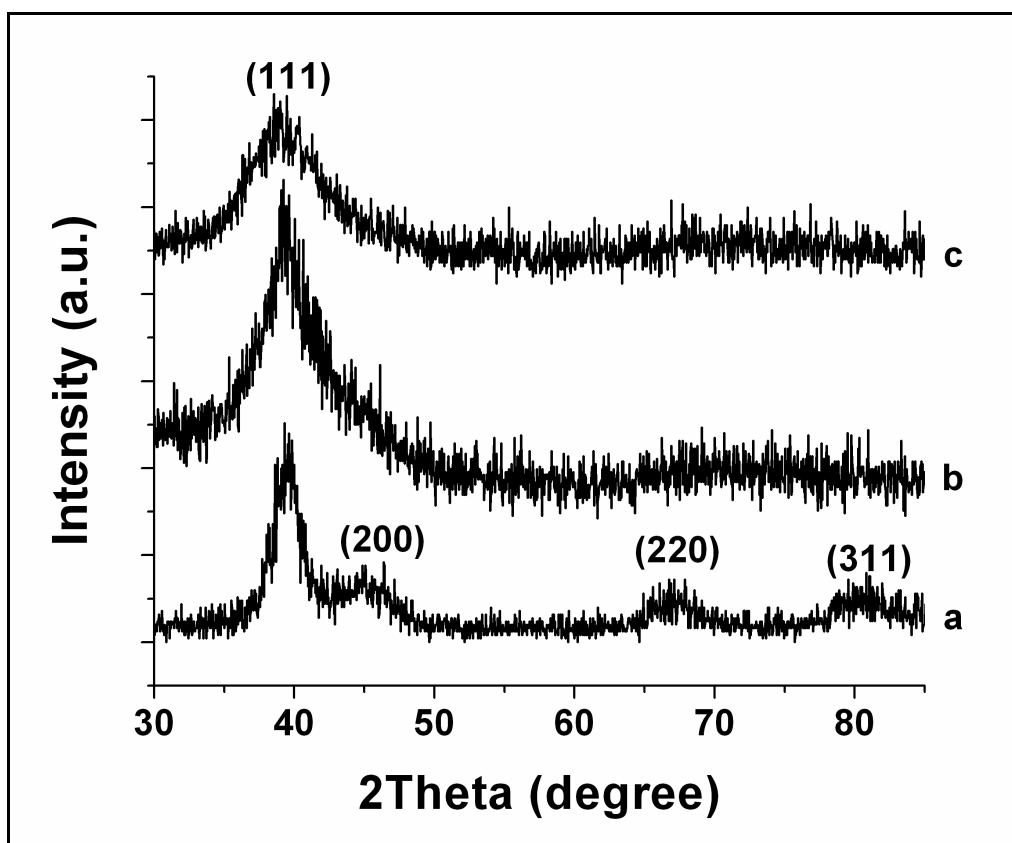


Figure 4.3. Powder XRD patterns of Sample (0.4 ×) (a), Sample (0.6 ×) (b) and Sample (1.0 ×) (c).

The typical TEM images of the obtained samples are shown in Figure 4.4 (also see Supporting Information Figure 4.S2 for the histogram patterns). Generally speaking, when increasing the molar ratio of TOP to Pd(II), the particles become smaller in size and rounder in shape. Sample (0.4 ×) shows irregular faceted particles with an average diameter of 10.7 ± 2.9 nm. The standard deviation (SD) is 27%. For Sample (0.6 ×), the average diameter is 10.8 ± 2.0 nm (SD = 19%). While the average particle size remains almost the same compared with Sample (0.4 ×), the narrowing in particle size distribution is noticeable. Sample (1.0 ×) shows smaller and more spherical particles with an average diameter of 9.5 ± 1.2 nm (SD = 13%). These particles self-assemble into hexagonal close-packing superlattices, as shown by TEM. For Sample (1.4 ×), the particles become further smaller, but the monodispersity becomes poorer (average particle size: 7.6 ± 1.9 nm; SD: 25%).

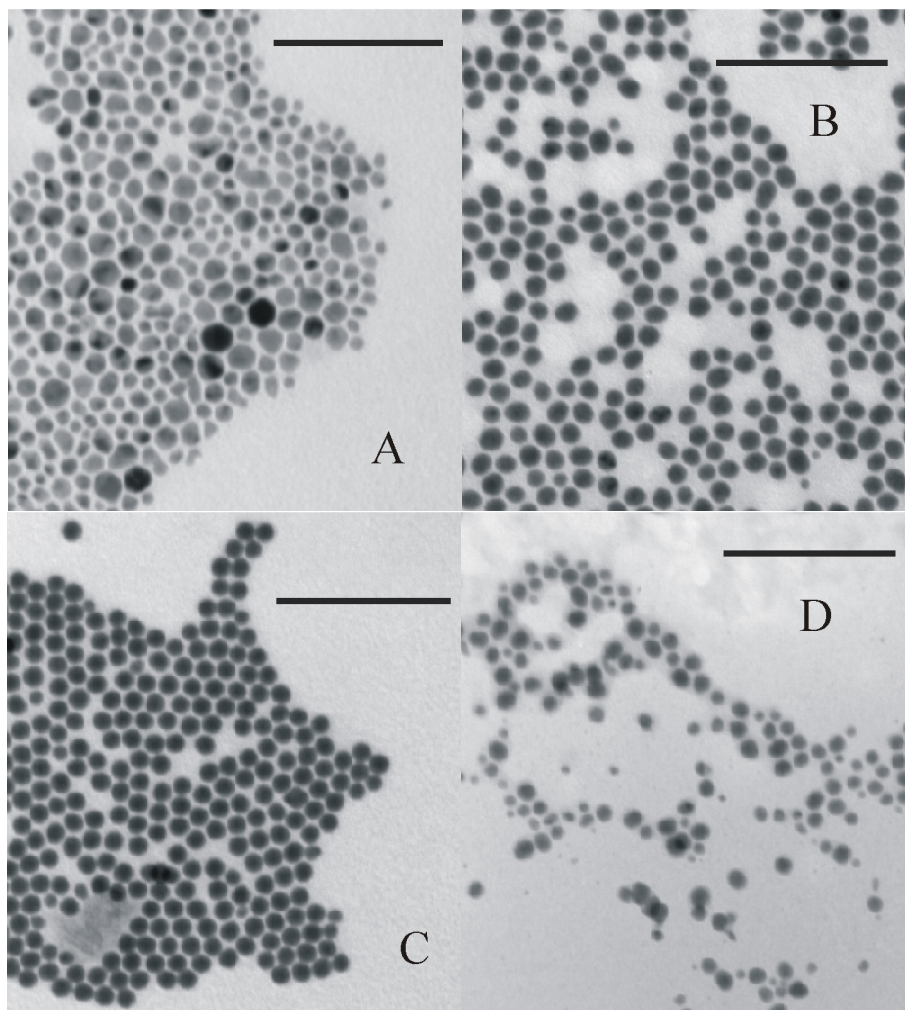


Figure 4.4. TEM images of (a) Sample ($0.4 \times$), (b) Sample ($0.6 \times$), (c) Sample ($1.0 \times$), (d) Sample ($1.4 \times$). Scale bar = 100 nm.

Due to the damping effect of the d-d transitions, Pd nanoparticles usually do not show a surface plasmon (SP) absorbance in UV/vis spectra.²⁶ Consistent with this observation, an UV/vis measurement of Sample (1.0 ×), which was washed and then redissolved in hexane, presents no SP band (see Supporting Information Figure 4.S3).

4.3.3 The function of TOP

As mentioned above, when the source Pd(II) salt was dissolved in 4-*tert*-butyltoluene with oleylamine at room temperature, certain Pd(II)-amine complexes were formed. When TOP was added into such a system, the Pd(II)-amine complexes were converted to Pd(II)-TOP complexes due to the stronger coordinating potency to Pd(II) ions of phosphine ligands over amine ligands. To prove this, the change of the UV/vis absorbance for Sample (1.0 ×) before and after adding TOP was measured. When TOP was added to the Pd(II)-oleylamine system, a new peak at ca. 318nm was generated (Figure 4.5). To indicate such a peak was not due to the pure TOP ligands, the UV/vis absorbance of TOP in hexane was measured and no peak was found at this position. Furthermore, when adding Na₂PdCl₄ to this TOP/hexane mixture, a peak came out at 318 nm (see Supporting Information Figure 4.S4). All of these results confirm that the absorbance at 318 nm for Sample (1.0 ×) after adding TOP was really due to the generation of certain Pd(II)-TOP complexes.

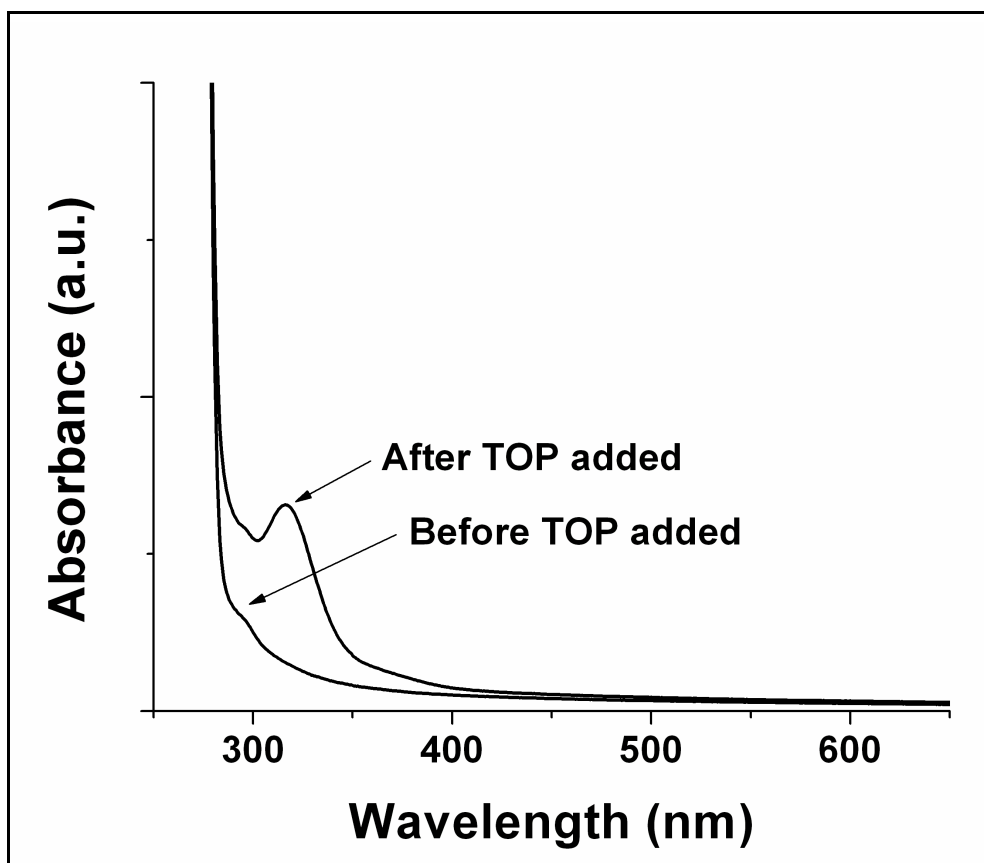


Figure 4.5. UV/vis absorbance for Sample (1.0 ×) before and after adding TOP at room temperature to show the generation of Pd(II)-TOP complexes. For each measurement, 30 ul of the solution was taken and then mixed with 3 ml of hexane, which was also used as the reference.

After heat treatment, different final products were generated, highly depending on the concentration of TOP. A preliminary explanation for this phenomenon is as follows: When no TOP was applied, only aggregated Pd(0) particles were obtained due to the amine-induced reduction and the poor protecting ability of amine ligands for the as-synthesized Pd(0) particles. However, for Sample (2.0 ×), only certain Pd(II)-TOP complexes were produced, which were quite stable in the reaction system. For Sample (0.4 ×) to Sample (1.4 ×), since the amounts of TOP ligands were inadequate, some Pd(II) ions were consumed to form Pd(II)-TOP complexes, while the remaining Pd(II) ions would still be reduced by oleylamine. Since well-protected particles were generated in these cases, the chemical binding of TOP (from the free Pd(II)-TOP complexes in solution) on the as-synthesized Pd(0) particles is assumed. So, some TOP ligands were consumed to protect the Pd nanoparticles, while the others still remained in solution as Pd(II)-TOP complexes. Figure 4.6 shows the UV/vis absorbance of the solutions after heating. A peak at 318 nm was found for all the samples except Sample (0 ×).

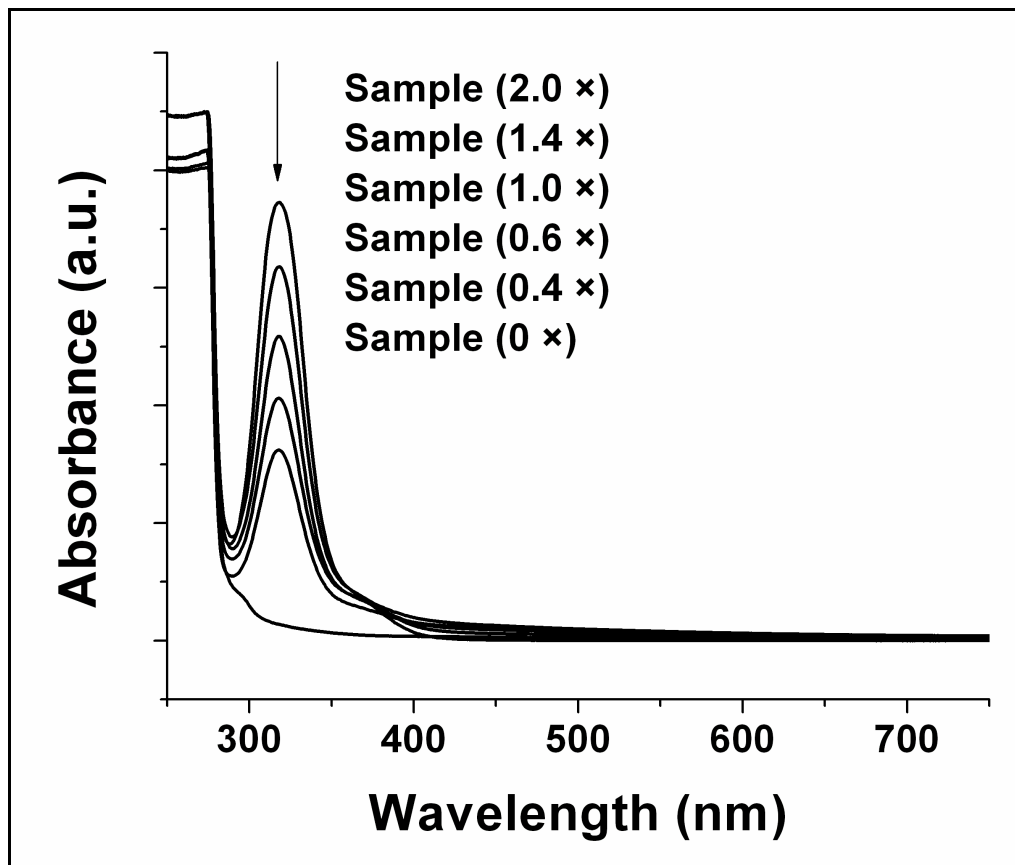
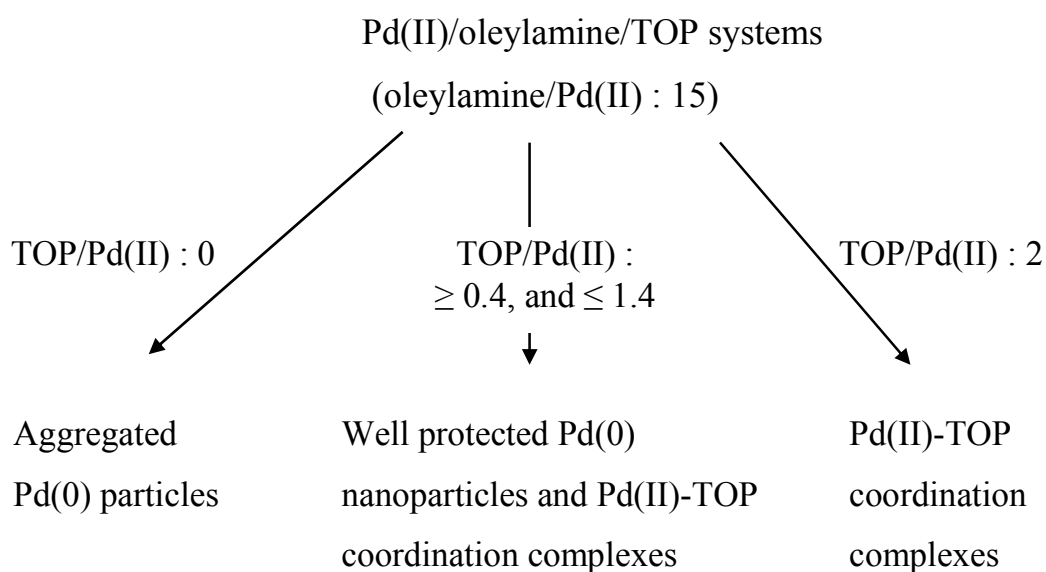


Figure 4.6. UV/vis patterns of the sample solutions after heating. For each measurement, an aliquot of 30 μ l was taken and then mixed with 3 ml of hexane. Reference: hexane.

According to the above discussion, the influence of different amounts of TOP on the final products is systematically shown in Scheme 4.1. It should be pointed out, for collecting Pd(0) nanoparticles, the Pd(II)-TOP complexes could be removed by washing with acetone.

Scheme 4.1. Influence of TOP on the final products. (Note: all the ratios are molar ratios.)



A similar influence of thiol ligands on a Pd(II)/octylamine system was reported previously.²⁴ With increasing thiol concentration, the final products changed from sulfur rich Pd nanoparticles to a tiara-like Pd(II)-thiolate complex. Another similar example was reported regarding the influence of oleic acid on the preparation of Co(0) nanocrystals.²⁷ Increasing the concentration of oleic acid also resulted in the transformation of Co(0) nanoparticles to Co(II) cluster compounds. The results described herein add to our understanding of these sensitive chemical processes that are ligand-controlled.

4.3.4 The cooperative protecting effects of oleylamine

As mentioned previously, the main function of oleylamine in this system was to reduce Pd(II) ions. Without TOP added, only aggregated Pd nanoparticles were obtained even when the molar ratio of oleylamine to Pd(II) reached to 150. But further studies indicated that, addition of an appropriate amount of oleylamine as a supplementary capping ligand was very important and necessary even when TOP was added. The experiments were carried out according to Sample (0.6 ×) except changing the concentration of oleylamine. In Sample (0.6 ×), the molar ratio of oleylamine to Pd(II) was set as 15 arbitrarily. When the molar ratio was decreased to 3, only aggregated Pd(0) particles were generated (Figure 4.7, a). However, when the molar ratio was increased to 60, well-protected Pd(0) nanoparticles were obtained with a little bigger size but narrower distribution (size: 11.6 ± 1.4 nm, SD = 12%) compared with Sample (0.6 ×) (Figure 4.7, b. Also see Supporting Information Figure 4.S5 for the histogram of the size distribution). Furthermore, this sample has been found to be quite stable toward long-term digestive ripening. After boiling for 17 h, a typical TEM picture shows Pd

nanoparticles with an average diameter of 14.9 ± 1.2 nm (SD = 8%). A close-up TEM picture indicates that, when the size increases, it is more likely to form quasi-spherical particles with certain crystal facets (Figure 4.8. Also see Supporting Information Figure 4.S5 for the histogram of the size distribution).

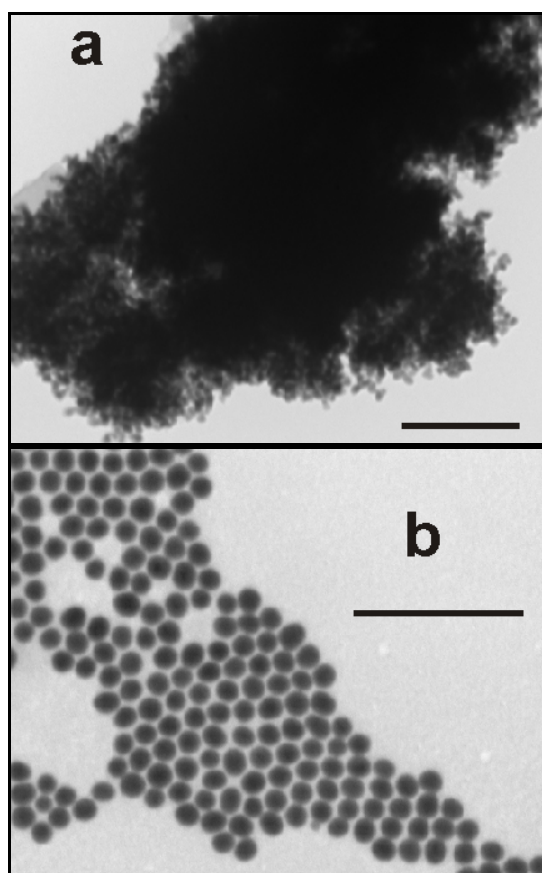


Figure 4.7. TEM images of the particles prepared according to Sample (0.6 ×) except changing the molar ratio of oleylamine to Pd(II). (a) Decreasing the ratio to 3, (b) increasing the ratio to 60. Scale bar = 100 nm. Also see the TEM image of Sample (0.6 ×) in Figure 4.4 (b) for comparison.

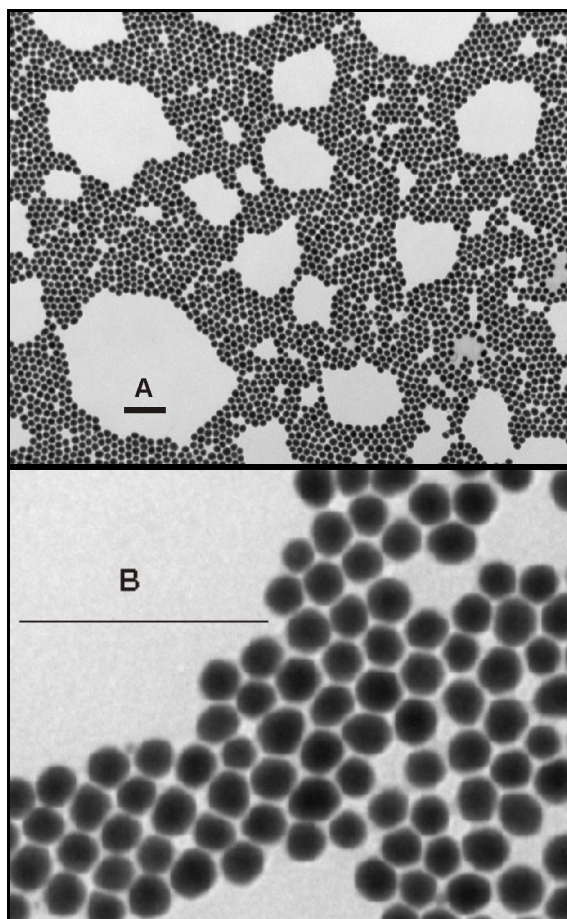


Figure 4.8. TEM images of the sample prepared according to Sample (0.6 ×) except increasing the molar ratio of oleylamine to Pd(II) to 60 and heating for 17 h. (A) Small magnification to show the hexagonal close-packing pattern in short range. (B) Large magnification to show the faceted quasi-spherical shape. Scale bar = 100 nm.

4.4 Conclusions

In this chapter, we report the influence of TOP ligand on the synthesis of Pd nanoparticles by oleylamine-induced reduction of Pd(II) ions. Without TOP, only aggregated Pd particles were generated. When an appropriate amount of TOP was added, nearly monodisperse Pd nanoparticles could be obtained. But further increasing the molar ratio of TOP/Pd(II) to 2 resulted in the formation of Pd(II)-TOP coordination complexes. Also, the function of oleylamine as a supplementary ligand was discussed, which will be helpful for understanding the cooperation of mixed protecting ligands in certain systems.

4.5 References

1. Klabunde, K. J. in *Nanoscale Materials in Chemistry* Wiley-Interscience, 2001 and references therein.
2. Narayanan, R.; El-Sayed, M. A. *Journal of the American Chemical Society* **2003**, 125(27), 8340-8347.
3. Semagina, N.; Renken, A.; Kiwi-Minsker, L. *Journal of Physical Chemistry C* **2007**, 111(37), 13933-13937.
4. Veisz, B.; Kiraly, Z. *Langmuir* **2003**, 19(11), 4817-4824.
5. Scott, R. W. J.; Ye, H.; Henriquez, R. R.; Crooks, R. M. *Chemistry of Materials* **2003**, 15(20), 3873-3878.
6. Ye, H.; Scott, R. W. J.; Crooks, R. M. *Langmuir* **2004**, 20(7), 2915-2920.
7. Tan, H.; Zhan, T.; Fan, W. Y. *Chemical Physics Letters* **2006**, 428, 352-355.

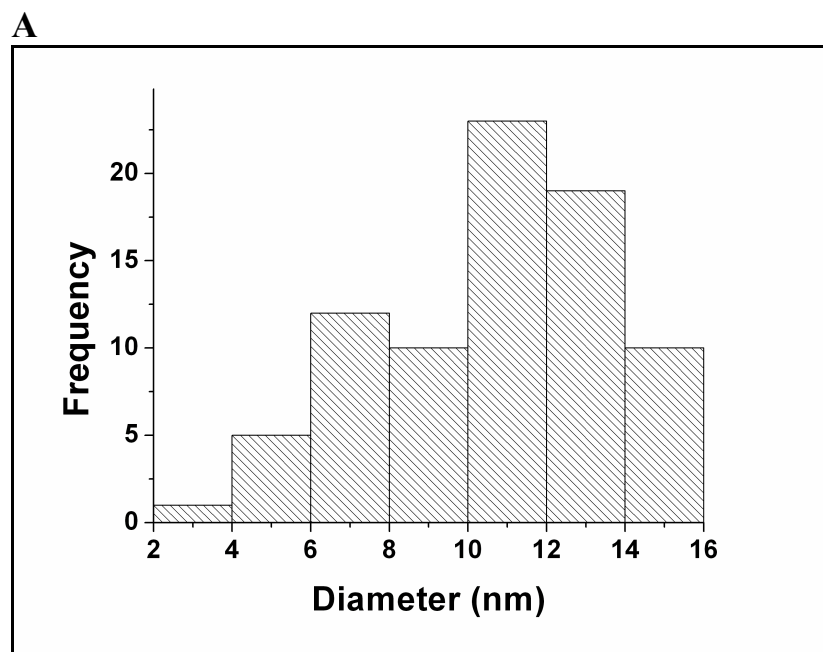
8. Martin, J. E.; Wilcoxon, J. P.; Odinek, J.; Provencio, P. *Journal of Physical Chemistry B* **2002**, 106(5), 971-978.
9. Chen, M.; Falkner, J.; Guo, W.-H.; Zhang, J.-Y.; Sayes, C.; Colvin, V. L. *Journal of Colloid and Interface Science* **2005**, 287, 146-151.
10. Son, S. U.; Jang, Y.; Yoon, K. Y.; Kang, E.; Hyeon, T. *Nano Letters* **2004**, 4(6), 1147-1151.
11. Kim, S.-W.; Park, J.; Jang, Y.; Chung, Y.; Hwang, S.; Hyeon, T.; Kim, Y. W. *Nano Letters* **2003**, 3(9), 1289-1291.
12. Yee, C. K.; Jordan, R.; Ulman, A.; White, H.; King, A.; Rafailovich, M.; Sokolov, J. *Langmuir* **1999**, 15(10), 3486-3491.
13. Zamborini, F. P.; Gross, S. M.; Murray, R. W. *Langmuir* **2001**, 17(2), 481-488.
14. Xiong, Y.; Chen, J.; Wiley, B.; Xia, Y. *Journal of the American Chemical Society* **2005**, 127(20), 7332-7333.
15. Xiong, Y.; Chen, J.; Wiley, B.; Xia, Y.; Yin, Y.; Li, Z.-Y. *Nano Letters* **2005**, 5(7), 1237-1242.
16. Teranishi, T.; Miyake, M. *Chemistry of Materials* **1998**, 10(2), 594-600.
17. Thomas, P. J.; Kulkarni, G. U.; Rao, C. N. R. *Journal of Physical Chemistry B* **2000**, 104(34), 8138-8144.
18. Zhou, Y.; Itoh, H.; Uemura, T.; Naka, K.; Chujo, Y. *Langmuir* **2002**, 18(1), 277-283.
19. Scott, R. W. J.; Wilson, O. M.; Crooks, R. M. *Journal of Physical Chemistry B* **2005**, 109(2), 692-704.

20. Ganesan, M.; Freemantle, R. G.; Obare, S. O. *Chemistry of Materials* **2007**, 19(14), 3464-3471.
21. Horinouchi, S.; Yamanoi, Y.; Yonezawa, T.; Mouri, T.; Nishihara, H. *Langmuir* **2006**, 22(4), 1880-1884.
22. Hiramatsu, H.; Osterloh, F. E. *Chemistry of Materials* **2004**, 16(13), 2509-2511.
23. Aslam, M.; Fu, L.; Su, M.; Vijayamohanan, K.; Dravid, V. P. *Journal of Materials Chemistry* **2004**, 14, 1795-1797.
24. Yang, Z.; Klabunde, K. J.; Sorensen, C. M. *Journal of Physical Chemistry C* **2007**, 111(49), 18143-18147.
25. Capdevielle, P.; Lavigne, A.; Sparfel, D.; Baranne-Lafont, J.; Nguyen, K. C.; Maumy, M. *Tetrahedron Letters* **1990**, 31(23), 3305-3308.
26. Shon, Y. S.; Dawson, G. B.; Porter, M.; Murray, R.W. *Langmuir* **2002**, 18(10), 3880-3885.
27. Samia, A. C. S.; Hyzer, K.; Schlueter, J. A.; Qin, C.-J.; Jiang, J. S.; Bader, S. D.; Lin, X.-M. *Journal of the American Chemical Society* **2005**, 127(12), 4126-4127.

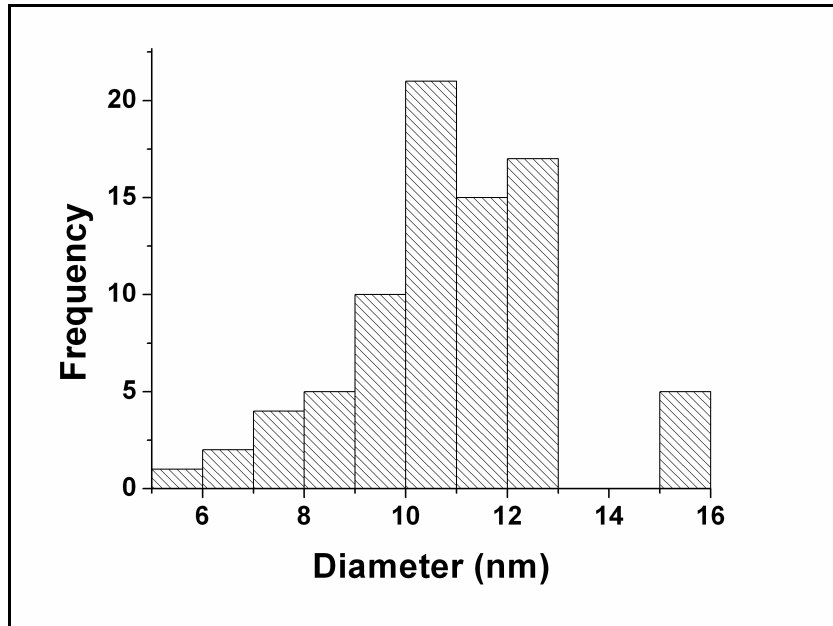
4.6 Supporting Information



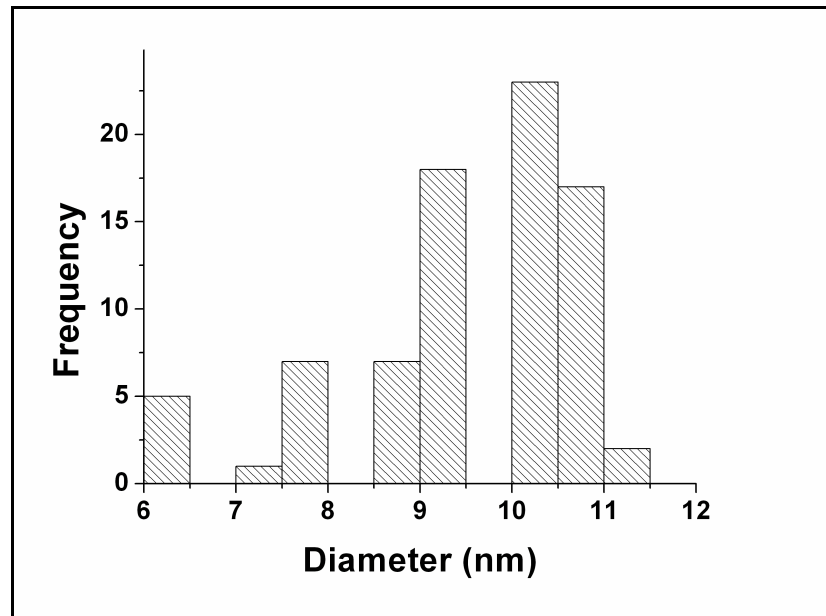
Figure 4.S1. Different appearance of the as-synthesized samples. The molar ratios of TOP to Pd(II) were 0, 0.4, 0.6, 1.0, 1.4, and 2.0 from left to right.



B



C



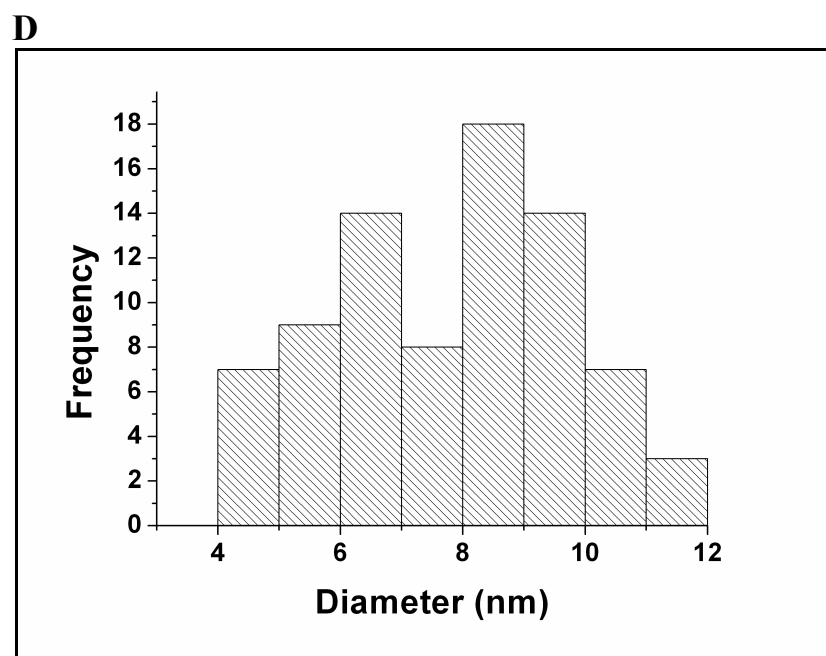


Figure 4.S2. Histograms indicating the size distribution. (A) Sample (0.4 ×), diameter = 10.7 ± 2.9 nm; (B) Sample (0.6 ×), diameter = 10.8 ± 2.0 nm; (C) Sample (1.0 ×), diameter = 9.5 ± 1.2 nm; (D) Sample (1.4 ×), diameter = 7.6 ± 1.9 nm. For each sample, 80 particles were measured.

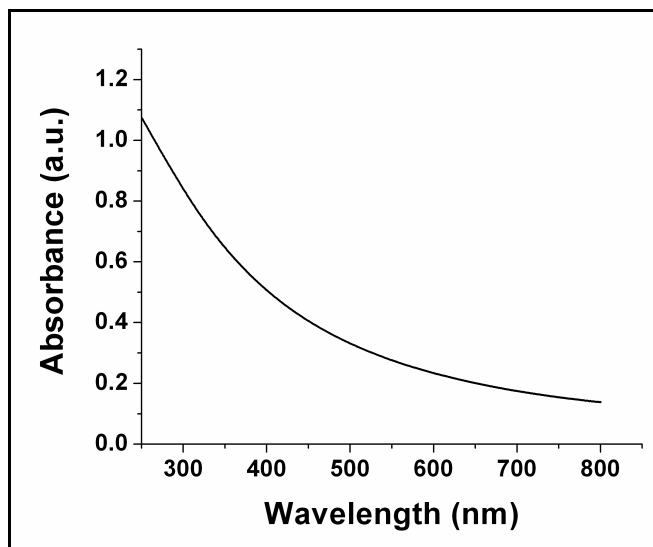


Figure 4.S3. UV/vis absorbance of Sample (1.0 ×) after wash. For the measurement, the washed sample was redissolved in hexane, and hexane was used as the reference.

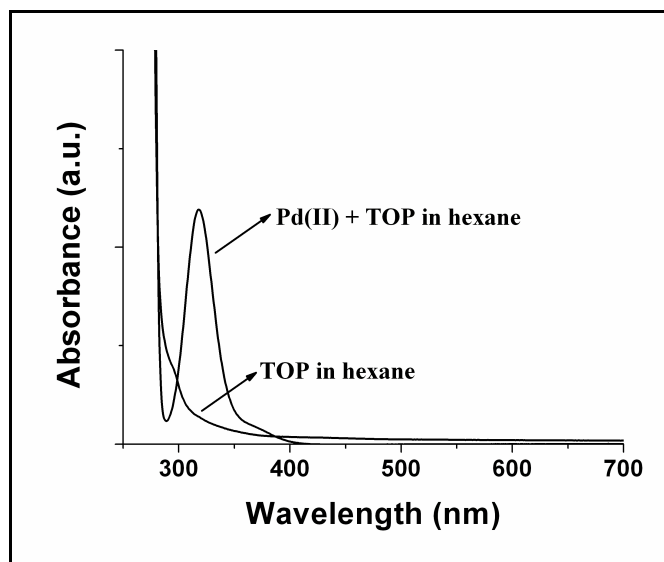


Figure 4.S4. UV/vis absorbance to show the generation of Pd(II)-TOP complexes at room temperature. Reference: hexane.

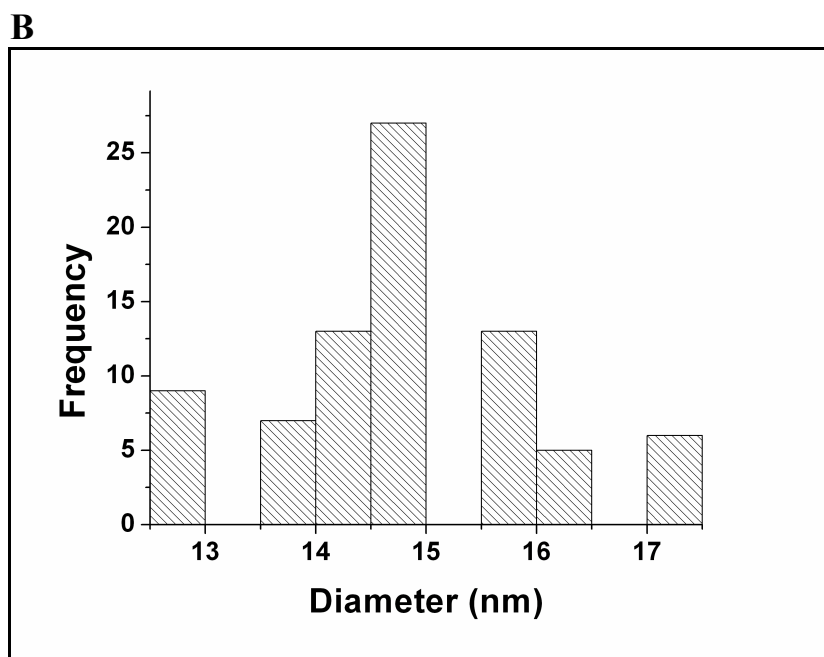
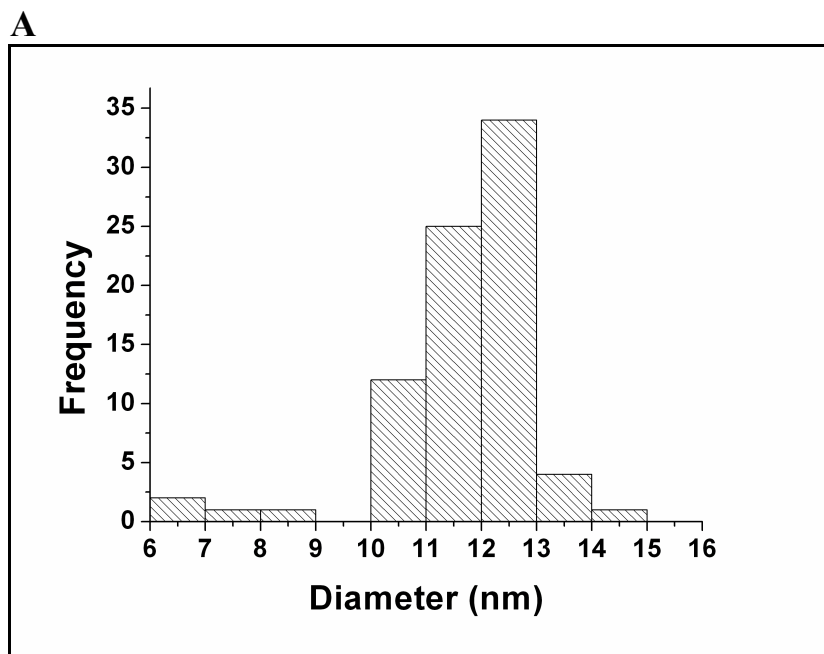


Figure 4.S5. Histograms indicating the size distribution for the sample prepared according to Sample (0.6 ×) except increasing the molar ratio of oleylamine to Pd(II) to 60. (A) Boiling for 1 h, diameter = 11.6 ± 1.4 nm; (B) Boiling for 17 h, diameter = 14.9 ± 1.2 nm. For each sample, 80 particles were measured.

CHAPTER 5 - An unusual fluorescence evolution of cadmium selenide (CdSe) nanoparticles generated from a cadmium oxide / trioctylphosphine selenide / trioctylphosphine heterogeneous system

5.1 Introduction

Among all the semiconductor quantum dots, cadmium selenide (CdSe) particles have been investigated intensively due to their size-dependent luminescent properties and the related applications in bio-labeling^{1, 2} and other light-emitting devices.³⁻⁵ To make high quality CdSe nanoparticles with tunable sizes and controllable fluorescence properties, a variety of synthetic routes have been established. The most common protocol is to grow CdSe nanoparticles from hot organic solvents containing protecting ligands. Murray and co-workers first reported the synthesis of nearly monodisperse CdE (E = S, Se, Te) semiconductor nanocrystallites by using dimethyl cadmium ($\text{Cd}(\text{CH}_3)_2$) as the cadmium source and trioctylphosphine (TOP)/trioctylphosphine oxide (TOPO) as the capping agents.⁶ Because $\text{Cd}(\text{CH}_3)_2$ is volatile, unstable, and highly toxic, other cadmium sources have been eagerly explored since then. Compared with $\text{Cd}(\text{CH}_3)_2$, more complicated and stable organometallic cadmium precursors⁷ or even single-source precursors composed of both cadmium and selenium^{8, 9} have been specially synthesized and applied to prepare CdSe nanoparticles. On the other hand, the preparation could be conducted more readily by using simple cadmium sources such as CdO plus some

organic acids. For example, Peng et al. applied CdO along with hexylphosphonic acid or tetradecylphosphonic acid to synthesize high-quality CdSe nanocrystals.¹⁰ In this case, soluble cadmium-phosphonic acid complexes were generated first, which then reacted with trioctylphosphine selenide (TOPSe) to generate CdSe nanoparticles. Other organic acids with long C-chains such as stearic acid and oleic acid were also successfully employed.¹¹⁻¹⁵ In addition to the routes using high-boiling-point organic solvents, CdSe nanoparticles could also be prepared from aqueous phase,¹⁶ water-oil interface,¹⁷ or continuous aerosol flow.¹⁸

It's well known that, the fluorescence properties of CdSe nanoparticles are greatly influenced by the particle size. When the particle size increases, the band edge emission red-shifts to lower energies. On the other hand, due to the high surface to volume ratio of CdSe quantum dots, the fluorescence properties are also considerably affected by the surface-related defects or traps, which insert extra electronic states in the band gap and then result in the red-shift of the band edge emission and the broadening of the photoluminescence (PL) peak.

A continual red-shift of the fluorescence peak of CdSe quantum dots during the reaction period is often observed, which is mostly due to the quick growth of the particle size under the applied experimental conditions. Also due to the quick growth, the investigation of the PL evolution during the early reaction stages is very difficult and is usually not explored.^{19, 20}

Here we present a strategy to prepare CdSe nanoparticles directly from commercially available CdO powder in a heterogeneous system without using any acids. Only three starting materials (CdO, Se, and TOP) were engaged. Compared to other methods using homogeneous liquid phase, the growth of CdSe nanoparticles under our experimental conditions was relatively slow. As a result, an unusual fluorescence evolution of CdSe nanoparticles, i.e., the blue-shift of the fluorescence peak in the early reaction periods, could be observed over a long time span. This phenomenon is attributed to the gradual removal of the surface defects/traps during the slow growth and crystallization of the particles.

5.2 Experimental Section

5.2.1 Materials

Cadmium oxide (CdO, 99.998%) was purchased from Alfa Aesar, A Johnson Matthey Co. Trioctylphosphine ($\text{CH}_3(\text{CH}_2)_7\text{P}$, 90%) and selenium powder (Se, 99.99%) were bought from Aldrich Chem. Co. Other chemicals were purchased and used as received.

5.2.2 Preparation of CdSe nanoparticles from CdO/TOPSe/TOP system

A typical experiment is described as follows. In a glass tube, 0.128 g of CdO powder (ca. 1×10^{-3} mol) was added into 5 mL of TOP. The tube was then equipped with a rubber septum, which was connected to a vacuum line and an argon gas-tank through needles. Then, the mixture was degassed and then flushed with argon several times. After that, it was preheated in a hot sand-bath (ca. 320 °C). In another glass vial,

0.160 g (ca. 2×10^{-3} mol) of black Se powder was dissolved into 5 mL of TOP by supersonic vibration to form a clear solution with a slightly yellow color. Then, the TOPSe/TOP solution was quickly injected into the hot CdO/TOP mixture. The resulting mixture was then heated at 320 °C under the protection of argon for 4 h. The solution's color changed gradually to dark brown, which indicated the formation of CdSe nanoparticles. In order to track the changes in particle size and the optical properties, aliquots (0.4 mL of solution) were taken out using needles and syringes during the reaction. The collected samples were washed with acetone several times and then redispersed in hexane. Then another centrifugation was conducted to remove unreacted CdO. After these treatments, stable CdSe colloidal solutions in hexane were obtained and ready for further analysis.

5.2.3 Equipment and analysis

Fluorescence properties were measured by using a Fluoro Max-2 instrument from HORIBA Jobin Yvon Company. The samples were all excited at 400 nm. UV/vis absorption analysis was carried out on a Cary 500 UV-VIS-NIR spectrophotometer. Transmission electron microscopy (TEM) was performed on a Philips CM100 microscope operated at 100 kV. To prepare a TEM sample, a drop of colloidal solution was dropped onto a carbon-coated Formvar copper grid and then allowed to dry in air. Powder X-ray diffraction (XRD) patterns were recorded by a Bruker D8 X-ray diffractometer with Cu K α radiation.

5.3 Results and discussion

5.3.1 The fluorescence evolution at 320 °C

Before injecting TOPSe/TOP, it has been observed that CdO could not be dissolved into TOP. It remained as brown precipitates lying on the bottom of the reactor and no reaction could be noticed even if the system was heated at 320 °C for up to 5 h. After injecting TOPSe/TOP, the color of the solution gradually turned to yellow, then to brown, with the disappearance of solid CdO. After being heated at 320 °C for 4 h, a stable dark-brown-colored colloid solution was generated. The powder XRD pattern of the solid only showed the peaks for CdSe nanocrystallites with wurtzite structure, and no peaks for CdO could be found (Figure 5.1). So, this heterogeneous reaction was assumed to occur according to the following equation: CdO (solid) + TOPSe/TOP (liquid) → CdSe (nanoparticles) + TOPO/TOP (liquid).

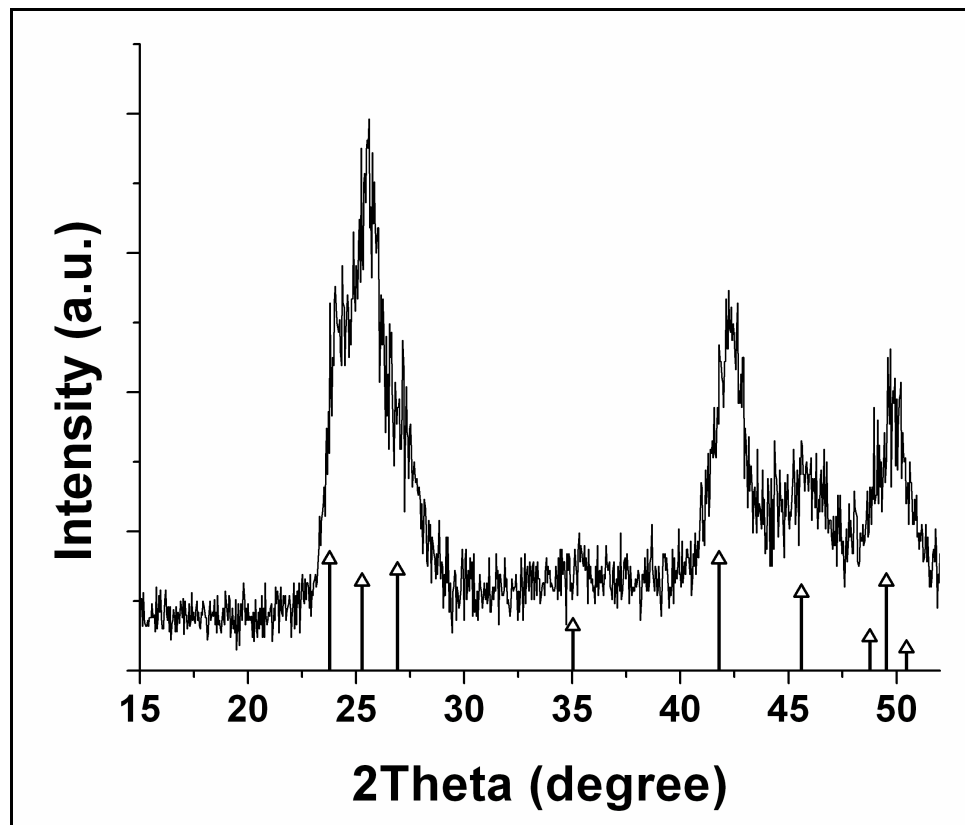


Figure 5.1. Powder XRD pattern of the sample collected after heating at 320 °C for 4 h to show the generation of CdSe nanocrystallites with wurtzite structure. The standard pattern (vertical lines) is drawn according to JCPDS file No. 02-0330.

During the reaction, a series of samples were collected after certain time intervals. The samples could be precipitated out of solution by adding polar solvents such as acetone or ethanol. And they were readily redissolved into nonpolar solvents such as hexane or toluene. These phenomena indicate that the particles are protected by certain organic ligands, which must be TOP/TOPO (generated from the reaction). Figure 5.2 shows the temporal evolution of the particle's morphology. For all the samples, it has been found that the particle's shape is not perfect spherical, but kind of irregular with some crystal-like facets. And the particles are well separated from one another, which further confirms the existence of the protecting ligands. According to the images, the average size increases quickly in the early periods (0.5 h: 4.3 nm; 1 h: 7.2 nm), then more slowly to 7.8 nm after 4h.

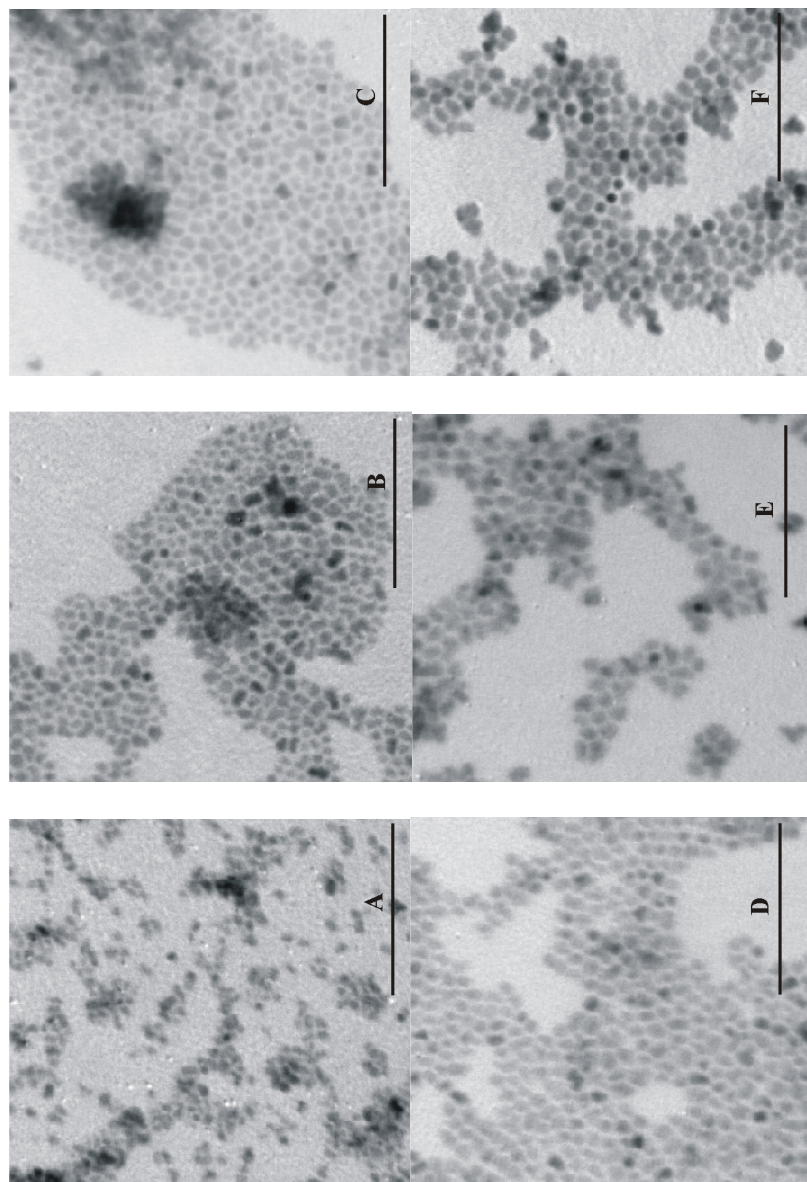


Figure 5.2. TEM images to show the temporal evolution of CdSe nanoparticles. A: 0.5 h; B: 1 h; C: 1.5 h; D: 2 h; E: 3 h; F: 4 h. scale bar = 100 nm. Heating temperature: 320 °C.

The temporal fluorescence evolution of the obtained CdSe nanoparticles is shown in Figure 5.3. After heating for 0.5 h, the sample has a relatively broad fluorescence peak centered at 628 nm. This peak blue-shifts to 612 nm and becomes narrow after 1h. Then, it continually red-shifts to 671 nm and becomes much narrower (full width of half-maximum (FWHM) = 39 nm) after 4h. Figure 5.4 clearly indicates both the shifting and the narrowing of the fluorescence peak along with the heating time.

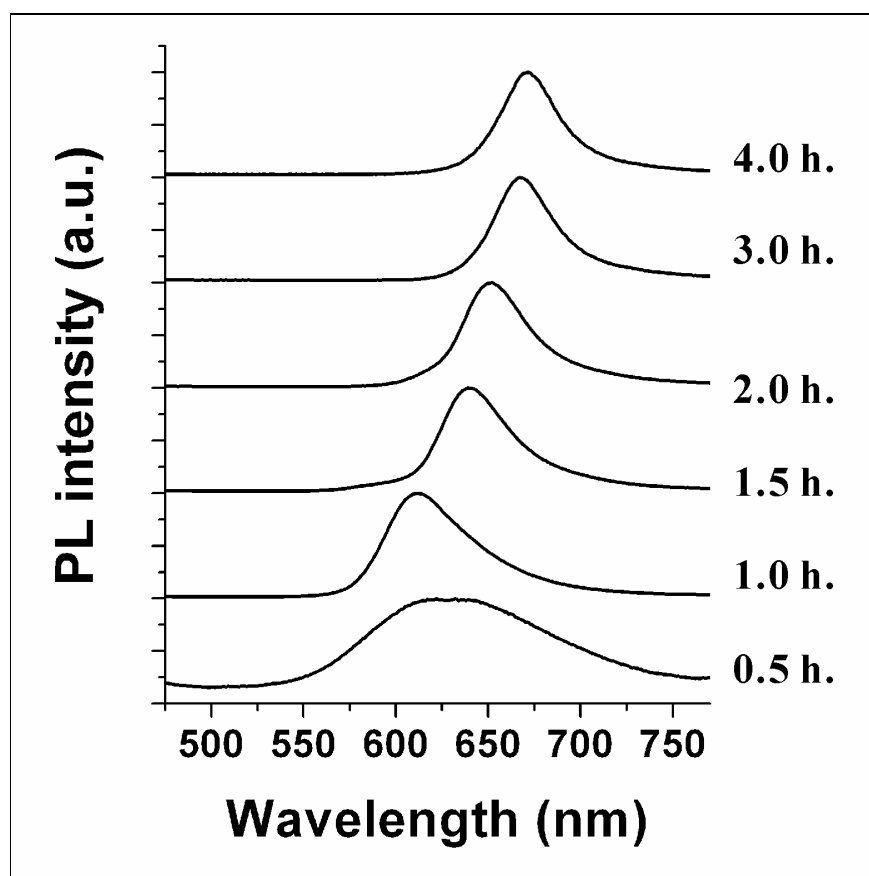


Figure 5.3. Photoluminescence (PL) evolution of CdSe nanoparticles. Heating temperature: 320 °C.

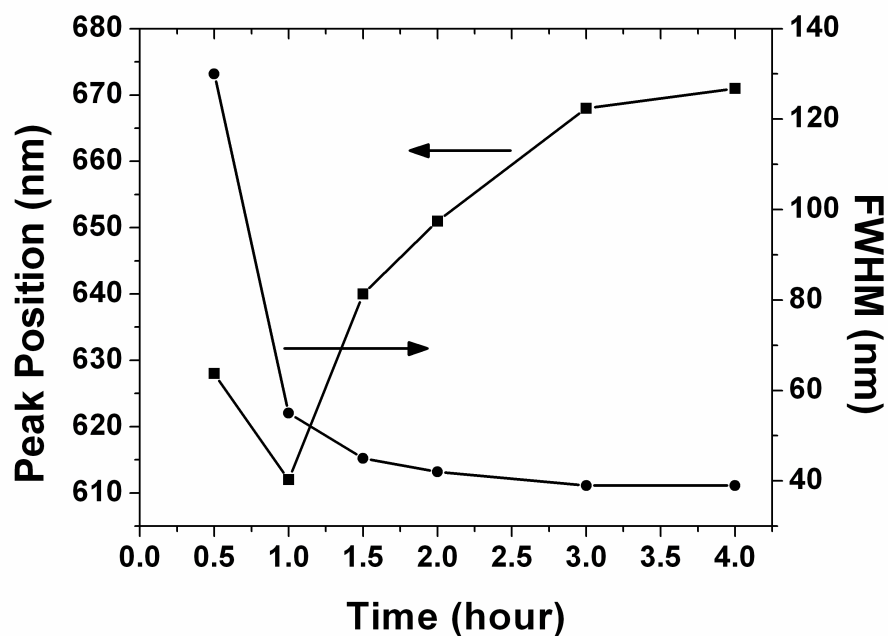


Figure 5.4. Changes of the PL peak position (labeled with solid squares) and the full width of half-maximum (FWHM, labeled with solid circles) as the function of heating time. Heating temperature: 320 °C.

The UV/vis absorbance patterns of the obtained samples are shown in Figure 5.5. No peak is observable for the sample heated for 0.5 h. For other samples, broad peaks are noticeable and red-shift continually (1.0 h: 608 nm; 1.5 h: 632 nm; 2.0 h: 646 nm; 3.0 h: 654 nm; 4.0 h: 666 nm).

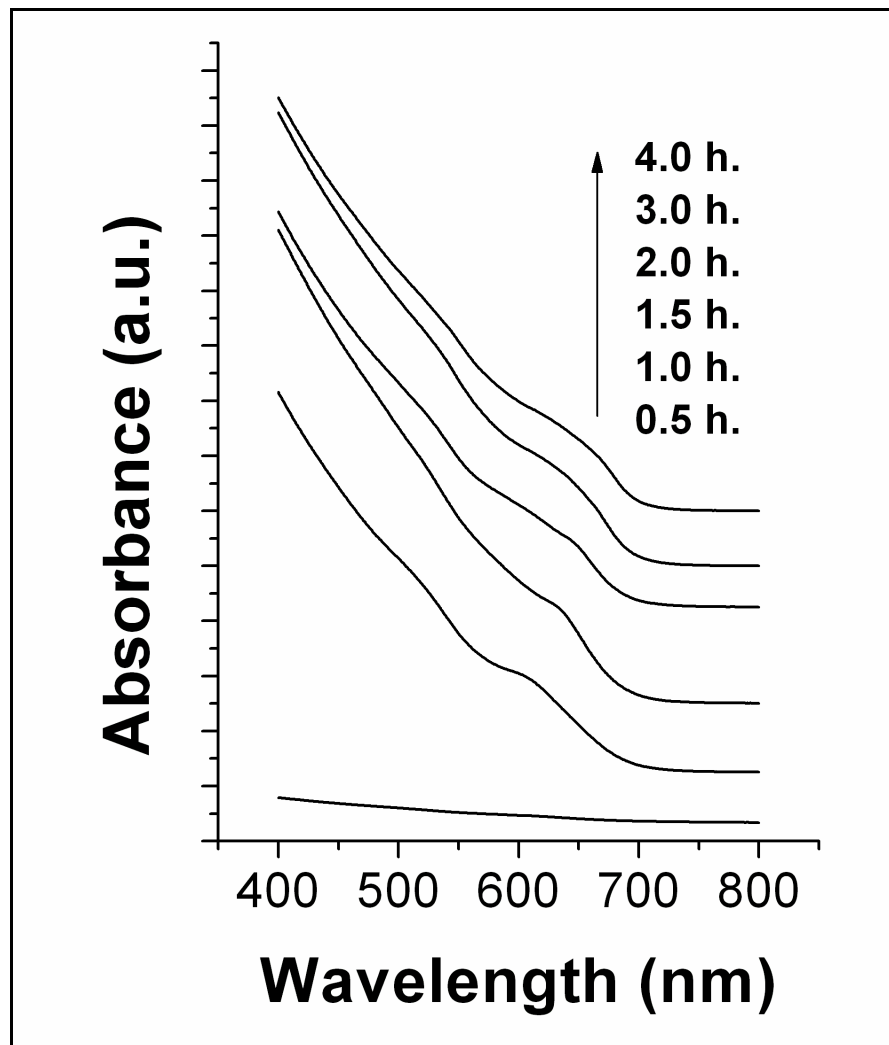


Figure 5.5. UV/vis absorbance patterns of the obtained samples.

5.3.2 The fluorescence evolution at 270 °C

Compared with the continual red-shift of the fluorescence peak generally reported by other researchers, the blue-shift during the early stages in our results is very interesting. To further investigate this phenomenon, another experiment was conducted at 270 °C instead of 320 °C. The fluorescence evolution at this lower temperature is shown in Figure 5.6.

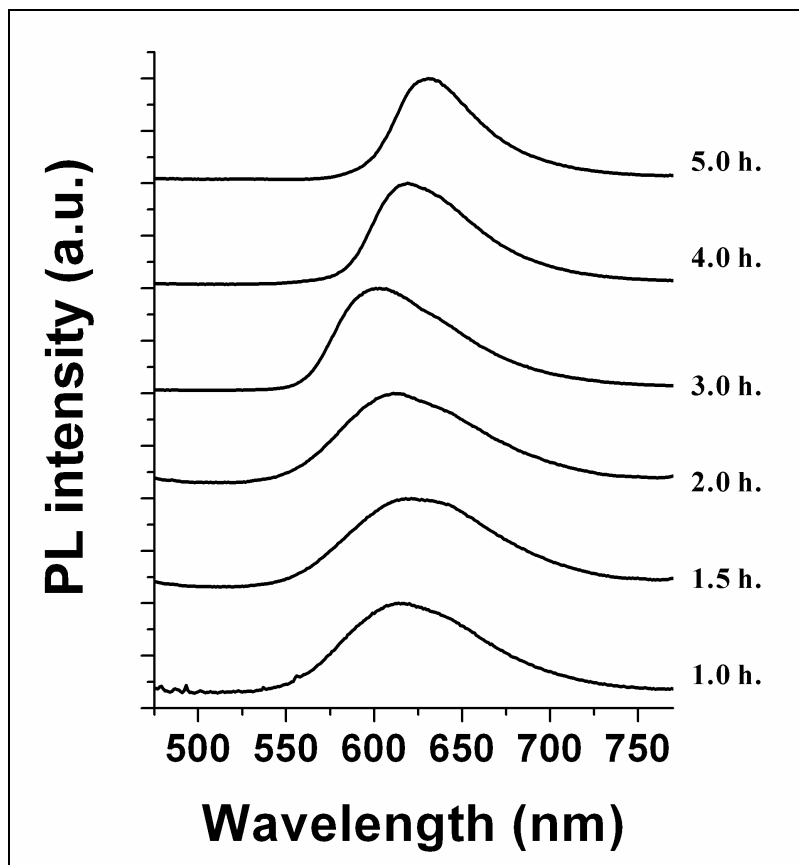


Figure 5.6. Temporal fluorescence evolution of CdSe nanoparticles. Heating temperature: 270 °C.

The changes in the peak position and the FWHM value are shown in Figure 5.7. After 1h, the sample shows a broad fluorescence peak centered at 614 nm. This peak first red-shifts to 621 nm after 1.5 h. Then it blue-shifts to 611 nm after 2 h and 601 nm after 3 h. After that, it begins to red-shift to 619 nm after 4 h, and then to 631 nm after 5 h. Also, unlike the continual narrowing occurred at 320 °C, the fluorescence peak becomes slightly broad after 1.5 h, and then it undergoes continual narrowing.

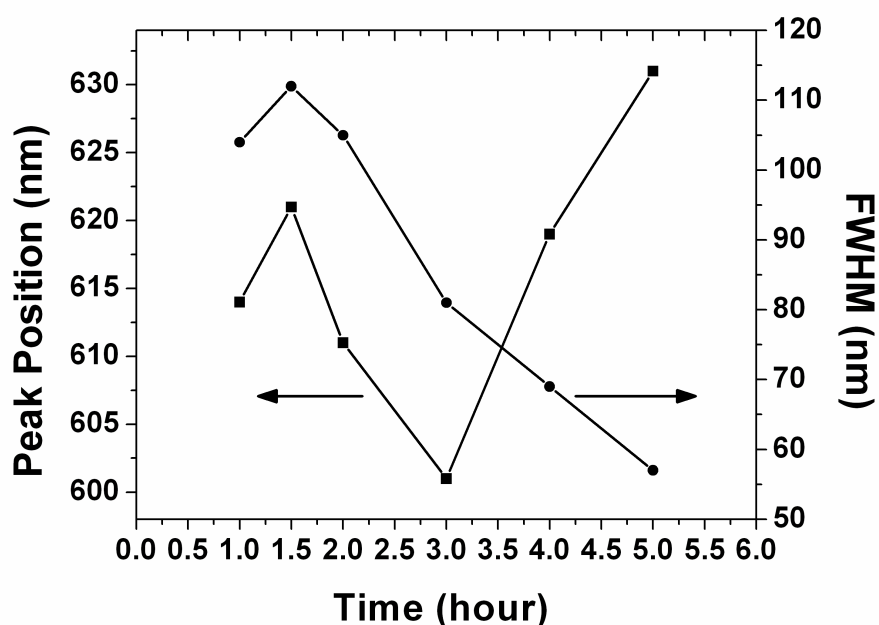


Figure 5.7. Changes of the peak position (labeled with solid squares) and the full width of half-maximum (FWHM, labeled with solid circles) as the function of heating time. Heating temperature: 270 °C.

5.3.3 Discussion

As mentioned previously, the fluorescence emission is influenced by both the particle size and the surface states. When heated at 320 °C, the broadness of the PL peak after 0.5 h is mostly due to the existence of a plenty of surface states, since the particle size is relatively narrow according to the TEM image. Also due to the surface states, this peak has been red-shifted from the band edge emission to a considerable extent. After 1h, the particle size increases from 4.3 nm to 7.2 nm. If only considering the size effect, the PL peak should red-shift. But, because the particles have been heated for a long time and become bigger, they have the chance to rearrange the surface atoms and most of the surface states disappear. As a result, the PL peak blue-shifts to a position close to the band edge emission and becomes much narrower. After that, the constant red-shift of the PL peak is attributed to the continual increase of the particle size.

When heated at 270 °C, the CdSe particles grow at a lower rate and the removal of the surface states also becomes slower. So, it takes a long time (up to 3 h) for the PL peak blue-shifting from a surface-state-dominated emission to an intrinsic-state-dominated emission.

5.4 Conclusions

The generation of CdSe nanoparticles from a CdO/TOPSe/TOP heterogeneous system has been investigated. A very convenient synthesis method has been developed. Also, unusual fluorescence evolutions have been observed at two different reaction temperatures. These phenomena are attributed to the slow removal of surface states due

to atom rearrangements and crystallization. The results and discussion presented herein are helpful for us to further understand the PL evolution of CdSe quantum dots, especially during the early stages.

5.5 References

- (1) Bruchez, M.; Moronne, M.; Gin, P.; Weiss, S.; Alivisatos, A. P. *Science* **1998**, 281, 2013.
- (2) Dubertret, B.; Skourides, P.; Norris, D. J.; Noireaux, V.; Brivanlou, A. H.; Libchaber, A. *Science* **2002**, 298, 1759.
- (3) Zhao, J.; Bardecker, J. A.; Munro, A. M.; Liu, M. S.; Niu, Y.; Ding, I.-K.; Luo, J.; Chen, B.; Jen, A. K.-Y.; Ginger, D. S. *Nano Letter* **2006**, 6, 463.
- (4) Caruge, J.-M.; Halpert, J. E.; Bulovic, V.; Bawendi, M. G. *Nano Letter* **2006**, 6, 2991.
- (5) Achermann, M.; Petruska, M. A.; Koleske, D. D.; Crawford, M. H.; Klimov, V. I. *Nano Letter* **2006**, 6, 1396.
- (6) Murray, C. B.; Norris, D. J.; Bawendi, M. G. *J. Am. Chem. Soc.* **1993**, 115, 8706.
- (7) Hambrock, J.; Birkner, A.; Fischer, R. A. *J. Mater. Chem.* **2001**, 11, 3197.
- (8) Malik, M. A.; Revaprasadu, N.; O'Brien, P. *Chem. Mater.* **2001**, 13, 913.
- (9) Cumberland, S. L.; Hanif, K. M.; Javier, A.; Khitrov, G. A.; Strouse, G. F.; Woessner, S. M.; Yun, C. S. *Chem. Mater.* **2002**, 14, 1576.
- (10) Peng, Z. A.; Peng, X. *J. Am. Chem. Soc.* **2001**, 123, 183.
- (11) Qu, L.; Peng, X. *J. Am. Chem. Soc.* **2002**, 124, 2049.
- (12) Bullen, C. R.; Mulvaney, P. *Nano Lett.* **2004**, 4, 2303.

- (13) Liu, H.; Owen, J. S.; Alivisatos, A. P. *J. Am. Chem. Soc.* **2007**, 129, 305.
- (14) Embden, J. V.; Mulvaney, P. *Langmuir* **2005**, 21, 10226.
- (15) Dai, Q.; Li, D.; Chen, H.; Kan, S.; Li, H.; Gao, S.; Hou, Y.; Liu, B.; Zou, G. *J. Phys. Chem. B* **2006**, 110, 16508.
- (16) Palaniappan, K.; Xue, C.; Arumugam, G.; Hackney, S. A.; Liu, J. *Chem. Mater.* **2006**, 18, 1275.
- (17) Pan, D.; Wang, Q.; Jiang, S.; Ji, X.; An, L. *J. Phys. Chem. C* **2007**, 111, 5661.
- (18) Didenko, Y. T.; Suslick, K. S. *J. Am. Chem. Soc.* **2005**, 127, 12196.
- (19) Bowers II, M. J.; McBride, J. R.; Rosenthal, S. J. *J. Am. Chem. Soc.* **2005**, 127, 15378.
- (20) Chen, X.; Samia, A. C. S.; Lou, Y.; Burda, C. *J. Am. Chem. Soc.* **2005**, 127, 4372.

CHAPTER 6 - Synthesis of magnesium oxychloride nanorods with controllable morphology and their transformation to magnesium hydroxide nanorods via treatment with sodium hydroxide

6.1 Introduction

At the present time considerable efforts have been made to synthesize one-dimensional (1D) nanostructures such as nanorods, nanowires, nanobelts and nanotubes. Because they have two quantum-confined dimensions (the radial directions) and one unconfined dimension (the axial direction), such 1D nanostructures may have a unique density of electronic states, which result in different optical, electronic, and magnetic properties compared to their bulk, two-dimensional (quantum wells), or 0-dimensional (quantum dots) counterparts. A variety of synthetic strategies have been established to obtain 1D nanostructures by using templates,¹⁻³ vapor-liquid-solid method,^{4, 5} solution-liquid-solid method,^{6, 7} capping-agent-directed growth,^{8, 9} intrinsically anisotropic growth without using any surfactants,^{10, 11} etc.

As important components in Sorel cement, magnesium oxychlorides ($\text{Mg}_x(\text{OH})_y\text{Cl}_z \cdot n\text{H}_2\text{O}$, also called hydrated basic magnesium chlorides) were first reported in 1867.¹² When mixing appropriate amounts of MgO, MgCl_2 , and H_2O

together, white marble-like materials can be obtained after solidification, which is due to the formation of a network of needle-like crystalline magnesium oxychlorides.¹³ As a result of good mechanical properties, good insulating ability, low thermal conductivity, and good fire resistance, such materials have a rather wide range of applications in coatings, binders, cements, and other architectural materials.¹⁴⁻¹⁶ Also, intensive studies have been performed in order to understand the chemical reactions and the phase equilibria in the system MgO-MgCl₂-H₂O.¹⁷⁻²² It is known that, at room temperature, three crystalline products can form in such a system, including 5Mg(OH)₂·MgCl₂·8H₂O (phase 5), 3Mg(OH)₂·MgCl₂·8H₂O (phase 3) and Mg(OH)₂. While at elevated temperature (for example, above 70 °C), other two crystalline magnesium oxychlorides, i.e., 2Mg(OH)₂·MgCl₂·4H₂O (phase 2) and 9Mg(OH)₂·MgCl₂·5H₂O (phase 9) can be obtained.^{23,24}

The previous studies in the system MgO-MgCl₂-H₂O were mainly focused on the chemical reactions and the phase equilibria. Few data about the morphology of the generated magnesium oxychlorides could be found in the literature. In our early paper, we reported the influence of different MgO samples (different crystal size and surface area) on the growth and the morphology of magnesium chloride nanorods.²⁵ In the present study, the influence of the concentrations of the starting materials is discussed in detail. Also, the transformation of the obtained magnesium oxychloride nanorods to Mg(OH)₂ nanorods via NaOH treatment at room temperature is presented.

6.2 Experimental section

6.2.1 Materials

Magnesium chloride hydrate ($\text{MgCl}_2 \cdot 6\text{H}_2\text{O}$, certified A.C.S. crystals, Fisher), magnesium oxide (MgO , 325 mesh, >99%, Sigma), and other chemicals were purchased and used as received.

6.2.2 Preparation of magnesium oxychlorides

The procedures for the preparation of samples A-F are described as follows. In Erlenmeyer flasks, different amounts of $\text{MgCl}_2 \cdot 6\text{H}_2\text{O}$ were dissolved in 48 mL (2.67 mol) of distilled water. Then, 4 g of MgO (0.10 mol) was added quickly while stirring the solutions violently. The surface area and the crystal size of this oxide were measured to be $45 \text{ m}^2/\text{g}$ and 23 nm.²⁵ The amounts of the applied starting materials and the experimental conditions are listed in Table 6.1. For sample A, the stirring was turned off manually after 8 h. For samples B-F, stirring stopped naturally when the suspensions became pastes (gelation process) that were too thick to be stirred anymore. After the stirring stopped, all the samples (sealed by rubber stoppers) were aged at room temperature on the bench up to 72 h after the addition of MgO . After aging, the samples were washed with water and ethanol several times. Dried powder could be obtained by heating the sample at 80 °C overnight. For example, 8.8 g of dry powder was obtained from sample D. The yield is 64% based on MgO . Sample G to sample M were prepared similarly to samples A-F.

6.2.3 Transformation of $\text{MgCl}_2 \cdot 6\text{H}_2\text{O}$ nanorods to $\text{Mg}(\text{OH})_2$ nanorods

Sample D was used as the model to describe the conversion of magnesium oxychloride to $\text{Mg}(\text{OH})_2$ by treated with NaOH solution. For this purpose, the wet filter cake from sample D after washing was applied directly without drying. The cake was redispersed into a solution of 24 g of NaOH dissolved in water (100 mL) and ethanol (300 mL). The conversion was carried out in a sealed flask at room temperature for 12 h with moderate stirring. The product was then collected by filtration and washed with water and ethanol. After dried at 80 °C overnight, 13.4 g of $\text{Mg}(\text{OH})_2$ powder was obtained. The yield was about 100%.

6.2.4 Equipment and analysis

Transmission electron microscopy (TEM) was performed on a Philips CM100 microscope operated at 100 kV. To prepare a TEM sample, the washed products were redispersed into ethanol and then a drop of suspension was dropped onto a carbon/Formvar co-coated copper grid, which was then allowed to dry in air. Powder X-ray diffraction (XRD) patterns were recorded by a Bruker D8 X-ray diffractometer with $\text{Cu K}\alpha$ radiation.

Table 6.1. Experimental conditions for the synthesis of magnesium oxychlorides

Expt. No.	MgO (g)	MgCl ₂ .6H ₂ O (g)	Water (mL)	Length (μm)	Width (μm)	Aspect Ratio
A	4	27.12	48	NA*	NA	NA
B	4	40.68	48	4.1±1.6	0.3±0.1	18.1±12.4
C	4	54.24	48	8.5±4.4	0.9±0.6	12.5±10.1
D	4	67.80	48	7.2±2.6	0.5±0.2	16.9±9.7
E	4	81.36	48	6.9±3.4	0.5±0.2	17.6±12.2
F	4	135.60	48	4.5±2.4	0.3±0.1	17.7±10.2
G	4	54.24	96	NA	NA	NA
H	4	81.36	96	6.2±2.6	0.6±0.2	13.2±8.0
I	4	108.48	96	8.7±3.6	1.1±0.4	8.7±5.0
J	4	135.60	96	8.3±2.9	0.9±0.4	10.6±6.4
K	4	162.72	96	7.1±1.8	0.6±0.3	14.0±7.0
L	4	6.78	6	0.7±0.2	~ 0.01	~ 70
M	4	20.34	12	3.0±1.0	~ 0.09	~ 35

*NA: not available

6.3 Results and discussion

6.3.1 Synthesis of magnesium oxychloride nanorods

From sample A to sample F, the quantity of $\text{MgCl}_2 \cdot 6\text{H}_2\text{O}$ was changed systematically while fixing the amounts of the other two starting materials (MgO : 4 g; H_2O : 48 mL) to indicate the influence on the final products. After the addition of MgO , at first, all the samples formed white suspensions and could be stirred smoothly. Then, with samples B-F, the suspensions became more and more sticky, and at last, could not be stirred anymore. The time periods for this gelation process were 1.5, 2.0, 3.3, 4.0, 6.5 h for sample B to sample F, respectively. It shows that, for a larger amount of $\text{MgCl}_2 \cdot 6\text{H}_2\text{O}$, a longer time period was needed for the gelation. In the case of sample A, no obvious change in viscosity was observed with time, so the stirring was stopped manually after 8.0 h.

The XRD patterns and the TEM images of sample A to F are shown in Figure 6.1 and Figure 6.2, respectively.

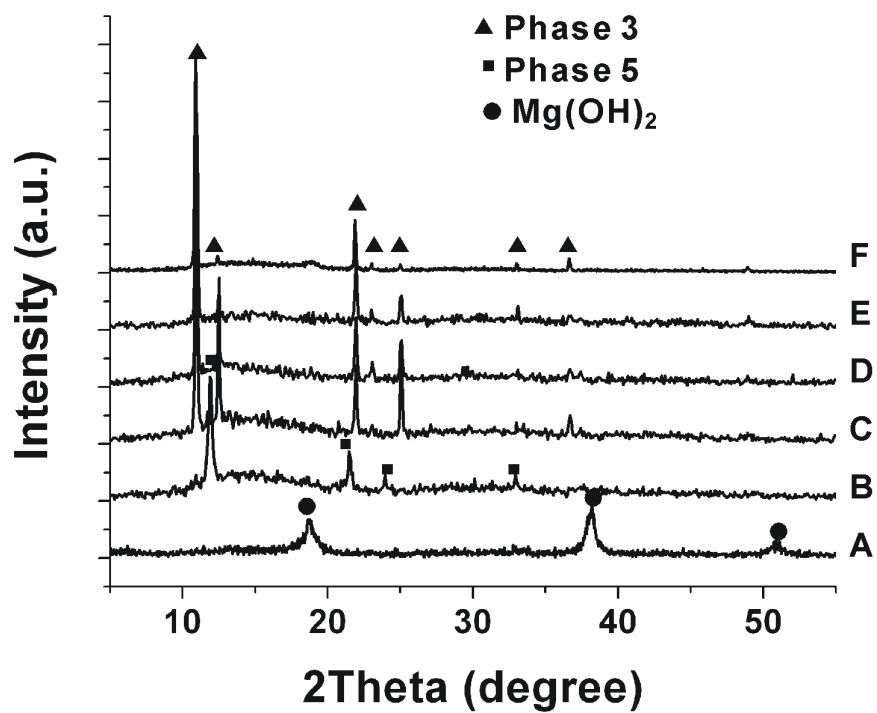


Figure 6.1. Powder XRD patterns of samples A-F (Exp. No. shown in Table 6.1). The peaks are appointed according to JCPDS file 73-2119 (phase 3), file 07-0420 (phase 5), and 75-1527 (Mg(OH)₂).

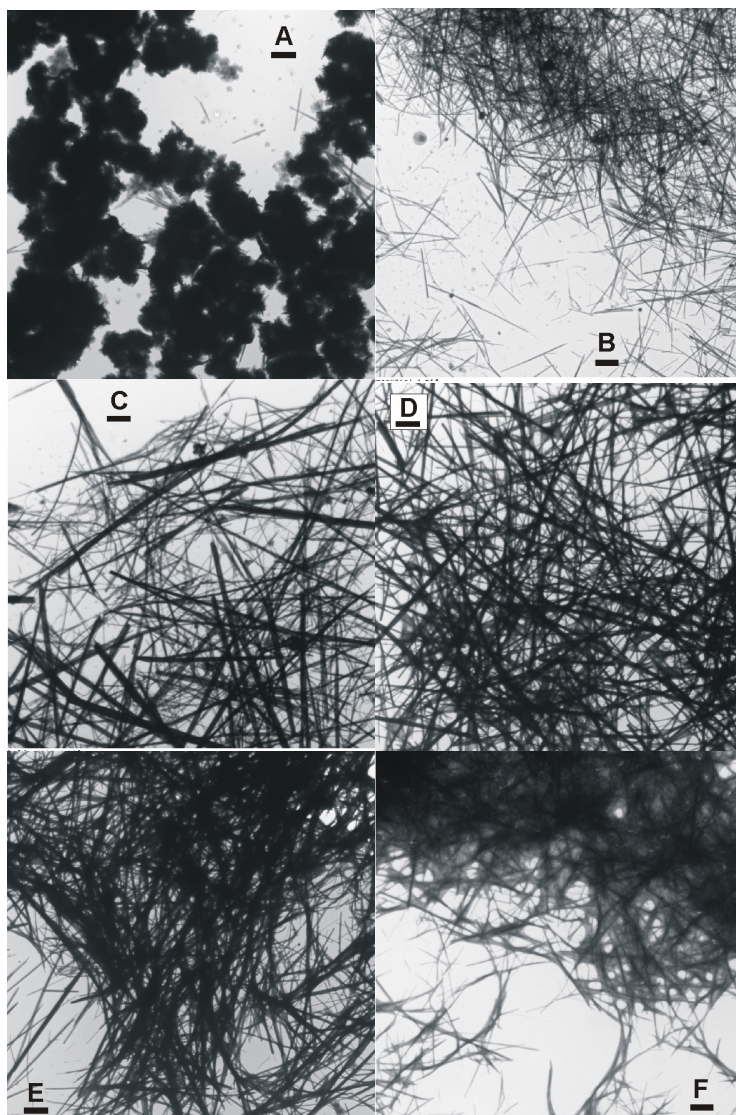
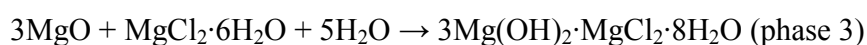
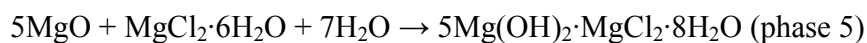


Figure 6.2. TEM images of samples A-F. The scale bar in each image is equal to 2 μm .

According to the results, it is obvious that the amount of $\text{MgCl}_2 \cdot 6\text{H}_2\text{O}$ is critical for the formation of magnesium oxychloride nanorods. At a low concentration of $\text{MgCl}_2 \cdot 6\text{H}_2\text{O}$, such as in sample A, $\text{Mg}(\text{OH})_2$ was obtained as the main product after aging; while at high concentrations, magnesium oxychloride nanorods were produced. Also, the crystalline phase of the products changed from phase 5 (sample B) to phase 3 (samples C-F) when the concentration of $\text{MgCl}_2 \cdot 6\text{H}_2\text{O}$ was increased. It is also notable that nanorods in sample B (phase 5) are much shorter and thinner than those in sample C (phase 3).

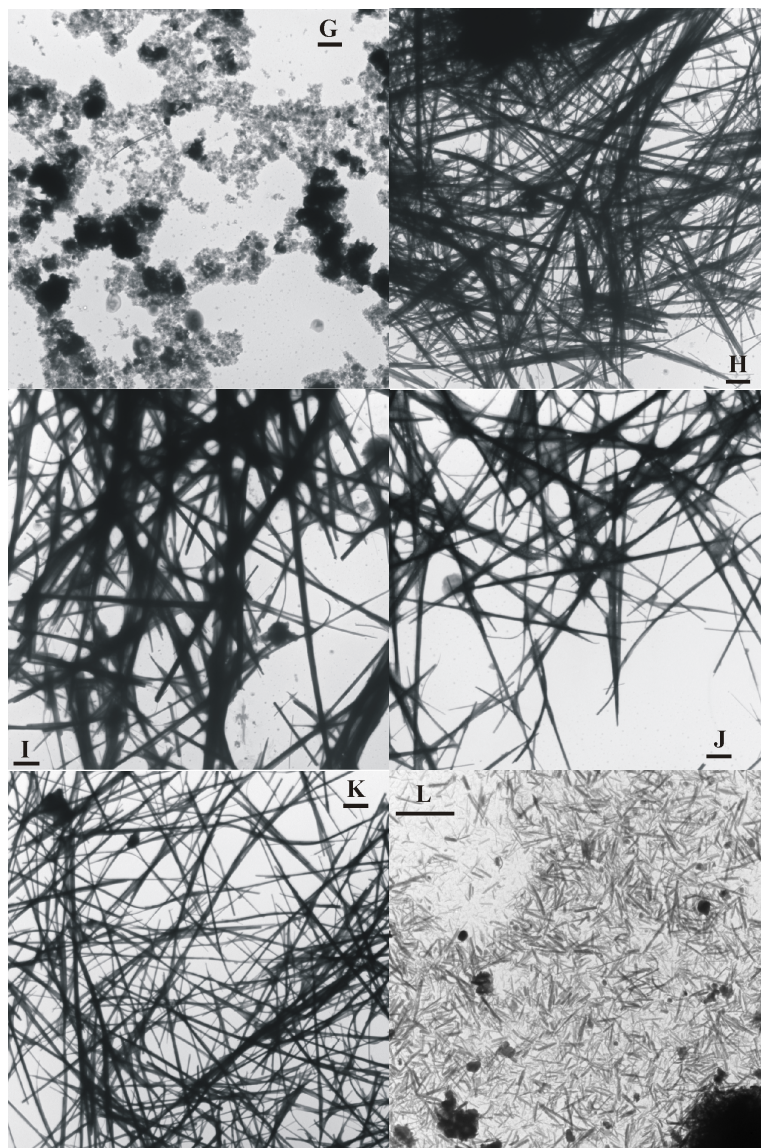
The mechanism of the formation of magnesium oxychlorides from the system $\text{MgO-MgCl}_2\text{-H}_2\text{O}$ and the preferable conditions for the crystallization of phase 5 or phase 3 have been investigated intensively in the literature, although there are very limited data on the morphology of the obtained products. The reactions begin with the dissolution of MgO in MgCl_2 aqueous solutions, and such a hydrolyzation process highly depends on the reactivity of MgO (related to crystalline size, surface area, etc.) and the concentration of MgCl_2 . It is facilitated by using MgO with high reactivity and MgCl_2 solutions with high concentrations.^{17, 18, 21} After the dissolution of MgO , the pH value of the mixture will increase. Then, in systems with inadequate MgCl_2 , $\text{Mg}(\text{OH})_2$ will form; while in the systems with high concentration of MgCl_2 , basic magnesium chloride crystals will grow slowly from gel-like supersaturated solutions. It has also been reported that, phase 5 is much easier to grow into crystals compared with phase 3, and the latter is generated from high concentration of MgCl_2 .²⁰ The overall reactions to form phase 5 and phase 3 in our systems can be expressed by the following equations:



The results obtained in our experiments are highly consistent with the reported results in the literature. In sample A, irregular aggregates of $\text{Mg}(\text{OH})_2$ were generated after aging due to the insufficient of MgCl_2 . When increasing the amount of magnesium salt, magnesium oxychloride nanorods were obtained and the crystal phase changed from phase 5 to phase 3. Also, due to the quick growth of phase 5 compared to phase 3 (which may result in more nucleation sites soon after the reaction begins), the nanorods in sample B (phase 5) were shorter and thinner than those in sample C (phase 3). When further increasing the concentration of MgCl_2 , the gelation of the systems and the crystallization of phase 3 were slowed down according to the experimental results. As a result, the nanorods decreased in both length and diameter from sample C to sample F.

In samples G-K, similar experiments were performed while increasing the added water to 96 mL. The same trend as in samples A-F was found. When increasing the amounts of $\text{MgCl}_2 \cdot 6\text{H}_2\text{O}$, the final products changed from irregular $\text{Mg}(\text{OH})_2$ aggregates to magnesium oxychloride nanorods. Typical TEM images for each sample are presented in Figure 6.3. The reason for the morphology changes of the nanorods in samples H-K could be assumed according to the discussion mentioned in samples A-F. Furthermore, when comparing these two series of experiments, it is noticeable that the nanorods in samples B-F are slightly shorter and thinner compared to the corresponding nanorods in samples H-K (for example, comparing sample B to sample H). These

results suggest that, using less water may result in smaller nanorods. To prove this assumption, sample L (6 mL of water added) and sample M (12 mL of water added) were carried out, and much shorter nanorods were obtained (Figure 6.3).



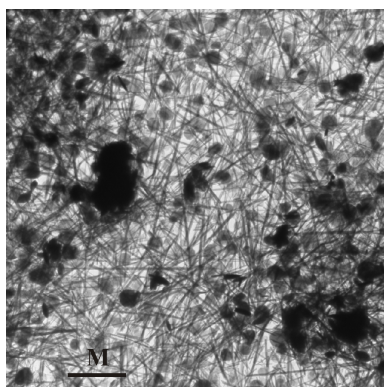


Figure 6.3. TEM images of samples G-M. The scale bar in each image is equal to 2 μm .

6.3.2 Conversion of magnesium oxychlorides to $\text{Mg}(\text{OH})_2$

As indicated by the literature, magnesium oxychloride nanorods can be transformed to $\text{Mg}(\text{OH})_2$ by basic treatment in water/ethanol mixed solvents at 60 $^\circ\text{C}$ with the rod-like morphology remained.²⁶ In addition, $\text{Mg}(\text{OH})_2$ nanotubes may be generated from magnesium oxychlorides nanorods via a solvothermal treatment using ethylenediamine.^{27, 28} In the present study, the transformation was carried out in water/ethanol solutions at room temperature for 12 h. The powder XRD pattern and the typical TEM picture of sample D after NaOH treatment are shown in Figure 6.4. The XRD pattern indicates that the conversion from magnesium oxychloride to $\text{Mg}(\text{OH})_2$ was quite complete, and the TEM image shows the retention of the rod-like morphology. The obtained $\text{Mg}(\text{OH})_2$ nanorods were $6.5 \pm 2.1 \mu\text{m}$ in length and 0.3 ± 0.1 in width, which were slightly shorter and thinner compared to sample D.

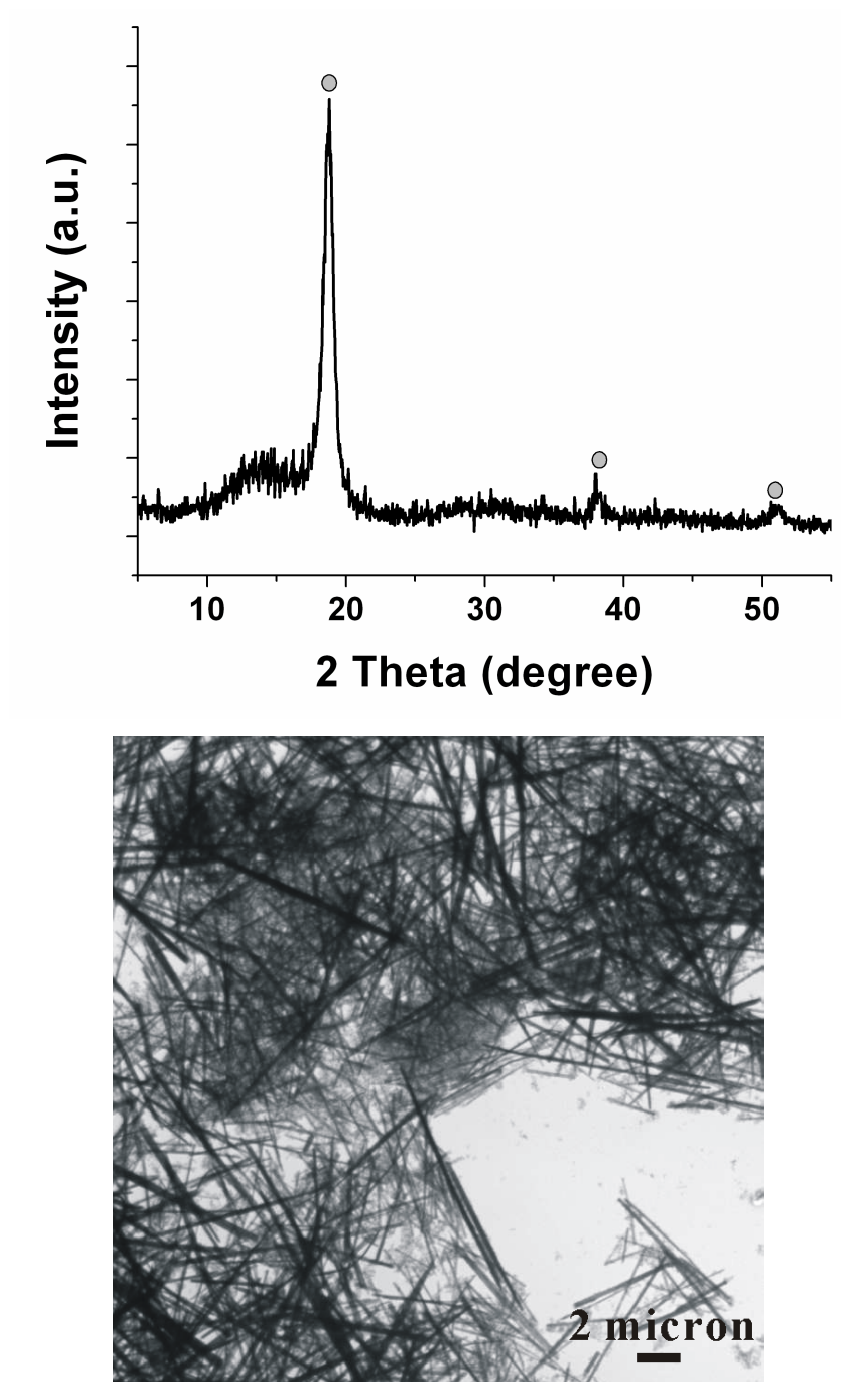


Figure 6.4. Powder XRD pattern and TEM image of sample D after NaOH treatment. The peaks in the XRD pattern are appointed according to JCPDS file 75-1527.

6.4 Conclusions

By changing the quantities of the starting materials in the system MgO-MgCl₂-H₂O, magnesium oxychloride nanorods were prepared with controllable morphology. The obtained nanorods could be converted to magnesium hydroxide nanorods via NaOH treatment. Due to the mild experimental conditions that were engaged, the results presented here can be used to produce both magnesium oxychloride nanorods and Mg(OH)₂ nanorods on large scale.

6.5 References

- (1) Tian, F.; Zhu, J.; Wei, D.; Shen, Y. T. *J. Phys. Chem. B* **2005**, 109, 14852.
- (2) Choi, J.; Oh, S. J.; Ju, H.; Cheon, J. *Nano Lett.* **2005**, 5, 2179.
- (3) Zach, M. P.; Inazu, K.; Ng, K. H.; Hemminger, J. C.; Penner, R. M. *Chem. Mater.* **2002**, 14, 3206.
- (4) Wang, D.; Chang, Y. L.; Liu, Z.; Dai, H. *J. Am. Chem. Soc.* **2005**, 127, 11871.
- (5) Chueh, Y. L.; Chou, L. J.; Hsu, C. M.; Kung, S. C. *J. Phys. Chem. B* **2005**, 109, 21831.
- (6) Lu, X.; Fanfair, D. D.; Johnston, K. P.; Korgel, B. A. *J. Am. Chem. Soc.* **2005**, 127, 15718.
- (7) Wang, Y.; Jiang, X.; Herricks, T.; Xia, Y. *J. Phys. Chem. B* **2004**, 108, 8631.
- (8) Chen, H. M.; Peng, H. C.; Liu, R. S.; Asakura, K.; Lee, C. L.; Lee, J. F.; Hu, S. F. *J. Phys. Chem. B* **2005**, 109, 19553.
- (9) Wang, W.; Banerjee, S.; Jia, S.; Steigerwald, M. L.; Herman, I. P. *Chem. Mater.* **2007**, 19, 2573.
- (10) Gates, B.; Yin, Y.; Xia, Y. *J. Am. Chem. Soc.* **2000**, 122, 12582.
- (11) Jiang, X.; Wang, Y.; Herricks, T.; Xia, Y. *J. Mater. Chem.* **2004**, 14, 695.

- (12) Sorel, S. *Comp. Rend.* **1867**, 65, 102.
- (13) Tooper, B.; Cartz, L. *Nature* **1966**, 211, 64.
- (14) Alley, R. I.; Caine, G. E. *Magnesium oxychloride cement compositions and methods for manufacture* U.S. Patent 5004505, **1991**.
- (15) Policastro, P. P. *Zinc-containing magnesium oxychloride cements providing fire resistance* U.S. Patent 5039454, **1991**.
- (16) Plekhanova, T. A.; Keriene, J.; Gailius, A.; Yakovlev, G. I. *Const. Build. Mater.* **2007**, 21, 1833.
- (17) Sorrell, C. A.; Armstrong, C. R. *J. Am. Ceram. Soc.* **1976**, 59, 51.
- (18) Matkovic, B.; Popovic, S.; Rogic, V.; Zunic, T.; Young, J. F. *J. Am. Ceram. Soc.* **1977**, 60, 504.
- (19) Urwongse, L.; Sorrell, C. A. *J. Am. Ceram. Soc.* **1980**, 63, 501.
- (20) Bilinski, H.; Matkovic, B.; Mazuranic, C.; Zunic, T. B. *J. Am. Ceram. Soc.* **1984**, 67, 266.
- (21) Christensen, A. N. *Mater. Res. Soc. Symp. Proc.* **1992**, 205, 259.
- (22) Li, Z.; Chau, C. K. *J. Mater. Civ. Eng.* **2008**, 20, 239.
- (23) Christensen, A. N.; Norby, P.; Hanson, J. C. *Acta Chem. Scand.* **1995**, 49, 331.
- (24) Christensen, A. N.; Norby, P.; Hanson, J. C. *J. Solid State Chem.* **1995**, 114, 556.
- (25) Jeevanandam, P.; Mulukutla, R. S.; Yang, Z.; Kwen, H.; Klabunde, K. J. *Chem. Mater.* **2007**, 19, 5395.
- (26) Wei, Q.; Lieber, C. M. *Mater. Res. Soc. Symp. Proc.* **2000**, 581, 3.
- (27) Fan, W.; Sun, S.; You, L.; Cao, G.; Song, X.; Zhang, W.; Yu, H. *J. Mater. Chem.* **2003**, 13, 3062.
- (28) Fan, W.; Sun, S.; Song, X.; Zhang, W.; Yu, H.; Tan, X.; Cao, G. *J. Solid State Chem.* **2004**, 177, 2329.